

DISSERTATION

GLOBAL OMEGA EQUATION: DERIVATION AND APPLICATION TO TROPICAL
CYCLOGENESIS IN THE NORTH ATLANTIC OCEAN

Submitted by

John F. Dostalek

Department of Atmospheric Science

In partial fulfillment of the requirements

For the Degree of Doctor of Philosophy

Colorado State University

Fort Collins, Colorado

Fall 2012

Doctoral Committee:

Advisor: Wayne Schubert

Co-Advisor: Mark DeMaria

Don Estep

Richard Johnson

Tom Vonder Haar

Copyright by John Francis Dostalek 2012

All Rights Reserved

ABSTRACT

GLOBAL OMEGA EQUATION: DERIVATION AND APPLICATION TO TROPICAL CYCLOGENESIS IN THE NORTH ATLANTIC OCEAN

The quasi-geostrophic omega equation has been used extensively to examine the large-scale vertical velocity patterns of atmospheric systems. It is derived from the quasi-geostrophic equations, a balanced set of equations based on the partitioning of the horizontal wind into a geostrophic and an ageostrophic component. Its use is limited to higher latitudes, however, as the geostrophic balance is undefined at the equator. In order to derive an omega equation which can be used at low latitudes, a new balanced set of equations is developed. Three key steps are used in the formulation. First, the horizontal wind is decomposed into a nondivergent and an irrotational component. Second, the Coriolis parameter is assumed to be slowly varying, such that it may be moved in and out of horizontal derivative operators as necessary to simplify the derivation. Finally, the mass field is formulated from the nondivergent wind field. The resulting balanced set of equations and the omega equation derived from them are valid over the whole sphere. In addition, they take a similar form to the quasi-geostrophic equations.

The global omega equation is applied to the problem of tropical cyclogenesis in the Atlantic Ocean. The omega fields are used to compare those disturbances that eventually undergo cyclogenesis with those that dissipate. Composite analysis is employed and, in order to account for the different regional behavior of tropical cyclogenesis, the Atlantic is divided into three subbasins: the Tropics, the Subtropics, and the Gulf of Mexico. It is found that the large-scale omega is not strong enough to account for the magnitude of vertical velocities found in tropical cyclones, but acts to provide a favorable environment for convection to develop. The greatest difference between the developing composite and dissipating composite is seen in the Tropics, where the large-scale ascent at low levels on the leading edge of the disturbance due to frictional forcing in the developing composite is significantly greater than the ascent at the leading edge of the dissipating disturbance. The other two subbasins do not exhibit such large statistical differences, but examining the omega fields and the dominant forcing terms do lend insight into the physical differences between those disturbances which develop and those that do not.

As an additional application, the 850-hPa omega is used as a predictor in an operational tropical cy-

clonogenesis probability product. Overall, the inclusion of the omega field improves the performance of the product, as measured in terms of the Brier skill score. Due to a difficulty in interpreting how the linear discriminant analysis handles the omega field however, it may be that the large-scale omega may be of more value in the genesis product's screening step than in its prediction step.

ACKNOWLEDGEMENTS

I owe thanks to many people for their part in helping me to finish this work. First of all I thank my wife, Erin, for her encouragement, prayers, and many sacrifices during my studies. I love you.

I thank also my co-advisors, Wayne Schubert and Mark DeMaria for their guidance and for the many discussions I had with them during the course of this project. Additional thanks to Mark, my day-to-day boss, for accomodating my desire to pursue this degree. Gratitude is also owed to the rest of my committe— Dick Johnson and Tom Vonder Haar from the Department of Atmospheric Sciences and Don Estep from the Department of Mathematics—for their additional insight and comments. Thanks also to Gerhard Dangelmayr from the Department of Mathematics for substituting for Don Estep during the oral defense of this dissertation.

The members of the Schubert group provided overall support and encouragement, but I would like to acknowledge in particular Scott Fulton, also Professor of Mathematics and Computer Science at Clarkson University, for providing the code for the vertical normal mode transform. Rick Taft helped in the setting up of the vertical normal mode transform code, as well as the spherical harmonic transform code (SPHEREPACK), and for providing coding simplifications used in solving the omega equation. Matt Masarik and Levi Silvers provided assistance with LaTeX.

The members of the Regional and Mesoscale Meteorology Branch at the Cooperative Institute for Research in the Atmosphere also encouraged me during my studies. I would like to especially thank Andrea Schumacher for performing the computations associated with the tropical cyclone genesis product discussed in Chapter 5. Thanks also to Deb Molenaar, who helped with various computer issues and Kevin Micke for his assistance in figure preparation.

Josh Cossuth from Florida State University was kind enough to share the data set which included the Dvorak fixes of the dissipating systems, information which was critical for this work.

Finally, thanks to my children—Kyle, Nate, and Janessa—for their patience and encouragement during my studies, and to my parents, in-laws, and church friends for their prayers and support.

This research was supported by NOAA Grant NA090AR4320074.

“Who then is this, that even the wind and the sea obey Him?”

-Mark 4:41 (NASB)

TABLE OF CONTENTS

1	Introduction	1
1.1	Vertical Motions in the Atmosphere	1
1.2	The Development of Quasi-geostrophic Theory	2
1.3	Introduction to the Omega Equation	4
1.4	Vertical Motion and Tropical Cyclogenesis	5
1.5	Structure of the Paper	6
2	Balance Theory on the Sphere	8
2.1	Considerations in Extending Quasi-geostrophic Theory to the Sphere	8
2.2	From the Primitive Equations to the Balanced System	9
2.2.1	Approximations to the Divergence Equation	12
2.2.2	Approximations to the Vorticity Equation	14
2.2.3	Approximations to the Thermodynamic Equation and the Static Stability	15
2.3	The Balanced System of Equations	15
3	The Quasi-geostrophic Omega Equation on the Sphere	20
3.1	Derivation of the omega equation and its boundary conditions	20
3.1.1	The Traditional Form of the Omega Equation	20
3.1.2	Q vector form of the omega equation	22
3.1.3	Boundary Conditions on the Omega Equation	25
3.2	Solution of the Omega Equation	26
3.2.1	Vertical Normal Mode Transform	26
3.2.2	Spherical Harmonic Transform	29
3.3	The Form of the Frictional Forcing	35
3.4	A Mid-Latitude Example	37
4	Application of the Global Omega Equation to Tropical Cyclogenesis in the Atlantic Ocean	41
4.1	Environmental Influences on Tropical Cyclogenesis	41
4.2	Effects of Large-Scale Vertical Motion on Tropical Cyclogenesis	42
4.2.1	Datasets	46
4.2.2	Compositing Procedure	48
4.3	Results	50
4.3.1	Tropical Atlantic Systems	50
4.3.2	Subtropical Atlantic Systems	65
4.3.3	Gulf of Mexico Systems	74
4.4	Significance Testing	83
5	The Use of the Global Omega as a Predictor of Tropical Cyclogenesis in the Atlantic	87
6	Conclusion	92

References	99
A Appendix: Derivation of the vertical transform pair for ω	104
A.1 Derivation of the inverse transform for ω	104
A.2 Derivation of the forward transform for ω	105

LIST OF FIGURES

3.1	Plot the function g , which describes the decay of the effects of the surface wind stress through the boundary layer (1000 hPa-900 hPa), and into the free atmosphere (above 900 hPa), where the effects of surface friction vanish.	37
3.2	a) 700-mb ω calculated from the mid-latitude quasi-geostrophic equations using SOR, from Martin (2006). The 'L' marks the position of the surface low, and the fronts are drawn according to convention. ω is contoured every 2 dPa s ⁻¹ , starting at 1 and -1 dPa s ⁻¹ , with upward motions shaded in dark gray and downward motion shaded in light gray. The unshaded solid lines are the 900-500 hPa thickness, contoured every 4 dam. <i>Courtesy of the American Meteorological Society. Copyright 2006.</i>	39
3.3	700-mb ω calculated from the global balance equations using the technique described in Chapter 3. The units of ω are dPa s ⁻¹ , with upward motions shaded in dark gray and downward motion shaded in light gray. Contour interval is 2 dPa s ⁻¹ , starting at 1 and -1 dPa s ⁻¹	40
4.1	Tracks of the 154 tropical cyclones of the 2001-2009 seasons at 6, 12, 18, and 24 hours before genesis.	44
4.2	Tracks of the 100 dissipating disturbances of the 2001-2009 seasons at 6, 12, 18, and 24 hours before decay.	46
4.3	Map outlining the three subbasins: Tropical Atlantic, Subtropical Atlantic, and the Gulf of Mexico.	49
4.4	Location of the tropical Atlantic composite developing system (solid) and the composite dissipating system (dashed) at 24, 18, 12, and 6 hours before either genesis or dissipation.	51
4.5	850 hPa height (black) and omega (blue) for the developing and dissipating tropical Atlantic composites at 24, 18, 12, and 6 hours before either genesis or dissipation. The height field is contoured every 10 meters. The omega field is contoured every 1 hPa day ⁻¹ , with dashed contours indicating rising motion and solid contours indicating sinking motion. The zero contour is omitted, and the "+" indicates the surface position of the composite.	52
4.6	Cross section of height anomaly (black) and omega (blue) through the developing and dissipating composites at 24, 18, 12, and 6 hours before genesis or dissipation. The height anomaly is contoured every 2 meters and omega is contoured every 2 hPa day ⁻¹ . In both cases solid represents positive values and dashed represents negative values. The zero contour is omitted, and the "+" sign is placed at the longitude of the surface location of the composite disturbance.	55
4.7	Vertical motions associated with the omega field forced by vorticity advection alone.	56
4.8	Vertical motions associated with convectively coupled equatorial waves as depicted by Kiladis et al. (2009). The wide arrows corresponding to the large-scale balanced motion attributed to vorticity advection (Fig. 4.7) have been added.	58
4.9	The contributions to the omega field for the tropical developing composite at 6 hours before development: a) total omega, b) vorticity effects, c) thermal effects d) friction effects. The omega field is contoured every 2 hPa day ⁻¹ , with dashed contours indicating rising motion and solid contours indicating sinking motion. The zero contour is omitted, and the "+" is located at the longitude of the surface location of the composite system.	59
4.10	Same as 4.9, only for the dissipating composite.	60

4.11	Perturbation height (black) and advection of the balanced vorticity by the balanced wind (blue) at -6 hours for: a) Developing composite and b) Dissipating composite. Perturbation height (black) and vorticity forcing for c) Developing composite and d) Dissipating composite. Perturbation height is contoured every 2 m, vorticity advection is contoured every $5 \times 10^{-11} \text{ s}^{-2}$, and vorticity forcing contoured every $0.5 \times 10^{-19} \text{ Pa}^{-1} \text{ s}^{-3}$. For all variables, solid contours denote positive values and dashed contours denote negative values. The zero contour is omitted, and the “+” is positioned at the surface longitude of the composite system.	61
4.12	850-hPa heights (black, m) and temperatures (red, K) at 6 hours before development or dissipation for a) the developing composite, b) the dissipating composite. 850-hPa heights, mean 850-500 hPa relative humidity (green, %), and 700-hPa GFS wind vectors at 6 hours before development or dissipation for c) the developing composite, and d) the dissipating composite. The “+” indicates the surface position of the composite.	63
4.13	Same as 4.4, but for the subtropical Atlantic composites.	65
4.14	850 hPa height (black) and omega (blue) for the developing and dissipating subtropical Atlantic composites at 24, 18, 12, and 6 hours before either genesis or dissipation. The height field is contoured every 10 meters. The omega field is contoured every 4 hPa day^{-1} , with dashed contours indicating rising motion and solid contours indicating sinking motion. The zero contour is omitted, and the “+” indicates the surface position of the composite.	68
4.15	Cross section of height anomaly (black) and omega (blue) through the Subtropical developing and dissipating composites at 24, 18, 12, and 6 hours before genesis or dissipation. The height anomaly is contoured every 8 meters and omega is contoured every 4 hPa day^{-1} . In both cases solid represents positive values and dashed represents negative values. The zero contour is omitted, and the “+” is located at the longitude of the surface location of the composite system.	70
4.16	The contributions to the omega field for the subtropical developing composite at 6 hours before development: a) total omega, b) vorticity effects, c) thermal effects d) friction effects. The omega field is contoured every 4 hPa day^{-1} , with dashed contours indicating rising motion and solid contours indicating sinking motion. The zero contour is omitted, and the “+” sign marks the surface longitude of the composite system.	71
4.17	Same as 4.16, only for the dissipating composite.	72
4.18	The 850-hPa height(black) and temperature(red) from the GFS analysis for the developing and dissipating composite at 24, 18, 12, and 6 hours before either development or dissipation. The height field is contoured every 10 m and the temperature field is contoured every 1 K. The “+” indicates the surface position of the composite.	73
4.19	Same as 4.4, but for the Gulf of Mexico systems.	75
4.20	850-hPa height (black) and omega (blue) for the developing and dissipating Gulf of Mexico composites at 24, 18, 12, and 6 hours before either genesis or dissipation. The height field is contoured every 10 meters. The omega field is contoured every 4 hPa day^{-1} , with dashed contours indicating rising motion and solid contours indicating sinking motion. The zero contour is omitted, and the “+” indicates the surface position of the composite.	76
4.21	Cross section of height anomaly (black) and omega (blue) through the developing and dissipating composites at 24, 18, 12, and 6 hours before genesis or dissipation. The height anomaly is contoured every 8 meters and omega is contoured every 4 hPa day^{-1} . In both cases solid represents positive values and dashed represents negative values. The zero contour is omitted, and the “+” sign marks the surface longitude of the composite system.	77

4.22	The contributions to the omega field for the Gulf of Mexico developing composite at 6 hours before development: a) total omega, b) vorticity effects, c) thermal effects d) friction effects. The omega field is contoured every 2 hPa day ⁻¹ , with dashed contours indicating rising motion and solid contours indicating sinking motion. The zero contour is omitted, and the “+” sign marks the surface longitude of the composite system.	80
4.23	Same as 4.22, only for the dissipating composite.	81
4.24	250-hPa heights (black, m), temperature (red K), and thermal forcing for omega (blue,) for a) developing and b) dissipating composites at -6 hours. The height field is contoured every 10 m, the temperature field every 1 K, and the forcing field every 1x10 ⁻¹⁸ Pa ⁻¹ s ⁻³ . The “+” indicates the surface position of the composite.	82
4.25	Cross sections of omega at a) -24 hours, b) -18 hours, c) -12 hours, d) -6 hours for the tropical developing composite. Areas where the developing composite has significantly greater rising motion are shaded light gray and areas where the developing composite has significantly greater sinking motion are shaded dark gray. Omega is contoured every 2 hPa day ⁻¹ with dashed contours indicating rising motion and solid contours indicating sinking motion. The “+” sign marks the surface longitude of the composite system.	84
4.26	Same as Figure 4.25 but for the subtropical developing composite.	85
4.27	Same as Figure 4.25 but for the Gulf of Mexico developing composite.	86
5.1	The five subregions of the Atlantic used in Schumacher et al. (2009).	89

LIST OF TABLES

4.1	The distribution of the 154 developing systems and the 100 dissipating systems among the three Atlantic subbasins.	48
4.2	The 850-200 hPa shear (ms^{-1}) and the SST of the Tropical developing and dissipating composites at 24, 18, 12, and 6 hours before development or dissipation. The shear calculations are using the winds averaged over a $4^\circ \times 4^\circ$ latitude-longitude box centered over the surface location, and the SSTs are taken at the surface location.	53
4.3	The CAPE, CIN, and LFC calculated from the 1-D cloud model using three different soundings, the Jordan sounding (Control), the Jordan sounding with the moisture profile altered by the divergence profile of the developing composite (Developing) and the dissipating composite (Dissipating).	64
4.4	As in Table 4.2, but for the Subtropical systems.	66
4.5	As in Table 4.2, but for the Gulf of Mexico systems.	74
5.1	Comparison of the Brier skill score for the forecast probability without 850-hPa omega and with 850-hPa omega as a discriminant. The third line shows the percent change when the 850-hPa omega is included. The results are given for the Atlantic Ocean as a whole and for each subbasin. The abbreviations are ATL=entire Atlantic, TAT=tropical Atlantic CAR=Caribbean, SAT=subtropical Atlantic, ECO=East Coast, GOM=Gulf of Mexico. . . .	90
5.2	Normalized coefficients of the LDA listed in order of decreasing magnitude. The abbreviations are: CPRB=climatological formation probability, CIRC=850-hPa circulation, DNST=distance to any existing tropical cyclone, PCCD=percentage of cold pixel coverage, VSHR=850–200-hPa vertical wind shear, HDIV=850-hPa horizontal divergence, QGOM=850-hPa omega, and PLND=percent land coverage.	91

Chapter 1

INTRODUCTION

1.1 Vertical Motions in the Atmosphere

It has long been known that most high impact weather events occur in areas of upward vertical motion. Besides a few notable exceptions such as droughts and downslope windstorms, potentially destructive weather – severe thunderstorms, blizzards, monsoonal rains, hurricanes – all occur where the air is rising. As such, much thought has gone into developing methods to determine the vertical motions of the atmosphere.

On the synoptic scale, horizontal winds are relatively easy to measure. Anemometers reliably measure surface winds, and GPS tracking of radiosondes gives accurate measurements of wind speeds aloft. Accurate measurements of vertical velocities, however, are more difficult. A scale analysis such as performed by Bluestein (1992) demonstrates the difficulty. Typical vertical wind speeds in synoptic-scale systems (10^{-2} m s^{-1}) are three orders of magnitude smaller than the speeds normally seen in horizontal winds (10 m s^{-1}). Certainly instrumented aircraft can measure vertical motions, but the coverage is limited. What is needed is a method to measure vertical motions over vast distances, such as the surface stations and radiosonde network can with the horizontal wind. Various techniques have been developed, therefore, to use those quantities which are more accurately measured, such as horizontal wind speed, to arrive at a measurement of the vertical wind speed. Miller and Panofsky (1958) review many of these techniques, but the two methods most commonly found in today's literature are the kinematic method and the omega equation.

In the kinematic method, vertical velocities are computed using the mass continuity equation in pressure coordinates. The vertical velocity at any pressure level is equal to the integral of the divergence above it. Because divergences in the atmosphere are generally small, errors in the measurement of the horizontal

wind components can result in considerable uncertainty in the divergence, and ultimately in the resulting omega computed from the kinematic method. These errors are typically mitigated by applying a correction scheme such as the one developed by O'Brien (1970).

Although the kinematic method is still in use today, the method most often used to calculate large-scale vertical velocities is the quasi-geostrophic omega equation. This method has an advantage in that it is accurate for large-scale flows, and it gives insight into the processes which force the rising or sinking motions. As the name implies, the quasi-geostrophic omega equation is derived from the quasi-geostrophic equations, a set of equations approximating the primitive equations for large-scale flows. Before discussing the quasi-geostrophic omega equation itself, therefore, an overview of the quasi-geostrophic equations is given. Also, in discussing the omega equation, the issue of scale arises. In this paper, the term large scale will be used synonymously with synoptic scale to mean flows with Rossby number much less than one. The terms small scale and mesoscale will be used interchangeably to mean flows with Rossby number greater than one. The definition of the Rossby number as used here is given in Section 2.2.

1.2 The Development of Quasi-geostrophic Theory

In the mid-twentieth century, meteorologists watched with interest as the first computers were undergoing development. The computer's ability to quickly perform mathematical calculations would be necessary to integrate the equations of motion forward in time in order to produce a numerical forecast of the atmosphere. Meteorologists recognized however, that the first numerical weather forecast would not be realized by the sole efforts of the computer engineers. The basic set of equations governing the flow of the atmosphere (the so-called primitive equations) were still too complex for the new technology to handle. It was necessary, therefore, to simplify the primitive equations in order to be used by the computer. As with any complex system, the simplification process is one of compromise. The goal is to produce a new set of equations which retains the most important aspects of the problem, but which discards those aspects which are secondary and do not contribute to the general understanding of the system, but merely make the manipulations of the equations cumbersome.

In addressing this problem, Charney (1948) began with the observations of the synoptic meteorolo-

gists that the atmospheric flow is approximately hydrostatic and adiabatic. In addition, the horizontal motions are larger than the vertical motions, and the flow of air is in approximate geostrophic balance. Charney used these characteristics to perform a scale analysis on the primitive equations of motion. The result was the development of what is now known as quasi-geostrophic theory. Building upon this work, Charney and other researchers were able to produce the first numerical weather forecast (Charney et al., 1950).

The utility of the quasi-geostrophic system of equations extends well beyond numerical weather prediction. The year after his work on quasi-geostrophic theory was published, Charney noted that the quasi-geostrophic system permits a simplified treatment of certain theoretical problems (Charney, 1949). The equations are simple enough to often be treated analytically, yet still contain enough of the physics of the motion of the atmosphere to allow an understanding of many phenomena in geophysical fluid dynamics. In his own work, Charney used the quasi-geostrophic equations to investigate such topics as the vertical propagation of planetary waves (Charney and Drazin, 1961), geostrophic turbulence (Charney, 1971), and the stability of jet streams (Charney and Stern, 1962).

Because it is such a powerful tool, the use of the quasi-geostrophic system naturally extended well beyond Charney's own research. For example, it has been used in the study of mid-latitude cyclones, severe weather, stratospheric dynamics, and ocean dynamics, as covered by modern textbooks (e.g. Andrews et al., 1987; Bluestein, 1993; Carlson, 1998; Gill, 1982; Holton, 1992; Pedlosky, 1987; Vallis, 2006). In fact, because of its usefulness in reducing the complexity of many atmospheric flows without entirely removing the essential features, the quasi-geostrophic approximation to the primitive equations is covered in virtually every modern textbook on the dynamics of the atmosphere or ocean. Arakawa (2000) notes "I was particularly inspired by the concept of quasi-geostrophy and then fascinated by the fact that even highly simplified dynamical models such as the quasi-geostrophic barotropic model have some relevance to extremely complicated day-to-day weather changes." The application of quasi-geostrophic theory is so widespread in atmospheric science, that it has been called the cornerstone of modern dynamic meteorology (Hoskins et al., 1978).

1.3 Introduction to the Omega Equation

The quasi-geostrophic omega equation is a second order, linear, partial differential equation derived from the quasi-geostrophic approximations to the vorticity equation and to the thermodynamic equation.

The equation may be written as

$$\frac{R\bar{\Gamma}}{p^2}\nabla^2\omega + f_0^2\frac{\partial^2\omega}{\partial p^2} = f_0\left\{\frac{\partial}{\partial p}[\mathbf{v}_g \cdot \nabla(\zeta_g + f)] - \frac{1}{f_0}\nabla^2\left[\mathbf{v}_g \cdot \nabla\left(\frac{\partial\Phi}{\partial p}\right)\right]\right\}, \quad (1.1)$$

where ω is the vertical pressure (p) velocity, $\mathbf{v}_g = \frac{1}{f_0}\mathbf{k} \times \nabla\Phi$ is the geostrophic wind, and ζ_g is the vertical component of the geostrophic vorticity (i.e. $\zeta_g = \mathbf{k} \cdot \nabla \times \mathbf{v}_g$). In this form, which will be called the traditional form, two terms are responsible for forcing the vertical motion. The left hand side is of a form resembling a three-dimensional Laplacian. For the purpose of qualitative interpretation of the equation, it is often assumed that omega is sinusoidal in both the horizontal and the vertical. This assumption leads to the result that the left hand side is proportional to $-\omega$ (Holton, 1992). Looking at the forcing terms, it is seen that the first term on the right hand side involves the absolute vorticity of the flow. In particular, advection of cyclonic vorticity which increases with height forces rising motion. The second term relates the thickness field to the vertical motion. The thickness field is related to the temperature field by the hydrostatic equation such that $\frac{\partial\Phi}{\partial p} = -\frac{RT}{p}$, so the term can be written $-\frac{1}{f_0}\nabla^2\left[-\mathbf{v}_g \cdot \nabla\left(\frac{RT}{p}\right)\right]$, meaning that the horizontal Laplacian of the temperature advection forces vertical motions. If, as in the case of ω , a sinusoidal form of the advection is assumed, then operating with the Laplacian results in a value which is proportional to the negative of the temperature advection, resulting in an approximate form of the forcing $\frac{1}{f_0}\left[-\mathbf{v}_g \cdot \nabla\left(\frac{RT}{p}\right)\right]$. The advection of warm air is associated with rising motion, and the advection of cold air is associated with sinking motion. A more complicated form of this equation was developed by Krishnamurti (1968a) and used in the analysis of a midlatitude cyclone (Krishnamurti, 1968b) and in a study of a tropical easterly wave (Baumhefner, 1968). In both of these studies, the total omega, as well as the omega resulting from the individual components was examined for relative importance.

Despite the relative ease in the interpretation of the forcing terms, there are drawbacks to using (1.1). Bluestein (1992) summarizes these issues. First, the two forcing functions can both be written entirely in terms of the height field so they never really act independently of one another. Second, there can be large

cancellation between the two forcing terms. This cancellation involves a term of the form $\mathbf{v}_g \cdot \nabla \frac{\partial \zeta_g}{\partial p}$, or the geostrophic advection of the thermal vorticity. Third, two pressure levels are needed to specify the vorticity forcing term. Finally, the two forcing terms are not Galilean invariant, although their sum is.

To address these issues, Trenberth (1978) approximated the forcing for the omega equation by the advection of vorticity by the thermal wind. His forcing is an approximation, however, in that he neglected a term involving the geostrophic deformation of the flow. Hoskins et al. (1978) devised an alternative to the traditional form of the omega equation which retains the deformation terms neglected by Trenberth. In their formulation, the omega equation is forced by the divergence of a vector, \mathbf{Q} :

$$\frac{R\bar{\Gamma}}{p^2} \nabla^2 \omega + f_0^2 \frac{\partial^2 \omega}{\partial p^2} = -2\nabla \cdot \mathbf{Q}. \quad (1.2)$$

As seen in Holton (1992), \mathbf{Q} is typically written in one of two equivalent forms:

$$\mathbf{Q} = \left(-\frac{R}{p} \frac{\partial \mathbf{v}_g}{\partial x} \cdot \nabla T, -\frac{R}{p} \frac{\partial \mathbf{v}_g}{\partial y} \cdot \nabla T \right) \quad (1.3)$$

or

$$\mathbf{Q} = \frac{D_g}{Dt} \left(\frac{R}{p} \nabla T \right) \quad (1.4)$$

In (1.4), it can be seen that \mathbf{Q} is proportional to the horizontal frontogenesis following the geostrophic flow.

1.4 Vertical Motion and Tropical Cyclogenesis

Convection is the primary source for vertical motions in tropical cyclones, whereas most omega equations (including the omega equations discussed here) assume adiabatic conditions. In that sense the study of a mature tropical cyclone should be undertaken using an omega equation which includes latent heating. But given that tropical cyclones are characterized by intense upward motion, it is reasonable to expect that an environment of large-scale rising motion would be favorable to the development of any nascent disturbances. Clearly tropical cyclones do have surrounding regions of subsidence which compensate the vigorous rising motions produced by the convection (Frank, 1977), and the eye of a hurricane is a well-known area of sinking motion (Shea and Gray, 1973; Willoughby, 1998). But it is the upward motions due to convection which drives the system, so any help in creating convection would benefit a pre-cyclone

disturbance. The focus in this paper, then, will be on the environmental conditions a disturbance experiences before either development or dissipation. In this sense, the relationship between omega and the development of a tropical cyclone will be similar to the relationship between omega and the development of severe convective storms proposed by Doswell (1987). In his view, rising motion created by synoptic-scale systems aids in removing any capping inversion which may be present, in addition to reducing the stability of the sounding overall. For this purpose the adiabatic omega equation is an appropriate tool.

The use of either (1.1) or (1.2) is well suited for midlatitude applications, but at low latitudes, the geostrophic wind becomes a less-valid approximation to the actual wind. At the equator, it is undefined altogether. In addition, tropical cyclones can form at a wide range of latitudes, especially in the Atlantic and West Pacific basins, so an omega equation which includes a variable Coriolis parameter is desirable. This paper introduces an omega equation which is based on a balanced set of equations valid for the whole sphere, therefore making it suitable for use in the Tropics. The derivation of the system relies on three key steps. First, the horizontal wind field is not decomposed into a geostrophic component and an ageostrophic component, but rather into a nondivergent component and an irrotational component. Second, the Coriolis parameter is allowed to vary with latitude, but this variation is assumed to be small compared to the variation of the streamfunction. As will be seen, this approximation allows the Coriolis parameter to be moved in and out of the del or Laplacian operators, ultimately creating an omega equation which has the same general appearance as the quasi-geostrophic omega equation. Finally, in creating the balanced mass and momentum fields, the mass field is computed from the nondivergent wind field, as opposed to the typical definition of the geostrophic balance, which gives the wind field as a function of the mass field. With the global omega equation, the large-scale vertical motions associated with Atlantic disturbances may be studied in much the same way as the quasi-geostrophic omega equation has been used to study extratropical weather systems.

1.5 Structure of the Paper

The remainder of this work is divided into 5 chapters. In Chapter 2, the primitive equations in spherical coordinates are used to derive the balanced system valid for the whole sphere. The derivation follows similar steps as are used to derive the quasi-geostrophic equations for midlatitudes. Not surprisingly,

the equations governing this balanced system appear very similar to the quasi-geostrophic equations. In the development of the quasi-geostrophic system, friction is often neglected; in this work, it will be retained. In Chapter 3, the global balanced system is used to derive a global omega equation and boundary conditions for its solution on the sphere. Both the traditional and the Q form are derived. The details of the method of solution of the omega equation, which includes a normal mode decomposition in the vertical and a spherical harmonic decomposition in the horizontal, are given. In Chapter 4, the global omega equation is applied to the problem of tropical cyclogenesis in the Atlantic Ocean in conjunction with the more traditional measures of tropical cyclogenesis likelihood such as vertical wind shear and sea-surface temperature. Here composite systems composed of disturbances which eventually became tropical cyclones are compared with composite systems composed of disturbances which dissipated before becoming tropical cyclones. The variations in the mechanisms of cyclogenesis are attempted to be captured by creating composite systems according to the subbasin of genesis or dissipation—the Tropical Atlantic, the Subtropical Atlantic, and the Gulf of Mexico. In Chapter 5, the predictive potential of the global omega is tested by including it in a statistical model which predicts the probability of cyclogenesis within 24 hours for each 5° latitude \times 5° longitude box in the Atlantic Ocean. Chapter 6 concludes the paper by summarizing the findings and suggesting avenues of further research.

Chapter 2

BALANCE THEORY ON THE SPHERE

2.1 Considerations in Extending Quasi-geostrophic Theory to the Sphere

In order to develop an omega equation applicable to the entire sphere, a set of equations governing a balanced flow on the sphere must be derived. Quasi-geostrophic theory, which has seen such extensive use in mid-latitudes, relies on the decomposition of the horizontal velocity into a geostrophic and an ageostrophic component. In this decomposition, there are two ways to define the geostrophic wind (Blackburn, 1985). The first is to replace the Coriolis parameter, f , with a constant, f_0 , associated with a particular latitude. While such an assumption is often used in mid-latitude studies, it is hardly appropriate to consider one value for the Coriolis parameter as applicable to the entire Earth. The second option is to retain the latitudinal variation in f in the definition of the geostrophic wind. This option cannot be applied to low latitudes, however, as the geostrophic balance breaks down due to the decrease in magnitude of the Coriolis parameter, resulting in a singularity at the equator where $f = 0$ (Daley, 1983). Therefore, an approach alternate to geostrophic balance is needed.

Bluestein (1992) notes that, for large-scale mid-latitude flows, the divergence can be up to an order of magnitude smaller than the relative vorticity. In his analysis, Charney (1963), reports that large-scale flows in the Tropics are also characterized by a small value of divergence. A balance theory relying on the assumption of the approximate nondivergence of the horizontal wind is therefore better suited to global motions than a theory based on geostrophic balance of the horizontal winds. This approach to obtaining a global balance theory was used by Kuo (1959) and Charney (1960). Schubert et al. (2009) and Verkley (2009) recently revisited the topic, examining the behavior of balanced, shallow-water Rossby waves on the

sphere. Although the theory uses similar scaling arguments applied to the derivation of mid-latitude quasi-geostrophic theory (Charney, 1948; Phillips, 1963), the horizontal wind is decomposed into a nondivergent and an irrotational component rather than a geostrophic and an ageostrophic component.

2.2 From the Primitive Equations to the Balanced System

In order to derive the equations governing a balance theory on the sphere, approximations to the primitive equations will be made which isolate the features characterized by a vertical scale which is small compared to the horizontal scale and having a small Rossby number. The Rossby number is typically defined as $Ro = \frac{U}{2\Omega\mu L}$, where U is a characteristic velocity, Ω is the angular rotation rate of the earth, μ is the sine of the latitude, and L is a characteristic length. This form of the Rossby number presents a problem for global applications, however, as it is unbounded at the equator. For this work the Rossby number will take the form used by Charney and Drazin (1961) and Charney and Stern (1962), namely, $Ro = \frac{U}{2\Omega L}$. This form remains finite at the equator. With pressure as the vertical coordinate, the dry, adiabatic, hydrostatic, primitive equations obeying the ideal gas law may be written as

$$\frac{D_3 \mathbf{v}}{Dt} + 2\Omega\mu \mathbf{k} \times \mathbf{v} + \nabla\Phi = \mathbf{F} \quad (2.1)$$

$$\frac{\partial\Phi}{\partial p} + \frac{RT}{p} = 0 \quad (2.2)$$

$$\nabla \cdot \mathbf{v} + \frac{\partial\omega}{\partial p} = 0 \quad (2.3)$$

$$\frac{\partial T}{\partial t} + \mathbf{v} \cdot \nabla T - \frac{\Gamma}{p}\omega = 0 \quad (2.4)$$

$$\Gamma = \left(\frac{RT}{c_p} - p \frac{\partial T}{\partial p} \right) \quad (2.5)$$

with the following definitions:

λ longitude

μ sine of the latitude

p pressure

t time

$2\Omega\mu$ Coriolis parameter

R gas constant for dry air

c_p specific heat of dry air at constant pressure

T temperature

Φ geopotential

\mathbf{v} horizontal velocity

ω vertical p -velocity

\mathbf{k} vertical unit vector

∇ gradient operator at constant p

$\frac{D_3}{Dt}$ total derivative $\equiv \frac{\partial}{\partial t} + \mathbf{v} \cdot \nabla + \omega \frac{\partial}{\partial p}$

The above six equations (the momentum equation (2.1) has two components) constitute a closed system in the six variables \mathbf{v} , ω , Φ , T , and Γ , which are all functions of the independent variables \mathbf{r} , p , and t , where $\mathbf{r} = (\lambda\mathbf{i}, \mu\mathbf{j})$ is a horizontal position vector.

A vector representing the effects of boundary layer friction, \mathbf{F} , has been included in the horizontal momentum equation. In mid-latitude studies, this term is often neglected because of the strength of the quasi-geostrophic forcing. In the Tropics, however, the quasi-geostrophic effects are much weaker, even to the point of being equaled or surpassed in magnitude by the frictional contribution (Krishnamurti, 1968a; Baumhefner, 1968). The frictional term has therefore been retained in the equations of motion in the layer

1000-900 hPa. The atmosphere above 900 hPa is considered to be frictionless. The description of its representation will be given in Chapter 3.

Before applying the necessary approximations to the primitive equations to arrive at the balanced system, it is convenient to replace the horizontal momentum equation (2.1) with equations governing the divergence and the vertical component of the vorticity of the flow. These equations are derived, respectively, by taking $\nabla \cdot$ and $\mathbf{k} \cdot \nabla \times$ of the momentum equation (2.1):

$$\begin{aligned} \frac{\partial \delta}{\partial t} + \nabla^2 \left(\Phi + \frac{1}{2} \mathbf{v} \cdot \mathbf{v} \right) - \zeta (\zeta + 2\Omega\mu) + \mathbf{v} \cdot \nabla (\zeta + 2\Omega\mu) \times \mathbf{k} + \omega \frac{\partial \delta}{\partial p} + \nabla \omega \cdot \frac{\partial \mathbf{v}}{\partial p} &= \nabla \cdot \mathbf{F}, \\ \frac{D_3 (\zeta + 2\Omega\mu)}{Dt} - (\zeta + 2\Omega\mu) \frac{\partial \omega}{\partial p} + \mathbf{k} \cdot \left(\nabla \omega \times \frac{\partial \mathbf{v}}{\partial p} \right) &= \nabla \times \mathbf{F}, \end{aligned}$$

where $\delta = \nabla \cdot \mathbf{v}$ is the divergence of the horizontal wind field, and $\zeta = \mathbf{k} \cdot \nabla \times \mathbf{v}$ is the vertical component of the isobaric relative vorticity.

Decomposing the horizontal wind field into nondivergent and irrotational components allows the horizontal wind vector to be written as $\mathbf{v} = \mathbf{v}_\psi + \mathbf{v}_\chi$. The nondivergent wind is given by $\mathbf{v}_\psi = \mathbf{k} \times \nabla \psi$, where ψ is the streamfunction, and the irrotational wind is given by $\mathbf{v}_\chi = \nabla \chi$, where χ is the velocity potential. The vertical component of the relative vorticity may then be written as:

$$\zeta = \mathbf{k} \cdot \nabla \times \mathbf{v} = \mathbf{k} \cdot \nabla \times (\mathbf{v}_\psi + \mathbf{v}_\chi) = \mathbf{k} \cdot \nabla \times (\mathbf{k} \times \nabla \psi) = \nabla^2 \psi$$

and the divergence of the horizontal wind may be written as:

$$\delta = \nabla \cdot \mathbf{v} = \nabla \cdot (\mathbf{v}_\psi + \mathbf{v}_\chi) = \nabla \cdot \nabla \chi = \nabla^2 \chi,$$

where by definition $\nabla \cdot \mathbf{v}_\psi = 0$ and $\nabla \times \mathbf{v}_\chi = 0$.

The system of equations from which the balance theory on the sphere are derived can now be written:

$$\begin{aligned} \frac{\partial (\nabla^2 \chi)}{\partial t} + \nabla^2 \left(\Phi + \frac{1}{2} \mathbf{v} \cdot \mathbf{v} \right) - \nabla^2 \psi (\nabla^2 \psi + 2\Omega\mu) \\ + \mathbf{v} \cdot \nabla (\nabla^2 \psi + 2\Omega\mu) \times \mathbf{k} + \omega \frac{\partial (\nabla^2 \chi)}{\partial p} + \nabla \omega \cdot \frac{\partial \mathbf{v}}{\partial p} &= \nabla \cdot \mathbf{F} \end{aligned} \quad (2.6)$$

$$\frac{D_3 (\nabla^2 \psi + 2\Omega\mu)}{Dt} - (\nabla^2 \psi + 2\Omega\mu) \frac{\partial \omega}{\partial p} + \mathbf{k} \cdot \left(\nabla \omega \times \frac{\partial \mathbf{v}}{\partial p} \right) = \nabla \times \mathbf{F} \quad (2.7)$$

$$\frac{\partial \Phi}{\partial p} + \frac{RT}{p} = 0 \quad (2.8)$$

$$\nabla^2 \chi + \frac{\partial \omega}{\partial p} = 0 \quad (2.9)$$

$$\frac{\partial T}{\partial t} + \mathbf{v} \cdot \nabla T - \frac{\Gamma}{p} \omega = 0 \quad (2.10)$$

$$\Gamma = \left(\frac{RT}{c_p} - p \frac{\partial T}{\partial p} \right) \quad (2.11)$$

$$\mathbf{v} = \mathbf{k} \times \nabla \psi + \nabla \chi \quad (2.12)$$

The system now consists of eight scalar equations in eight scalar variables: \mathbf{v} , ω , Φ , T , Γ , ψ , and χ . Although this system of equations is larger than the system introduced at the beginning of this section, it lends itself to the application of the approximations necessary to derive the balanced system. Approximations will be made to: the divergence equation, the vorticity equation, the thermodynamic equation, and the static stability parameter, Γ .

2.2.1 Approximations to the Divergence Equation

The approximate form of the divergence equation ultimately defines the balance assumed by the system. By neglecting the terms involving the divergent part of the wind, the term $\nabla \omega \cdot \frac{\partial \mathbf{v}}{\partial p}$, and the friction term, the divergence equation becomes

$$\nabla^2 \left(\Phi + \frac{1}{2} \mathbf{v}_\psi \cdot \mathbf{v}_\psi \right) - \zeta_a \nabla^2 \psi + \mathbf{v}_\psi \cdot \nabla \zeta_a \times \mathbf{k} = 0, \quad (2.13)$$

where $\zeta_a = (\nabla^2 \psi + 2\Omega\mu)$ is the absolute vorticity. The third term can be rewritten as

$$(\mathbf{k} \times \nabla \psi) \cdot (\nabla \zeta_a \times \mathbf{k}) = -\mathbf{k} \times \nabla \psi \cdot \mathbf{k} \times \nabla \zeta_a = -\nabla \psi \cdot \nabla \zeta_a,$$

which, when used in (2.13), gives the following:

$$\nabla^2 \left(\Phi + \frac{1}{2} \mathbf{v}_\psi \cdot \mathbf{v}_\psi \right) - \zeta_a \nabla^2 \psi - \nabla \psi \cdot \nabla \zeta_a =$$

$$\begin{aligned}
& \nabla^2 \left(\Phi + \frac{1}{2} \mathbf{v}_\psi \cdot \mathbf{v}_\psi \right) - \nabla \cdot (\zeta_a \nabla \psi) = \\
& \nabla^2 \Phi + \nabla^2 \left(\frac{1}{2} \mathbf{v}_\psi \cdot \mathbf{v}_\psi \right) - \nabla \cdot [(\nabla^2 \psi + 2\Omega\mu) \nabla \psi] = \\
& \nabla^2 \Phi - \nabla \cdot (f \nabla \psi) + \nabla^2 \left(\frac{1}{2} \mathbf{v}_\psi \cdot \mathbf{v}_\psi \right) - \nabla \cdot (\nabla^2 \psi \nabla \psi) = 0.
\end{aligned} \tag{2.14}$$

Equation (2.14) is known as the nonlinear balance equation (Charney, 1955). If further approximation is made by neglecting the nonlinear terms, the result is the linear balance equation,

$$\nabla^2 \Phi - \nabla \cdot (2\Omega\mu \nabla \psi) = 0. \tag{2.15}$$

The final approximation to the balance equation follows the arguments of Charney and Stern (1962). The variable μ will be considered a slowly-varying function of latitude in comparison to ψ . This approximation allows the factor $2\Omega\mu$, to be moved into the gradient operator in (2.15). Thus the balance equation can be written as $\nabla^2 (\Phi - 2\Omega\mu\psi) = 0$. The solution to this equation on a sphere is $\Phi - 2\Omega\mu\psi = C$, where C is a constant. This equation holds for each isobaric surface, and C will be chosen to be equal to the base-state geopotential of the isobaric surface. The final version of the balance equation becomes

$$2\Omega\mu\psi(\lambda, \mu, p) = \Phi(\lambda, \mu, p) - \bar{\Phi}(p), \tag{2.16}$$

where $\bar{\Phi}(p)$ is the base-state geopotential which is related to the base-state temperature profile through the hydrostatic equation. Thus, the Coriolis parameter maintains its full latitudinal variation, but the balance condition will not be valid for motions with large meridional extent. The results of this approximation are shown by Schubert et al. (2009). In comparing the Rossby-Haurwitz wave frequencies of the shallow water version of the global balance theory with those derived from the primitive equations, they found excellent agreement in all cases but the sectoral harmonics, i.e. harmonics with low meridional wavenumber.

Equation (2.16) describes the relationship between the temperature, or mass, field (Φ) and the wind, or momentum, field (ψ). It does not in general require that one of the fields be derived from the other; one may choose which field is conformed to the other in order to satisfy the balance condition. Phillips (1958) explored this choice in the context of numerical weather prediction, using a mid-latitude cyclone over the

eastern United States as an example. He came to the conclusion that it is more important to have an estimate of the wind field, and from that derive the associated temperature field through the balance relationship, than it is to have an estimate of the temperature field, and from that derive the wind field from the balance relationship. Although his domain covered only a portion of the midlatitudes, one might consider a verification of his conclusion to be borne out for the global balance theory by examining (2.16). If the balance is constructed by determining the streamfunction from the geopotential field, then $\psi = \frac{\Phi(\lambda, \mu, p) - \bar{\Phi}(p)}{2\Omega\mu}$, which is indeterminate or singular at the equator, depending on how $\bar{\Phi}(p)$ is defined. If, on the other hand, the balance is constructed by determining the geopotential field from the streamfunction, no such problem exists. It does require that, along the equator, the geopotential field is equal to the base-state geopotential for each pressure level, so that the geopotential perturbations are identically zero. This requirement will result in errors at very low latitudes, but should not effect the study of tropical cyclogenesis, as Gray (1968) shows that although most tropical cyclones form equatorward of 20° , formation is essentially nonexistent equatorward of 5° .

2.2.2 *Approximations to the Vorticity Equation*

The vorticity equation (2.7) will be approximated by neglecting the following (Kuo, 1959):

- (1) the horizontal advection of absolute vorticity by the irrotational component of the wind
- (2) the vertical advection of absolute vorticity
- (3) the stretching of the relative vorticity
- (4) the twisting term $\mathbf{k} \cdot \left(\nabla\omega \times \frac{\partial\mathbf{v}}{\partial p} \right)$.

In addition, the vertical component of the relative vorticity ζ should now be understood to be an approximation to the actual vertical component of the relative vorticity. The approximation comes from the use of \mathbf{v}_ψ as the balanced approximation to the actual nondivergent wind. The new vorticity equation is then given by

$$\frac{D(\nabla^2\psi + 2\Omega\mu)}{Dt} - 2\Omega\mu\frac{\partial\omega}{\partial p} = \mathbf{k} \cdot \nabla \times \mathbf{F},$$

where $\frac{D}{Dt} = \frac{\partial}{\partial t} + \mathbf{v}_\psi \cdot \nabla$ is the time derivative following the nondivergent component of the balanced wind. This form of the vorticity equation is consistent with Cases I and II of Charney (1960), only he includes the advection of the planetary vorticity by the irrotational wind and neglects friction.

2.2.3 *Approximations to the Thermodynamic Equation and the Static Stability*

Again following the arguments listed in Kuo (1959), a new version of the thermodynamic equation (2.10) is derived by:

(1) neglecting the horizontal advection of T by the irrotational component of the flow

(2) replacing the actual static stability Γ with a base-state static stability which is a function of pressure

$$\text{only } \bar{\Gamma} = \left(\frac{R\bar{T}}{c_p} - p \frac{d\bar{T}}{dp} \right)$$

With these changes the thermodynamic equation becomes

$$\frac{DT}{Dt} - \frac{\bar{\Gamma}}{p} \omega = 0$$

2.3 **The Balanced System of Equations**

The set of balanced equations on the sphere relates 7 equations to 7 variables: \mathbf{v}_ψ , ω , Φ , T , ψ , and χ .

Balance Theory on the Sphere

$$2\Omega\mu\psi = \Phi - \bar{\Phi} \quad (2.17)$$

$$\frac{D(\nabla^2\psi + 2\Omega\mu)}{Dt} - 2\Omega\mu\frac{\partial\omega}{\partial p} = \mathbf{k} \cdot \nabla \times \mathbf{F} \quad (2.18)$$

$$\frac{\partial\Phi}{\partial p} + \frac{RT}{p} = 0 \quad (2.19)$$

$$\nabla^2\chi + \frac{\partial\omega}{\partial p} = 0 \quad (2.20)$$

$$\frac{DT}{Dt} - \frac{\bar{\Gamma}}{p}\omega = 0 \quad (2.21)$$

$$\mathbf{v}_\psi = \mathbf{k} \times \nabla\psi \quad (2.22)$$

The derivation of the associated thermal wind relation, which will be used in the construction of the global omega equation, begins with the balance condition

$$2\Omega\mu\psi = \Phi - \bar{\Phi}.$$

Operating with $\partial/\partial p$ and using $\partial\Phi/\partial p = -\alpha$ and $d\bar{\Phi}/dp = -\bar{\alpha}$ gives

$$2\Omega\mu\frac{\partial\psi}{\partial p} = -(\alpha - \bar{\alpha}). \quad (2.23)$$

Applying the assumption of a slowly-varying μ , operating with $\mathbf{k} \times \nabla$ on the above equation results in the thermal wind equation for the balance theory on the sphere:

$$2\Omega\mu\frac{\partial\mathbf{v}_\psi}{\partial p} = -\mathbf{k} \times \nabla\alpha. \quad (2.24)$$

For comparison, the common frictionless, constant- f quasi-geostrophic system of equations is given in (2.25)-(2.30).

Quasi-geostrophic Theory on an f -Plane

$$f_0\psi = \Phi - \bar{\Phi} \quad (2.25)$$

$$\frac{D_g(\nabla^2\psi + f)}{Dt} - f_0\frac{\partial\omega}{\partial p} = 0 \quad (2.26)$$

$$\frac{\partial\Phi}{\partial p} + \frac{RT}{p} = 0 \quad (2.27)$$

$$\nabla^2\chi + \frac{\partial\omega}{\partial p} = 0 \quad (2.28)$$

$$\frac{D_g T}{Dt} - \frac{\bar{\Gamma}}{p}\omega = 0 \quad (2.29)$$

$$\mathbf{v}_g = \mathbf{k} \times \nabla\psi \quad (2.30)$$

In the derivation of the quasi-geostrophic system, such as given by Holton (1992), the same or similar approximations are made as in the derivation of the global balance equations:

- (1) the divergence equation is approximated by the geostrophic balance
- (2) the horizontal wind is decomposed into a geostrophic (\mathbf{v}_g) and an ageostrophic component (\mathbf{v}_a) with $|\mathbf{v}_g| \gg |\mathbf{v}_a|$
- (3) the three-dimensional total derivative is replaced with the two-dimensional total derivative $\frac{D_g}{Dt} = \frac{\partial}{\partial t} + \mathbf{v}_g \cdot \nabla$
- (4) the stretching and twisting term in the vorticity equation are neglected
- (5) the static stability, Γ is replaced by $\bar{\Gamma}$, which is a function of pressure only.

Further analysis of balanced systems typically involves the vorticity equation and the thermodynamic equation, and proceeds down one of two paths. The first is to combine the two equations in such a way as

to eliminate the streamfunction tendency. This operation leads to a partial differential equation in ω which governs the large-scale ascent and descent of air. This equation and its solution is the focus of this work. For completeness, however, the second option will be briefly discussed. In this case ω is eliminated between the two equations, which results in an equation governing the streamfunction tendency, analogous to the height tendency of the mid-latitude quasi-geostrophic theory. Following Holton (1992) use the hydrostatic equation along with the balance condition (2.17) to rewrite the thermodynamic equation as

$$\frac{\partial}{\partial t} \left(2\Omega\mu \frac{\partial\psi}{\partial p} \right) + \frac{R\bar{\Gamma}}{p^2} \omega = -\mathbf{v}_\psi \cdot \nabla \left(2\Omega\mu \frac{\partial\psi}{\partial p} \right). \quad (2.31)$$

If this result is multiplied by $\frac{2\Omega\mu}{\frac{R\bar{\Gamma}}{p^2}}$ and subsequently differentiated with respect to pressure, the result is

$$\frac{\partial}{\partial t} \left[\frac{\partial}{\partial p} \left(\frac{4\Omega^2\mu^2}{\frac{R\bar{\Gamma}}{p^2}} \frac{\partial\psi}{\partial p} \right) \right] = \frac{\partial}{\partial p} \left[-\mathbf{v}_\psi \cdot \nabla \left(\frac{4\Omega^2\mu^2}{\frac{R\bar{\Gamma}}{p^2}} \frac{\partial\psi}{\partial p} \right) \right] - 2\Omega\mu \frac{\partial\omega}{\partial p},$$

where the term $\frac{2\Omega\mu}{\frac{R\bar{\Gamma}}{p^2}}$ was moved inside the gradient operator using the slowly-varying μ approximation.

Adding this alteration of the thermodynamic equation to the vorticity equation gives

$$\nabla^2 \left(\frac{\partial\psi}{\partial t} \right) + \frac{\partial}{\partial t} \left[\frac{\partial}{\partial p} \left(\frac{4\Omega^2\mu^2}{\frac{R\bar{\Gamma}}{p^2}} \frac{\partial\psi}{\partial p} \right) \right] = -\mathbf{v}_\psi \cdot \nabla (\nabla^2\psi + 2\Omega\mu) - \frac{\partial}{\partial p} \left[\mathbf{v}_\psi \cdot \nabla \left(\frac{4\Omega^2\mu^2}{\frac{R\bar{\Gamma}}{p^2}} \frac{\partial\psi}{\partial p} \right) \right] + \mathbf{k} \cdot \nabla \times \mathbf{F}.$$

The second to the last term on the right may be written as

$$-\mathbf{v}_\psi \cdot \nabla \frac{\partial}{\partial p} \left(\frac{4\Omega^2\mu^2}{\frac{R\bar{\Gamma}}{p^2}} \frac{\partial\psi}{\partial p} \right) - 2\Omega\mu \frac{\partial\mathbf{v}_\psi}{\partial p} \cdot \nabla \left(\frac{2\Omega\mu}{\frac{R\bar{\Gamma}}{p^2}} \frac{\partial\psi}{\partial p} \right).$$

Using the balance relation and the thermal wind equation, it can be seen that the second term above is

$$\mathbf{k} \times \nabla\alpha \cdot \frac{2\Omega\mu}{\frac{R\bar{\Gamma}}{p^2}} \nabla\alpha = 0.$$

Gathering the remaining terms gives $\frac{Dq_\psi}{Dt} = \mathbf{k} \cdot \nabla \times \mathbf{F}$, or $\frac{Dq_\psi}{Dt} = 0$ for inviscid systems, where

$$q_\psi = \nabla^2\psi + 2\Omega\mu + \frac{\partial}{\partial p} \left(\frac{4\Omega^2\mu^2}{\frac{R\bar{\Gamma}}{p^2}} \frac{\partial\psi}{\partial p} \right)$$

is conserved following \mathbf{v}_ψ on an isobaric surface. As explained by Holton (1992), it is often referred to as the pseudo-potential vorticity. This name is used in order to distinguish q_ψ from Ertel's potential vorticity, which is materially conserved on an isentropic surface. In any event, q_ψ performs the role of the potential

vorticity for this set of equations. The essence of balanced systems is contained in the material conservation of potential vorticity and its invertibility. These properties are discussed at length in Hoskins et al. (1985). It is truly remarkable that all of the dynamics for adiabatic, frictionless, large-scale flows can be described by one variable. In fact Lorenz (2006) remarks of quasi-geostrophic theory “I personally regard the successful reduction of the dynamic equations to a single prognostic equation by means of the geostrophic relationship as the greatest single achievement of twentieth-century dynamic meteorology”.

Chapter 3

THE QUASI-GEOSTROPHIC OMEGA EQUATION ON THE SPHERE

3.1 Derivation of the omega equation and its boundary conditions

Although much insight into large-scale dynamics can be gained by examining the concepts of potential vorticity conservation and its invertibility, the focus of this work is on the global omega equation, its solution in spherical coordinates, and its application to the problem of tropical cyclogenesis. The omega equation is a diagnostic equation describing the large-scale vertical motion of the atmosphere. Whereas the streamfunction tendency, and subsequently the potential vorticity was derived in the previous chapter by eliminating omega from the vorticity and thermodynamic equations, the omega equation is derived by eliminating the streamfunction tendency term from the vorticity and thermodynamic equations. Just as with the mid-latitude omega equation, the global omega equation can be written in two ways, depending on the form of the forcing. The first – or traditional – form has the forcing divided into a vorticity component and a thermal component. In the second form, the forcing is written in terms of the the vector \mathbf{Q} . In this section, the derivation of both forms of the omega is presented, followed by the derivation of the boundary conditions.

3.1.1 *The Traditional Form of the Omega Equation*

In order to eliminate the streamfunction tendency from the balanced vorticity equation and the balanced thermodynamic equation, operate on (2.18) with $\frac{\partial}{\partial p}$ after multiplying by $-2\Omega\mu$, then add to ∇^2 of

(2.31). The result is

$$\begin{aligned} \frac{R\bar{\Gamma}}{p^2} \nabla^2 \omega + 4\Omega^2 \mu^2 \frac{\partial^2 \omega}{\partial p^2} &= \frac{\partial}{\partial p} [2\Omega \mu \mathbf{v}_\psi \cdot \nabla (\zeta + 2\Omega \mu)] \\ &- \nabla^2 \left[2\Omega \mu \mathbf{v}_\psi \cdot \nabla \left(\frac{\partial \psi}{\partial p} \right) \right] - \frac{\partial}{\partial p} (2\Omega \mu \mathbf{k} \cdot \nabla \times \mathbf{F}). \end{aligned} \quad (3.1)$$

Equation (3.1) shows that the forcing of the vertical velocity for the balance theory on the sphere is related to the vertical derivative of the vorticity advection by the balanced wind and to the Laplacian of the advection of $\frac{\partial \psi}{\partial p}$, which by (2.23) is essentially the Laplacian of the thermal advection.

Equation (3.1) is analogous to the mid-latitude quasi-geostrophic omega equation, given here in its frictionless form:

$$\frac{R\bar{\Gamma}}{p^2} \nabla^2 \omega + f_0^2 \frac{\partial^2 \omega}{\partial p^2} = f_0 \left\{ \frac{\partial}{\partial p} [\mathbf{v}_g \cdot \nabla (\zeta_g + f)] - \frac{1}{f_0} \nabla^2 \left[\mathbf{v}_g \cdot \nabla \left(\frac{\partial \Phi}{\partial p} \right) \right] \right\}. \quad (3.2)$$

The quasi-geostrophic omega is derived in the same manner as the global omega equation, only using the quasi-geostrophic vorticity equation (2.26) and the quasi-geostrophic thermodynamic equation (2.29).

In comparing (3.1) with (3.2), it can be seen that the forms of the two omega equations are identical – with a three-dimensional, Laplacian-type operator on the left-hand side, forced on the right-hand side by two terms. The first is the vertical derivative of the advection of the absolute vorticity. The second is the Laplacian of the advection of the vertical derivative of either the geopotential (3.2), or the streamfunction (3.1). By the hydrostatic equation, these derivatives are proportional to the temperature. Large-scale vertical motions on the sphere, then, are forced by the same mechanisms by which large-scale vertical motions at mid-latitudes are forced – by differential cyclonic vorticity advection and the Laplacian of the thermal advection.

In addition to the similarities, two differences can be seen. The advectations are accomplished in (3.11) by the geostrophic wind, and by the nondivergent wind component in (??). In the mid-latitude form, the Coriolis parameter assumes a constant value, f_0 , except in the vorticity advection term. In the global omega equation, the Coriolis parameter has its full variability in each term in which it exists. The complete range of values, however, includes $2\Omega \mu = 0$ at the equator, in which case (3.1) indicates that the forcing vanishes. Finally, the mid-latitude form contains the factor $\frac{1}{f_0}$ in the thermal advection term. This inclusion

is necessary as $\frac{\Phi}{f_0}$ has the proper units (m^2s^{-1}), i.e. that of a streamfunction. The term in fact could be written as $-\nabla^2 \left[\mathbf{v}_g \cdot \nabla \left(\frac{\partial \psi_g}{\partial p} \right) \right]$, where $\psi_g = \frac{\Phi}{f_0}$ is the geostrophic streamfunction.

3.1.2 \mathbf{Q} vector form of the omega equation

Similar to the quasi-geostrophic omega equation, the forcing of the omega equation derived here may also be written in the form of a vector, \mathbf{Q} . Using the slowly-varying μ approximation, the first two terms on the right-hand side of (3.1) can be written as:

$$2\Omega\mu \left\{ \frac{\partial}{\partial p} [\mathbf{v}_\psi \cdot \nabla (\zeta + 2\Omega\mu)] - \nabla^2 \left[\mathbf{v}_\psi \cdot \nabla \left(\frac{\partial \psi}{\partial p} \right) \right] \right\}.$$

Since \mathbf{v}_ψ is nondivergent, the advection by \mathbf{v}_ψ of the absolute vorticity is equal to the divergence of the vorticity flux, that is, $\mathbf{v}_\psi \cdot \nabla (\zeta + 2\Omega\mu) = \nabla \cdot [\mathbf{v}_\psi (\zeta + 2\Omega\mu)]$. Making this substitution and reversing the vertical derivative and the inner product and gradient operations, the forcing term becomes

$$2\Omega\mu \nabla \cdot \left\{ \frac{\partial}{\partial p} [\mathbf{v}_\psi (\zeta + 2\Omega\mu)] - \nabla \left[\mathbf{v}_\psi \cdot \frac{\partial}{\partial p} (\nabla \psi) \right] \right\}.$$

The term inside the second set of brackets can be rewritten as $\mathbf{v}_\psi \cdot \frac{\partial}{\partial p} (\nabla \psi) = \frac{\partial}{\partial p} (\mathbf{v}_\psi \cdot \nabla \psi) - \frac{\partial \mathbf{v}_\psi}{\partial p} \cdot \nabla \psi$. Because $\mathbf{v}_\psi = \mathbf{k} \times \nabla \psi$ is perpendicular to $\nabla \psi$, $\mathbf{v}_\psi \cdot \nabla \psi = 0$, from which it follows that $\mathbf{v}_\psi \cdot \frac{\partial}{\partial p} (\nabla \psi) = -\frac{\partial \mathbf{v}_\psi}{\partial p} \cdot \nabla \psi$. The forcing term for the omega equation can then be written as:

$$2\Omega\mu \nabla \cdot \left\{ \frac{\partial}{\partial p} [\mathbf{v}_\psi (\zeta + 2\Omega\mu)] + \nabla \left(\frac{\partial \mathbf{v}_\psi}{\partial p} \cdot \nabla \psi \right) \right\}.$$

Using the identity $\nabla (\mathbf{A} \cdot \mathbf{B}) = (\mathbf{A} \cdot \nabla) \mathbf{B} + (\mathbf{B} \cdot \nabla) \mathbf{A} + \mathbf{A} \times (\nabla \times \mathbf{B}) + \mathbf{B} \times (\nabla \times \mathbf{A})$ on the second term and noting that $\nabla \psi \times \left(\nabla \times \frac{\partial \mathbf{v}_\psi}{\partial p} \right) = \nabla \psi \times \frac{\partial \zeta}{\partial p} \mathbf{k} = -\frac{\partial \zeta}{\partial p} \mathbf{v}_\psi$ gives

$$2\Omega\mu \nabla \cdot \left\{ \frac{\partial}{\partial p} [\mathbf{v}_\psi (\zeta + 2\Omega\mu)] + \left(\frac{\partial \mathbf{v}_\psi}{\partial p} \cdot \nabla \right) \nabla \psi + (\nabla \psi \cdot \nabla) \frac{\partial \mathbf{v}_\psi}{\partial p} - \frac{\partial \zeta}{\partial p} \mathbf{v}_\psi \right\}.$$

Expanding the first term and adding $\left(\frac{\partial \mathbf{v}_\psi}{\partial p} \cdot \nabla \right) \nabla \psi - \left(\frac{\partial \mathbf{v}_\psi}{\partial p} \cdot \nabla \right) \nabla \psi = 0$ gives

$$2\Omega\mu \nabla \cdot \left[2 \left(\frac{\partial \mathbf{v}_\psi}{\partial p} \cdot \nabla \right) \nabla \psi + (2\Omega\mu) \frac{\partial \mathbf{v}_\psi}{\partial p} + \zeta \frac{\partial \mathbf{v}_\psi}{\partial p} + (\nabla \psi \cdot \nabla) \frac{\partial \mathbf{v}_\psi}{\partial p} - \left(\frac{\partial \mathbf{v}_\psi}{\partial p} \cdot \nabla \right) \nabla \psi \right].$$

Using the identity $\nabla \times (\mathbf{A} \times \mathbf{B}) = \mathbf{A} \nabla \cdot \mathbf{B} - \mathbf{B} \nabla \cdot \mathbf{A} + (\mathbf{B} \cdot \nabla) \mathbf{A} - (\mathbf{A} \cdot \nabla) \mathbf{B}$, the last three terms can be combined to give $\nabla \times \left(\frac{\partial \mathbf{v}_\psi}{\partial p} \times \nabla \psi \right)$. Using this in the forcing term gives

$$2\Omega\mu \nabla \cdot \left[2 \left(\frac{\partial \mathbf{v}_\psi}{\partial p} \cdot \nabla \right) \nabla \psi + 2\Omega\mu \frac{\partial \mathbf{v}_\psi}{\partial p} + \nabla \times \left(\frac{\partial \mathbf{v}_\psi}{\partial p} \times \nabla \psi \right) \right].$$

The last term, $\nabla \cdot \left[\nabla \times \left(\frac{\partial \mathbf{v}_\psi}{\partial p} \times \nabla \psi \right) \right] = 0$ because it is the divergence of a curl. Using this result, the forcing takes the form

$$2\Omega\mu\nabla \cdot \left[2 \left(\frac{\partial \mathbf{v}_\psi}{\partial p} \cdot \nabla \right) \nabla \psi + 2\Omega\mu \frac{\partial \mathbf{v}_\psi}{\partial p} \right],$$

or

$$2\Omega\mu\nabla \cdot \left[2 \left(\frac{\partial \mathbf{v}_\psi}{\partial p} \cdot \nabla \right) \nabla \psi \right] + 2\Omega\mu\nabla \cdot \left(2\Omega\mu \frac{\partial \mathbf{v}_\psi}{\partial p} \right).$$

Up to this point, the derivation has been independent of any coordinate system. To continue the derivation, however, it is necessary to begin using spherical coordinates. Therefore, expanding $\nabla \psi$ in spherical coordinates and using the assumption of a slowly-varying μ , the first term of the above equation may be written as

$$2\nabla \cdot \left[\left(2\Omega\mu \frac{\partial \mathbf{v}_\psi}{\partial p} \cdot \nabla \right) (v_\psi \mathbf{i} - u_\psi \mathbf{j}) \right].$$

If the product $\frac{\partial \mathbf{v}_\psi}{\partial p} \cdot \nabla$ is expanded and operates on $v_\psi \mathbf{i} - u_\psi \mathbf{j}$, the result is

$$\begin{aligned} \mathbf{Q} = (Q_1, Q_2, Q_3) = & 2\Omega\mu \left[\left(\frac{\partial u_\psi}{\partial p} \right) \left(\frac{\partial v_\psi}{a \cos \phi \partial \lambda} + \frac{u_\psi \tan \phi}{a} \right) + \left(\frac{\partial v_\psi}{\partial p} \right) \left(\frac{\partial v_\psi}{a \partial \phi} \right) \right] \mathbf{i} \\ & + 2\Omega\mu \left[\left(\frac{\partial u_\psi}{\partial p} \right) \left(-\frac{\partial u_\psi}{a \cos \phi \partial \lambda} + \frac{v_\psi \tan \phi}{a} \right) - \left(\frac{\partial v_\psi}{\partial p} \right) \left(\frac{\partial u_\psi}{a \partial \phi} \right) \right] \mathbf{j} \\ & + 2\Omega\mu \left[-\left(\frac{\partial u_\psi}{\partial p} \right) \left(\frac{v_\psi}{a} \right) + \left(\frac{\partial v_\psi}{\partial p} \right) \left(\frac{u_\psi}{a} \right) \right] \mathbf{k}. \end{aligned} \quad (3.3)$$

Here the variation with latitude and longitude of the unit vectors \mathbf{i} and \mathbf{j} has been taken into account, that is, $\frac{\partial \mathbf{i}}{a \cos \phi \partial \lambda} = \frac{\tan \phi}{a} \mathbf{j} - \frac{1}{a} \mathbf{k}$, $\frac{\partial \mathbf{i}}{a \partial \phi} = 0$, $\frac{\partial \mathbf{j}}{a \cos \phi \partial \lambda} = -\frac{\tan \phi}{a} \mathbf{i}$, $\frac{\partial \mathbf{j}}{a \partial \phi} = -\frac{1}{a} \mathbf{k}$ (Holton, 1992). In addition, because ∇ has been defined to be a horizontal operator, equation (3.3) implies that the component of \mathbf{Q} in the \mathbf{k} direction may be neglected.

\mathbf{Q} may be written in terms of variables at a single level by eliminating the terms involving vertical derivatives through the use of the components of the thermal wind equation $2\Omega\mu \frac{\partial u_\psi}{\partial p} = \frac{\partial \alpha}{a \partial \phi}$ and $2\Omega\mu \frac{\partial v_\psi}{\partial p} = -\frac{\partial \alpha}{a \cos \phi \partial \lambda}$. Using these relations in (3.3) gives

$$Q_1 = \left(\frac{\partial \alpha}{a \partial \phi} \right) \left(\frac{\partial v_\psi}{a \cos \phi \partial \lambda} + \frac{u_\psi \tan \phi}{a} \right) - \left(\frac{\partial \alpha}{a \cos \phi \partial \lambda} \right) \left(\frac{\partial v_\psi}{a \partial \phi} \right) \quad (3.4)$$

and

$$Q_2 = \left(\frac{\partial \alpha}{a \partial \phi} \right) \left(-\frac{\partial u_\psi}{a \cos \phi \partial \lambda} + \frac{v_\psi \tan \phi}{a} \right) + \left(\frac{\partial \alpha}{a \cos \phi \partial \lambda} \right) \left(\frac{\partial u_\psi}{a \partial \phi} \right). \quad (3.5)$$

Q_1 and Q_2 may now be computed using variables at only one level. The terms $\frac{u_\psi \tan \phi}{a}$ and $\frac{v_\psi \tan \phi}{a}$, however, present a difficulty as $\tan \phi$ is unbounded at the poles. To avoid singularities at the poles, the definition of vorticity and divergence will be used to eliminate these terms in the definitions of Q_1 and Q_2 , respectively.

The equation for the vertical component of the relative vorticity may be written as

$$\zeta = \frac{\partial v_\psi}{a \cos \phi \partial \lambda} - \frac{\partial (u_\psi \cos \phi)}{a \cos \phi \partial \phi} = \frac{\partial v_\psi}{a \cos \phi \partial \lambda} - \frac{\partial u_\psi}{a \partial \phi} + \frac{u_\psi \tan \phi}{a}.$$

Using this result in (3.4) gives

$$Q_1 = \left(\frac{\partial \alpha}{a \partial \phi} \right) \left(\frac{\partial u_\psi}{a \partial \phi} + \zeta \right) - \left(\frac{\partial \alpha}{a \cos \phi \partial \lambda} \right) \left(\frac{\partial v_\psi}{a \partial \phi} \right). \quad (3.6)$$

The two-dimensional divergence of \mathbf{v}_ψ is

$$\delta = \frac{\partial u}{a \cos \phi \partial \lambda} + \frac{\partial (v \cos \phi)}{a \cos \phi \partial \phi} = 0.$$

Expanding the second term, the above equation becomes

$$0 = \frac{\partial u_\psi}{a \cos \phi \partial \lambda} + \frac{\partial v_\psi}{a \partial \phi} - \frac{v_\psi \tan \phi}{a}.$$

Using this result in (3.5) gives

$$Q_2 = \left(\frac{\partial \alpha}{a \partial \phi} \right) \left(\frac{\partial v_\psi}{a \partial \phi} \right) + \left(\frac{\partial \alpha}{a \cos \phi \partial \lambda} \right) \left(\frac{\partial u_\psi}{a \partial \phi} \right). \quad (3.7)$$

The \mathbf{Q} form of the omega equation can now be written as

$$\frac{R\bar{\Gamma}}{p^2} \nabla^2 \omega + 4\Omega^2 \mu^2 \frac{\partial^2 \omega}{\partial p^2} = -2\nabla \cdot \mathbf{Q} + 2\Omega\mu \nabla \cdot \left(2\Omega\mu \frac{\partial \mathbf{v}_\psi}{\partial p} \right).$$

Note that the \mathbf{Q} forcing has been written as a convergence rather than a divergence. The forcing expressed in this way is consistent with what is found in the literature, and requires multiplying (3.6) and (3.7) by -1 . Also, the second term is typically of the same order of magnitude as $-2\nabla \cdot \mathbf{Q}$, and so will be retained (Blackburn, 1985). This term may also be written in terms of variables on a single level through the use of the thermal wind equation (2.24):

$$2\Omega\mu \nabla \cdot \left(2\Omega\mu \frac{\partial \mathbf{v}_\psi}{\partial p} \right) = 2\Omega\mu \nabla \cdot (-\mathbf{k} \times \nabla \alpha).$$

Returning friction to the forcing, the \mathbf{Q} form of the omega equation can then be written as

$$\frac{R\bar{T}}{p^2}\nabla^2\omega + 4\Omega^2\mu^2\frac{\partial^2\omega}{\partial p^2} = -2\nabla \cdot \mathbf{Q} - 2\Omega\mu\nabla \cdot (\mathbf{k} \times \nabla\alpha) - \frac{\partial}{\partial p}(2\Omega\mu\mathbf{k} \cdot \nabla \times \mathbf{F}). \quad (3.8)$$

3.1.3 Boundary Conditions on the Omega Equation

In order to solve a partial differential equation, the boundary conditions must be stated. To solve the omega equation (3.1) or (3.8), the atmosphere is considered to be bounded by two isobaric surfaces, $p = p_B$ and $p = p_T$. It is assumed that parcels do not cross the upper boundary, so that $\omega = 0$ at $p = p_T$. At the lower boundary it is assumed that parcels do not cross physical height surfaces, that is, $\frac{D_3z}{Dt} = 0$ at $p = p_B$. In practice, the condition on the lower boundary will be written in terms of the geopotential $\Phi = gz$, so that $g\frac{D_3z}{Dt} = \frac{D_3\Phi}{Dt} = 0$, where g is the acceleration due to gravity, which is assumed to be constant. Writing the geopotential in terms of the balance condition (2.17), as well as expanding the material derivative gives

$$\omega\frac{d\bar{\Phi}}{dp} + \frac{\partial(2\Omega\mu\psi)}{\partial t} + \mathbf{v}_\psi \cdot \nabla(2\Omega\mu\psi) = 0 \quad \text{at } p = p_B$$

where the horizontal advection of $\bar{\Phi}$ is zero because $\bar{\Phi} = \bar{\Phi}(p)$, the horizontal advection of $2\Omega\mu\psi$ is accomplished by \mathbf{v}_ψ only, and the vertical advection of $2\Omega\mu\psi$ has been neglected. These approximations are consistent with the approximations used to develop the balance theory on the sphere. Using the approximation of slowly-varying μ , the third term of the above equation can be rewritten as $\mathbf{v}_\psi \cdot 2\Omega\mu\nabla\psi$. Because $\mathbf{v}_\psi = \mathbf{k} \times \nabla\psi$ is perpendicular to $\nabla\psi$, $\mathbf{v}_\psi \cdot 2\Omega\mu\nabla\psi = 0$. The lower boundary condition becomes

$$\omega\frac{d\bar{\Phi}}{dp} + \frac{\partial(2\Omega\mu\psi)}{\partial t} = 0. \quad (3.9)$$

In order to apply the lower boundary condition, it will be convenient to rewrite it using the balanced vorticity equation (2.18). This equation applies at all levels, including the lower boundary, and can be written as

$$\frac{\partial\zeta}{\partial t} + \mathbf{v}_\psi \cdot \nabla(\zeta + 2\Omega\mu) - 2\Omega\mu\frac{\partial\omega}{\partial p} - \mathbf{k} \cdot \nabla \times \mathbf{F} = 0. \quad (3.10)$$

Multiplying (3.10) by $-2\Omega\mu$, adding it to ∇^2 of (3.9) and recognizing that $\frac{d\bar{\Phi}}{dp} = -\frac{R\bar{T}}{p}$, the lower boundary condition can be written as

$$4\Omega^2\mu^2\frac{\partial\omega}{\partial p} - \frac{R\bar{T}}{p}\nabla^2\omega = 2\Omega\mu\mathbf{v}_\psi \cdot \nabla(\zeta + 2\Omega\mu) - 2\Omega\mu\mathbf{k} \cdot \nabla \times \mathbf{F},$$

or by noting that \mathbf{v}_ψ is nondivergent,

$$4\Omega^2\mu^2\frac{\partial\omega}{\partial p} - \frac{R\bar{T}}{p}\nabla^2\omega = 2\Omega\mu\nabla \cdot [\mathbf{v}_\psi(\zeta + 2\Omega\mu)] - 2\Omega\mu\mathbf{k} \cdot \nabla \times \mathbf{F}.$$

The omega equation and its boundary conditions have now been defined and are repeated here.

Omega equation and its boundary conditions

$$\begin{aligned} \frac{R\bar{T}}{p^2}\nabla^2\omega + 4\Omega^2\mu^2\frac{\partial^2\omega}{\partial p^2} &= \frac{\partial}{\partial p} [2\Omega\mu\mathbf{v}_\psi \cdot \nabla(\zeta + 2\Omega\mu)] \\ &\quad - \nabla^2 \left[2\Omega\mu\mathbf{v}_\psi \cdot \nabla \left(\frac{\partial\psi}{\partial p} \right) \right] - \frac{\partial}{\partial p} (2\Omega\mu\mathbf{k} \cdot \nabla \times \mathbf{F}) \end{aligned}$$

or

$$\frac{R\bar{T}}{p^2}\nabla^2\omega + 4\Omega^2\mu^2\frac{\partial^2\omega}{\partial p^2} = -2\nabla \cdot \mathbf{Q} - 2\Omega\mu\nabla \cdot (\mathbf{k} \times \nabla\alpha) - \frac{\partial}{\partial p} (2\Omega\mu\mathbf{k} \cdot \nabla \times \mathbf{F}) \quad (3.11)$$

$$\omega = 0 \quad \text{at} \quad p = p_T \quad (3.12a)$$

$$4\Omega^2\mu^2\frac{\partial\omega}{\partial p} - \frac{R\bar{T}}{p}\nabla^2\omega = 2\Omega\mu\nabla \cdot [\mathbf{v}_\psi(\zeta + 2\Omega\mu)] - 2\Omega\mu\mathbf{k} \cdot \nabla \times \mathbf{F} \quad \text{at} \quad p = p_B \quad (3.12b)$$

3.2 Solution of the Omega Equation

Equation (3.11) with boundary conditions (3.12a)–(3.12b) will be solved using transform techniques — a normal mode transform in the vertical and a spherical harmonic transform in the horizontal. As this equation will be solved on the sphere, only vertical boundary conditions are needed, as there are no lateral boundaries.

3.2.1 Vertical Normal Mode Transform

A vertical normal mode transform is used to separate the vertical structure of the atmosphere from the horizontal structure. The procedure used here follows that developed by Fulton and Schubert (1985), although they performed the transform on equations involving u , v , and Φ . The forward and inverse transforms

on ω are, respectively,

$$\omega_\ell(\lambda, \mu) = \int_{p_T}^{p_B} \omega(\lambda, \mu, p) \frac{dV_\ell(p)}{dp} dp + \left[\omega \frac{p\bar{\Gamma}}{\bar{\Gamma}} \frac{dV_\ell(p)}{dp} \right]_{p_B}, \quad (3.13a)$$

and

$$\omega(\lambda, \mu, p) = \sum_{\ell=0}^{\infty} \omega_\ell(\lambda, \mu) \frac{c_\ell^2 p^2}{R\bar{\Gamma}(p_B - p_T)} \frac{dV_\ell(p)}{dp}. \quad (3.13b)$$

These two equations are derived in the Appendix. The vertical structure function $V_\ell(p)$ is determined by solving the Sturm-Liouville equation

$$\frac{d}{dp} \left(\frac{p^2}{R\bar{\Gamma}} \frac{dV_\ell}{dp} \right) + \frac{V_\ell}{c_\ell^2} = 0, \quad (3.14)$$

with boundary conditions

$$\frac{dV_\ell}{dp} = 0 \quad \text{at} \quad p = p_T \quad (3.15a)$$

and

$$p \frac{dV_\ell}{dp} + \frac{\bar{\Gamma}}{T} V_\ell = 0 \quad \text{at} \quad p = p_B, \quad (3.15b)$$

where c_ℓ^{-2} is the eigenvalue. The vertical structure functions obey the orthonormality condition

$$\frac{1}{p_B - p_T} \int_{p_T}^{p_B} V_\ell V_{\ell'} dp = \begin{cases} 1 & \ell' = \ell \\ 0 & \ell' \neq \ell. \end{cases}$$

The kernel of the vertical normal mode transform for ω , however, is $\frac{dV_\ell}{dp}$, which obeys the orthonormality condition:

$$\frac{c_\ell^2}{p_B - p_T} \left[\int_{p_T}^{p_B} \frac{dV_\ell}{dp} \frac{dV_{\ell'}}{dp} \frac{p^2}{R\bar{\Gamma}} dp + \left(\frac{p^3 \bar{\Gamma}}{R\bar{\Gamma}^2} \frac{dV_\ell}{dp} \frac{dV_{\ell'}}{dp} \right)_{p_B} \right] = \begin{cases} 1 & \ell' = \ell \\ 0 & \ell' \neq \ell. \end{cases} \quad (3.16)$$

The vertical transform of the omega equation begins by multiplying (3.11) by $\frac{p^2}{R\bar{\Gamma}} \frac{dV_\ell}{dp}$ and integrating from p_T to p_B :

$$\int_{p_T}^{p_B} \nabla^2 \omega \frac{dV_\ell}{dp} dp + 4\Omega^2 \mu^2 \int_{p_T}^{p_B} \frac{\partial^2 \omega}{\partial p^2} \frac{p^2}{R\bar{\Gamma}} \frac{dV_\ell}{dp} dp = \int_{p_T}^{p_B} \frac{p^2}{R\bar{\Gamma}} \frac{dV_\ell}{dp} F dp, \quad (3.17)$$

where $F = F(\lambda, \mu, p)$ is one of the forms of the forcing (rhs) of (3.11). Evaluate each term on the left-hand side, beginning with the first term

$$\int_{p_T}^{p_B} \nabla^2 \omega \frac{dV_\ell}{dp} dp.$$

If $\nabla^2 \left(\omega \frac{p\bar{T}}{\Gamma} \frac{dV_\ell}{dp} \right)_{p_B} - \nabla^2 \left(\omega \frac{p\bar{T}}{\Gamma} \frac{dV_\ell}{dp} \right)_{p_B} = 0$ is added, the result is

$$\nabla^2 \left[\int_{p_T}^{p_B} \omega \frac{dV_\ell}{dp} dp + \left(\omega \frac{p\bar{T}}{\Gamma} \frac{dV_\ell}{dp} \right)_{p_B} \right] - \nabla^2 \left(\omega \frac{p\bar{T}}{\Gamma} \frac{dV_\ell}{dp} \right)_{p_B}.$$

Use (3.13a) and the fact that in the second term only ω is dependent on λ and ϕ to get

$$\nabla^2 \omega_\ell - \left(\frac{dV_\ell}{dp} \frac{p\bar{T}}{\Gamma} \nabla^2 \omega \right)_{p_B}. \quad (3.18)$$

Using integration by parts, the second term on the left-hand side of (3.17) becomes

$$4\Omega^2 \mu^2 \left[\int_{p_T}^{p_B} \frac{\partial}{\partial p} \left(\frac{\partial \omega}{\partial p} \frac{p^2}{R\bar{\Gamma}} \frac{dV_\ell}{dp} \right) dp - \int_{p_T}^{p_B} \frac{\partial \omega}{\partial p} \frac{d}{dp} \left(\frac{p^2}{R\bar{\Gamma}} \frac{dV_\ell}{dp} \right) dp \right].$$

Evaluating the first integral and using (3.14) on the second gives

$$4\Omega^2 \mu^2 \left(\left[\frac{\partial \omega}{\partial p} \frac{p^2}{R\bar{\Gamma}} \frac{dV_\ell}{dp} \right]_{p_T}^{p_B} + \int_{p_T}^{p_B} \frac{\partial \omega}{\partial p} \frac{V_\ell}{c_\ell^2} dp \right).$$

Using the boundary condition (3.15a) on the first term and integrating by parts on the second term gives

$$\begin{aligned} & 4\Omega^2 \mu^2 \left[\left(\frac{\partial \omega}{\partial p} \frac{p^2}{R\bar{\Gamma}} \frac{dV_\ell}{dp} \right)_{p_B} + \int_{p_T}^{p_B} \frac{\partial}{\partial p} \left(\omega \frac{V_\ell}{c_\ell^2} \right) dp - \int_{p_T}^{p_B} \omega \frac{d}{dp} \left(\frac{V_\ell}{c_\ell^2} \right) dp \right] \\ &= 4\Omega^2 \mu^2 \left[\left(\frac{\partial \omega}{\partial p} \frac{p^2}{R\bar{\Gamma}} \frac{dV_\ell}{dp} \right)_{p_B} + \left(\omega \frac{V_\ell}{c_\ell^2} \right)_{p_T}^{p_B} - \int_{p_T}^{p_B} \omega \frac{1}{c_\ell^2} \frac{dV_\ell}{dp} dp \right]. \end{aligned}$$

Using the boundary conditions (3.12a) and (3.15b) gives

$$\begin{aligned} & 4\Omega^2 \mu^2 \left[\left(\frac{\partial \omega}{\partial p} \frac{p^2}{R\bar{\Gamma}} \frac{dV_\ell}{dp} \right)_{p_B} - \left(\omega \frac{p\bar{T}}{\Gamma} \frac{1}{c_\ell^2} \frac{dV_\ell}{dp} \right)_{p_B} - \frac{1}{c_\ell^2} \int_{p_T}^{p_B} \omega \frac{dV_\ell}{dp} dp \right] \\ &= 4\Omega^2 \mu^2 \left\{ \left(\frac{\partial \omega}{\partial p} \frac{p^2}{R\bar{\Gamma}} \frac{dV_\ell}{dp} \right)_{p_B} - \frac{1}{c_\ell^2} \left[\int_{p_T}^{p_B} \omega \frac{dV_\ell}{dp} dp + \left(\omega \frac{p\bar{T}}{\Gamma} \frac{dV_\ell}{dp} \right)_{p_B} \right] \right\}. \end{aligned}$$

Finally, use (3.13a) to get

$$4\Omega^2 \mu^2 \left(\frac{\partial \omega}{\partial p} \frac{p^2}{R\bar{\Gamma}} \frac{dV_\ell}{dp} \right)_{p_B} - 4\Omega^2 \mu^2 \frac{\omega_\ell}{c_\ell^2}. \quad (3.19)$$

Combining (3.18) and (3.19) with the right-hand side of (3.17) gives

$$\begin{aligned} \nabla^2 \omega_\ell - 4\Omega^2 \mu^2 \frac{\omega_\ell}{c_\ell^2} + 4\Omega^2 \mu^2 \left(\frac{\partial \omega}{\partial p} \frac{p^2}{R\bar{\Gamma}} \frac{dV_\ell}{dp} \right)_{p_B} - \left(\frac{dV_\ell}{dp} \frac{p\bar{\Gamma}}{\bar{\Gamma}} \nabla^2 \omega \right)_{p_B} \\ = \int_{p_T}^{p_B} \frac{p^2}{R\bar{\Gamma}} \frac{dV_\ell}{dp} F dp. \end{aligned}$$

Factoring out $\frac{p^2}{R\bar{\Gamma}} \frac{dV_\ell}{dp}$ from the terms evaluated at the lower boundary gives

$$\begin{aligned} \nabla^2 \omega_\ell - 4\Omega^2 \mu^2 \frac{\omega_\ell}{c_\ell^2} + \left[\frac{p^2}{R\bar{\Gamma}} \frac{dV_\ell}{dp} \left(4\Omega^2 \mu^2 \frac{\partial \omega}{\partial p} - \frac{R\bar{\Gamma}}{p} \nabla^2 \omega \right) \right]_{p_B} \\ = \int_{p_T}^{p_B} \frac{p^2}{R\bar{\Gamma}} \frac{dV_\ell}{dp} F dp. \end{aligned}$$

Using the lower boundary condition $4\Omega^2 \mu^2 \frac{\partial \omega}{\partial p} - \frac{R\bar{\Gamma}}{p} \nabla^2 \omega = G(\lambda, \mu, p)$ at $p = p_B$ (3.12b) and rearranging gives

$$\nabla^2 \omega_\ell - \frac{4\Omega^2 \mu^2}{c_\ell^2} \omega_\ell = \int_{p_T}^{p_B} \frac{p^2}{R\bar{\Gamma}} \frac{dV_\ell}{dp} F dp - \left(\frac{p^2}{R\bar{\Gamma}} \frac{dV_\ell}{dp} G \right)_{p_B}.$$

If the Laplacian operator is expanded in terms of λ and μ and the right-hand side is multiplied by $1 =$

$\left(\frac{p_B - p_T}{c_\ell} \right)^2 \left(\frac{c_\ell}{p_B - p_T} \right)^2$ the result is

$$\frac{\partial^2 \omega_\ell}{(1 - \mu^2) \partial \lambda^2} + \frac{\partial}{\partial \mu} \left[(1 - \mu^2) \frac{\partial \omega_\ell}{\partial \mu} \right] - \epsilon_\ell \mu^2 \omega_\ell = \left[\frac{a(p_B - p_T)}{c_\ell} \right]^2 F_\ell(\lambda, \mu), \quad (3.20)$$

where $\epsilon_\ell = 4\Omega^2 a^2 / c_\ell^2$ is Lamb's parameter and

$$F_\ell(\lambda, \mu) = \left(\frac{c_\ell}{p_B - p_T} \right)^2 \left[\int_{p_T}^{p_B} \frac{p^2}{R\bar{\Gamma}} \frac{dV_\ell}{dp} F dp - \left(\frac{p^2}{R\bar{\Gamma}} \frac{dV_\ell}{dp} G \right)_{p_B} \right].$$

In the next section, the spherical harmonic transform will be used to convert the partial differential equation (3.20) into an algebraic system.

3.2.2 Spherical Harmonic Transform

The spherical harmonic transform consists of a Fourier transform in λ and an associated Legendre transform in μ . Because of the variety in notations and normalizations used in the literature in conjunction with spherical harmonics, before proceeding with the derivation of the omega equation, the notations and normalizations used in this paper will be presented. The spherical harmonic transform pair will be given by

$$\omega_{\ell mn} = \int_{-1}^1 \int_0^{2\pi} \omega_\ell(\lambda, \mu) [Y_n^m(\lambda, \mu)]^* d\lambda d\mu$$

and

$$\omega_\ell(\lambda, \mu) = \sum_{m=-\infty}^{\infty} \sum_{n=|m|}^{\infty} \omega_{\ell mn} Y_n^m(\lambda, \mu),$$

where * denotes complex conjugation. The spherical harmonics, $Y_n^m(\lambda, \mu)$, are given by

$$Y_n^m(\lambda, \mu) = \sqrt{\frac{2n+1}{4\pi} \frac{(n-m)!}{(n+m)!}} P_n^m(\mu) \Phi_m(\lambda),$$

where $\Phi_m(\lambda) = e^{im\lambda}$ is the Fourier component, and $P_n^m(\mu) = (1-\mu^2)^{\frac{m}{2}} \frac{d^m}{d\mu^m} \left\{ \frac{1}{2^n n!} \frac{d^n}{d\mu^n} [(\mu^2-1)^n] \right\}$ are the associated Legendre functions, with the term in the braces the Legendre polynomials. The value m is the zonal wavenumber and the value n is obtained by adding to m the number of meridional nodal lines, thus $-\infty < m < \infty$ and $n \geq |m|$. The term $\sqrt{\frac{2n+1}{4\pi} \frac{(n-m)!}{(n+m)!}}$ is a normalization factor and can be divided between the Fourier and associated Legendre components such that

$$\bar{\Phi}_m(\lambda) = \frac{1}{\sqrt{2\pi}} \Phi_m(\lambda) \quad (3.21a)$$

and

$$\bar{P}_n^m(\mu) = \sqrt{\frac{2n+1}{2} \frac{(n-m)!}{(n+m)!}} P_n^m(\mu). \quad (3.21b)$$

This normalization for the associated Legendre functions is used by Belousov (1962) and also in SPHEREPACK (Adams and Swarztrauber, 1999), the software package which is used in the numerical computations. With these definitions, the following normalizations hold:

$$\begin{aligned} \int_{-1}^1 \int_0^{2\pi} [Y_n^m(\lambda, \mu)] [Y_{n'}^{m'}(\lambda, \mu)]^* d\lambda d\mu &= \delta_{mm'} \delta_{nn'} \\ \int_0^{2\pi} [\bar{\Phi}_m(\lambda)] [\bar{\Phi}_{m'}(\lambda)]^* d\lambda &= \delta_{mm'} \\ \int_{-1}^1 \bar{P}_n^m(\mu) \bar{P}_{n'}^m(\mu) d\mu &= \delta_{nn'}. \end{aligned}$$

Using these normalizations, the Fourier transform pair and the associated Legendre transform pair are respectively given by

$$\omega_{\ell m}(\mu) = \int_0^{2\pi} \omega_\ell(\lambda, \mu) [\bar{\Phi}_m(\lambda)]^* d\lambda \quad (3.22a)$$

$$\omega_\ell(\lambda, \mu) = \sum_{m=-\infty}^{\infty} \omega_{\ell m}(\mu) \bar{\Phi}_m(\lambda) \quad (3.22b)$$

and

$$\omega_{\ell mn} = \int_{-1}^1 \omega_{\ell m}(\mu) \bar{P}_n^m(\mu) d\mu \quad (3.23a)$$

$$\omega_{\ell m}(\mu) = \sum_{n=|m|}^{\infty} \omega_{\ell mn} \bar{P}_n^m(\mu). \quad (3.23b)$$

Because $\omega_{\ell}(\lambda, \mu)$ is real valued, the spherical harmonic coefficients for $m < 0$ are the complex conjugates of the spherical harmonic coefficients for $m > 0$. Thus it is necessary to only consider the Fourier and associated Legendre transformations for $m \geq 0$. SPHEREPACK also assumes that the variable being transformed is real valued, so only considering the case $m \geq 0$ for the theoretical development transfers well to the numerical computations.

With the notation and normalizations defined, the derivation of the omega equation continues with the application of the forward Fourier transform (3.22a) to (3.20). The result is

$$\frac{d}{d\mu} \left[(1 - \mu^2) \frac{d\omega_{\ell m}}{d\mu} \right] - \left(\epsilon_{\ell} \mu^2 + \frac{m^2}{1 - \mu^2} \right) \omega_{\ell m} = \left[\frac{a(p_B - p_T)}{c_{\ell}} \right]^2 F_{\ell m}. \quad (3.24)$$

Applying the forward associated Legendre transform (3.23a) to the first term on the left-hand side of (3.24) gives

$$\begin{aligned} & \int_{-1}^1 \left\{ \frac{d}{d\mu} \left[(1 - \mu^2) \frac{d\omega_{\ell m}(\mu)}{d\mu} \right] \right\} \bar{P}_n^m(\mu) d\mu \\ &= \int_{-1}^1 \frac{d}{d\mu} \left[(1 - \mu^2) \frac{d\omega_{\ell m}(\mu)}{d\mu} \bar{P}_n^m(\mu) \right] d\mu - \int_{-1}^1 (1 - \mu^2) \frac{d\omega_{\ell m}(\mu)}{d\mu} \frac{d\bar{P}_n^m(\mu)}{d\mu} d\mu \\ &= \left[(1 - \mu^2) \frac{d\omega_{\ell m}(\mu)}{d\mu} \bar{P}_n^m(\mu) \right]_{-1}^1 - \int_{-1}^1 (1 - \mu^2) \frac{d\omega_{\ell m}(\mu)}{d\mu} \frac{d\bar{P}_n^m(\mu)}{d\mu} d\mu \\ &= - \int_{-1}^1 (1 - \mu^2) \frac{d\omega_{\ell m}(\mu)}{d\mu} \frac{d\bar{P}_n^m(\mu)}{d\mu} d\mu \\ &= - \int_{-1}^1 \frac{d}{d\mu} \left[\omega_{\ell m}(\mu) (1 - \mu^2) \frac{d\bar{P}_n^m(\mu)}{d\mu} \right] d\mu + \int_{-1}^1 \omega_{\ell m}(\mu) \frac{d}{d\mu} \left[(1 - \mu^2) \frac{d\bar{P}_n^m(\mu)}{d\mu} \right] d\mu \\ &= - \left[\omega_{\ell m}(\mu) (1 - \mu^2) \frac{d\bar{P}_n^m(\mu)}{d\mu} \right]_{-1}^1 + \int_{-1}^1 \omega_{\ell m}(\mu) \frac{d}{d\mu} \left[(1 - \mu^2) \frac{d\bar{P}_n^m(\mu)}{d\mu} \right] d\mu \\ &= \int_{-1}^1 \omega_{\ell m}(\mu) \frac{d}{d\mu} \left[(1 - \mu^2) \frac{d\bar{P}_n^m(\mu)}{d\mu} \right] d\mu. \end{aligned}$$

The normalized associated Legendre functions (as well as the associated Legendre functions) are solutions

in the interval $-1 \leq \mu \leq 1$ to the differential equation

$$\frac{d}{d\mu} \left[(1 - \mu^2) \frac{d\bar{P}_n^m(\mu)}{d\mu} \right] + \left[n(n+1) - \frac{m^2}{1 - \mu^2} \right] \bar{P}_n^m(\mu) = 0.$$

Using this result the derivation continues with

$$\begin{aligned} \int_{-1}^1 \omega_{\ell m}(\mu) \frac{d}{d\mu} \left[(1 - \mu^2) \frac{d\bar{P}_n^m(\mu)}{d\mu} \right] d\mu &= - \int_{-1}^1 \omega_{\ell m}(\mu) \left[n(n+1) - \frac{m^2}{1 - \mu^2} \right] \bar{P}_n^m(\mu) d\mu \\ &= -n(n+1) \int_{-1}^1 \omega_{\ell m}(\mu) \bar{P}_n^m(\mu) d\mu + \int_{-1}^1 \omega_{\ell m}(\mu) \frac{m^2}{1 - \mu^2} \bar{P}_n^m(\mu) d\mu. \end{aligned}$$

Applying (3.23a) to the first integral on the right-hand side gives

$$-n(n+1) \omega_{\ell mn} + \int_{-1}^1 \omega_{\ell m}(\mu) \frac{m^2}{1 - \mu^2} \bar{P}_n^m(\mu) d\mu. \quad (3.25)$$

The forward associated Legendre transform of the second term on the left-hand side of (3.24) is

$$-\epsilon_\ell \int_{-1}^1 \omega_{\ell m}(\mu) \mu^2 \bar{P}_n^m(\mu) d\mu - \int_{-1}^1 \omega_{\ell m}(\mu) \frac{m^2}{1 - \mu^2} \bar{P}_n^m(\mu) d\mu. \quad (3.26)$$

Finally, transforming the right-hand side of (3.24) gives

$$\left[\frac{a(p_B - p_T)}{c_\ell} \right]^2 F_{\ell mn}. \quad (3.27)$$

Combining (3.25), (3.26), and (3.27) gives the omega equation which has been transformed using vertical normal modes and spherical harmonics:

$$n(n+1) \omega_{\ell mn} + \epsilon_\ell \int_{-1}^1 \omega_{\ell m}(\mu) \mu^2 \bar{P}_n^m(\mu) d\mu = - \left[\frac{a(p_B - p_T)}{c_\ell} \right]^2 F_{\ell mn}. \quad (3.28)$$

To get the integral $\int_{-1}^1 \omega_{\ell m}(\mu) \mu^2 \bar{P}_n^m(\mu) d\mu$ into a more workable form, use the following recurrence relation for the normalized associated Legendre functions (Belousov, 1962):

$$\bar{P}_n^m(\mu) = 2a_n^m \mu \bar{P}_{n-1}^m(\mu) - b_n^m \bar{P}_{n-2}^m(\mu), \quad (3.29)$$

where

$$a_n^m = \sqrt{\frac{n^2 - \frac{1}{4}}{n^2 - m^2}}$$

and

$$b_n^m = \sqrt{\frac{(2n+1)(n-m-1)(n+m-1)}{(2n-3)(n^2-m^2)}}.$$

By substituting $n + 1$ for n , equation (3.29) can be written as

$$\mu \bar{P}_n^m(\mu) = \left(\frac{1}{2a_{n+1}^m} \right) \bar{P}_{n+1}^m(\mu) + \left(\frac{b_{n+1}^m}{2a_{n+1}^m} \right) \bar{P}_{n-1}^m(\mu). \quad (3.30)$$

Multiplying by μ gives

$$\mu^2 \bar{P}_n^m(\mu) = \left(\frac{1}{2a_{n+1}^m} \right) \mu \bar{P}_{n+1}^m(\mu) + \left(\frac{b_{n+1}^m}{2a_{n+1}^m} \right) \mu \bar{P}_{n-1}^m(\mu). \quad (3.31)$$

Using (3.30) with n first replaced by $n + 1$ and then with n replaced by $n - 1$, the factor of μ outside the normalized associated Legendre functions may be eliminated from the right-hand side of (3.31), giving

$$\begin{aligned} \mu^2 \bar{P}_n^m(\mu) &= \left(\frac{1}{2a_{n+1}^m} \right) \left[\frac{1}{2a_{n+2}^m} \bar{P}_{n+2}^m(\mu) + \frac{b_{n+2}^m}{2a_{n+2}^m} \bar{P}_n^m(\mu) \right] \\ &\quad + \left(\frac{b_{n+1}^m}{2a_{n+1}^m} \right) \left[\frac{1}{2a_n^m} \bar{P}_n^m(\mu) + \frac{b_n^m}{2a_n^m} \bar{P}_{n-2}^m(\mu) \right]. \end{aligned}$$

Combining the $\bar{P}_n^m(\mu)$ terms gives

$$\mu^2 \bar{P}_n^m(\mu) = \left(\frac{b_n^m b_{n+1}^m}{4a_n^m a_{n+1}^m} \right) \bar{P}_{n-2}^m(\mu) + \left(\frac{a_n^m b_{n+2}^m + a_{n+2}^m b_{n+1}^m}{4a_n^m a_{n+1}^m a_{n+2}^m} \right) \bar{P}_n^m(\mu) + \left(\frac{1}{4a_{n+1}^m a_{n+2}^m} \right) \bar{P}_{n+2}^m(\mu). \quad (3.32)$$

Mathematica, developed by Wolfram Research, can be used to simplify complicated coefficients such as those on the right-hand side of (3.32). It found that with the introduction of three new variables, A_{mn} , B_{mn} , and C_{mn} , the coefficients can be greatly simplified. Define:

$$\begin{aligned} A_{mn} &= n^2 - m^2 \\ B_{mn} &= 4n^2 - 1 \\ C_{mn} &= \left(\frac{A_{mn}}{B_{mn}} \right)^{\frac{1}{2}}. \end{aligned}$$

then

$$\frac{b_n^m b_{n+1}^m}{4a_n^m a_{n+1}^m} = C_{mn} C_{mn-1} = \alpha_{mn}.$$

$$\frac{a_n^m b_{n+2}^m + a_{n+2}^m b_{n+1}^m}{4a_n^m a_{n+1}^m a_{n+2}^m} = C_{mn+1}^2 + C_{mn}^2 = \beta_{mn},$$

and

$$\frac{1}{4a_{n+1}^m a_{n+2}^m} = C_{mn+2} C_{mn+1} = \gamma_{mn}.$$

Equation (3.32) can now be written as

$$\mu^2 \bar{P}_n^m(\mu) = \alpha_{mn} \bar{P}_{n-2}^m(\mu) + \beta_{mn} \bar{P}_n^m(\mu) + \gamma_{mn} \bar{P}_{n+2}^m(\mu),$$

which can be used in (3.28) to give

$$\begin{aligned} n(n+1)\omega_{\ell,m,n} + \epsilon_\ell \int_{-1}^1 \omega_{\ell,m}(\mu) [\alpha_{mn} \bar{P}_{n-2}^m(\mu) + \beta_{mn} \bar{P}_n^m(\mu) + \gamma_{mn} \bar{P}_{n+2}^m(\mu)] d\mu \\ = - \left[\frac{a(p_B - p_T)}{c_\ell} \right]^2 F_{\ell,m,n}. \end{aligned}$$

Applying (3.23a) to the integral results in

$$n(n+1)\omega_{\ell,m,n} + \epsilon_\ell \alpha_{mn} \omega_{\ell,m,n-2} + \epsilon_\ell \beta_{mn} \omega_{\ell,m,n} + \epsilon_\ell \gamma_{mn} \omega_{\ell,m,n+2} = - \left[\frac{a(p_B - p_T)}{c_\ell} \right]^2 F_{\ell,m,n}.$$

This equation can also be written as

$$A_{\ell,m,n} \omega_{\ell,m,n-2} + B_{\ell,m,n} \omega_{\ell,m,n} + C_{\ell,m,n} \omega_{\ell,m,n+2} = - \left[\frac{a(p_B - p_T)}{c_\ell} \right]^2 F_{\ell,m,n}, \quad (3.33)$$

where $A_{\ell,m,n} = \epsilon_\ell \alpha_{mn}$, $B_{\ell,m,n} = n(n+1) + \epsilon_\ell \beta_{mn}$, and $C_{\ell,m,n} = \epsilon_\ell \gamma_{mn}$.

According to (3.33), the spherical harmonic coefficients of the quasi-geostrophic omega for each vertical mode $\omega_{\ell,m,n}$ are related to the spherical harmonic coefficients of the corresponding vertical mode of the forcing $F_{\ell,m,n}$, and are also coupled to the spherical harmonic coefficients $\omega_{\ell,m,n+2}$ and $\omega_{\ell,m,n-2}$, resulting in a system of equations for each vertical mode ℓ and each zonal mode m . The indices m and n take on the respective values of $0 \leq m < \infty$ and $n \geq m$. For computational purposes, however, an upper limit to the spherical harmonic coefficients must be defined. Here triangular truncation at $n = N$ is used.

For a given vertical mode ℓ and zonal mode m , the system of equations for obtaining the spherical harmonic coefficients of the global omega equation is given by:

$$\begin{pmatrix} B_{\ell,m,m} & 0 & C_{\ell,m,m} & 0 & 0 & 0 & \cdots & 0 \\ 0 & B_{\ell,m,m+1} & 0 & C_{\ell,m,m+1} & 0 & 0 & \cdots & 0 \\ A_{\ell,m,m+2} & 0 & B_{\ell,m,m+2} & 0 & C_{\ell,m,m+2} & 0 & \cdots & 0 \\ \vdots & \vdots \\ 0 & \cdots & 0 & A_{\ell,m,N-2} & 0 & B_{\ell,m,N-2} & 0 & C_{\ell,m,N-2} \\ 0 & \cdots & 0 & 0 & A_{\ell,m,N-1} & 0 & B_{\ell,m,N-1} & 0 \\ 0 & \cdots & 0 & 0 & 0 & A_{\ell,m,N} & 0 & B_{\ell,m,N} \end{pmatrix} \begin{pmatrix} \omega_{\ell,m,m} \\ \omega_{\ell,m,m+1} \\ \omega_{\ell,m,m+2} \\ \vdots \\ \omega_{\ell,m,N-2} \\ \omega_{\ell,m,N-1} \\ \omega_{\ell,m,N} \end{pmatrix}$$

$$= - \left[\frac{a(p_B - p_T)}{c_\ell} \right]^2 \begin{pmatrix} F_{\ell,m,m} \\ F_{\ell,m,m+1} \\ F_{\ell,m,m+2} \\ \vdots \\ F_{\ell,m,N-2} \\ F_{\ell,m,N-1} \\ F_{\ell,m,N} \end{pmatrix}. \quad (3.34)$$

Note that the number of equations in the system depends on m . As m increases from 0 to N , the number of equations in the system decreases from $N + 1$ to 1.

The reconstruction of $\omega(\lambda, \mu, p)$ from the spherical harmonic coefficients $\omega_{\ell,m,n}$ is a three-step process. First, the inverse associated Legendre transform (3.23b) is used to compute $\omega_{\ell m}(\mu)$. Next, the inverse Fourier transform (3.22b) is used to get $\omega_\ell(\lambda, \mu)$. Finally, $\omega_\ell(\lambda, \mu)$ is summed over ℓ according to the inverse vertical normal mode transfer (3.13b) to achieve the solution $\omega(\lambda, \mu, p)$.

3.3 The Form of the Frictional Forcing

In the solution of the omega equation, frictional effects appear not only in the omega equation itself ($-\frac{\partial}{\partial p}(2\Omega\mu\mathbf{k} \cdot \nabla \times \mathbf{F})$), but also in the lower boundary condition ($-2\Omega\mu\mathbf{k} \cdot \nabla \times \mathbf{F}$). \mathbf{F} is given by the standard bulk formula (Haltiner, 1971) involving the vertical derivative of the wind stress:

$$\mathbf{F} = -g \frac{\partial \boldsymbol{\tau}(\lambda, \mu, p)}{\partial p}.$$

The wind stress itself is given by a surface wind stress multiplied by a function of pressure which describes the decay of the stress away from the surface:

$$\boldsymbol{\tau}(\lambda, \mu, p) = \boldsymbol{\tau}_s(\lambda, \mu) g(p).$$

The surface wind stress is given by the formula:

$$\boldsymbol{\tau}_s(\lambda, \mu) = \frac{C_D [U(\lambda, \mu)]}{\alpha(\lambda, \mu, p_0)} |\mathbf{v}_\psi(\lambda, \mu, p_0)| [u_\psi(\lambda, \mu, p_0) \mathbf{i} + v_\psi(\lambda, \mu, p_0) \mathbf{j}],$$

where $p_0=1000\text{hPa}$, α is the specific volume associated with the balanced flow, and $C_D [U (\lambda, \mu)]$ is the drag coefficient given by (Williams et al., 2012):

$$C_D [U (\lambda, \mu)] = \begin{cases} \frac{2.70}{U} + 0.142 + 0.0764U & \text{if } U \leq 25 \\ 2.16 + 0.5406 \left\{ 1 - \exp \left[\frac{-(U-25)}{7.5} \right] \right\} & \text{if } U \geq 25 \end{cases}$$

with

$$U (\lambda, \mu) = 0.78 \left\{ [\bar{u}_{\psi, PBL} (\lambda, \mu)]^2 + [\bar{v}_{\psi, PBL} (\lambda, \mu)]^2 \right\}^{\frac{1}{2}}.$$

The planetary boundary layer is assumed to be from 1000 hPa to 900 hPa.

The function $g(p)$ governs the decrease of the effect of surface friction with height through the boundary layer. Since the effects of friction are often discussed in terms of physical height and not pressure, $-\ln p$ will be used instead of p . The decay was chosen to be quadratic in $-\ln p$:

$$g(p) = a \left[\ln \left(\frac{p_0}{p} \right) \right]^2 + b \left[\ln \left(\frac{p_0}{p} \right) \right] + c.$$

This form is convenient because the coefficients a , b , and c can be uniquely determined by enforcing the following boundary conditions: $g(p) = 1$ at 1000 hPa, $g(p) = 0$ at 900 hPa, and $g'(p) = 0$ at 900 hPa. The last condition assures a smooth transition of $g(p)$ from the boundary layer to the free atmosphere, where friction is assumed to vanish. Using these boundary conditions, $a = 90.08$, $b = -18.98$, and $c = 1.00$. A plot of $g(p)$ is shown in (Fig. 3.1).

There is still another benefit from using the quadratic decay of $g(p)$. For this function, $g(p)$ is positive, which give the correct sign for frictionally-induced vertical motion in low pressure and high pressure regions. Consider the omega equation forced only by friction:

$$\frac{R\bar{\Gamma}}{p^2} \nabla^2 \omega + 4\Omega^2 \mu^2 \frac{\partial^2 \omega}{\partial p^2} = -\frac{\partial}{\partial p} (2\Omega \mu \mathbf{k} \cdot \nabla \times \mathbf{F}) = g \frac{d^2 g}{dp^2} 2\Omega \mu \mathbf{k} \cdot \nabla \times \boldsymbol{\tau}_s (\lambda, \mu).$$

For a low (cyclonic) weather system, $\mathbf{k} \cdot \nabla \times \boldsymbol{\tau}_s (\lambda, \mu) > 0$, and with $g''(p) > 0$ the right-hand (forcing) side is positive, so that

$$\frac{R\bar{\Gamma}}{p^2} \nabla^2 \omega + 4\Omega^2 \mu^2 \frac{\partial^2 \omega}{\partial p^2} > 0.$$

Holton (1992) shows that for sinusoidal motion $\frac{R\bar{\Gamma}}{p^2} \nabla^2 \omega + 4\Omega^2 \mu^2 \frac{\partial^2 \omega}{\partial p^2} \propto -\omega$, which results in $\omega < 0$, or rising motion, for low pressure systems. In high pressure (anticyclonic systems), $\mathbf{k} \cdot \nabla \times \boldsymbol{\tau}_s (\lambda, \mu) < 0$, but

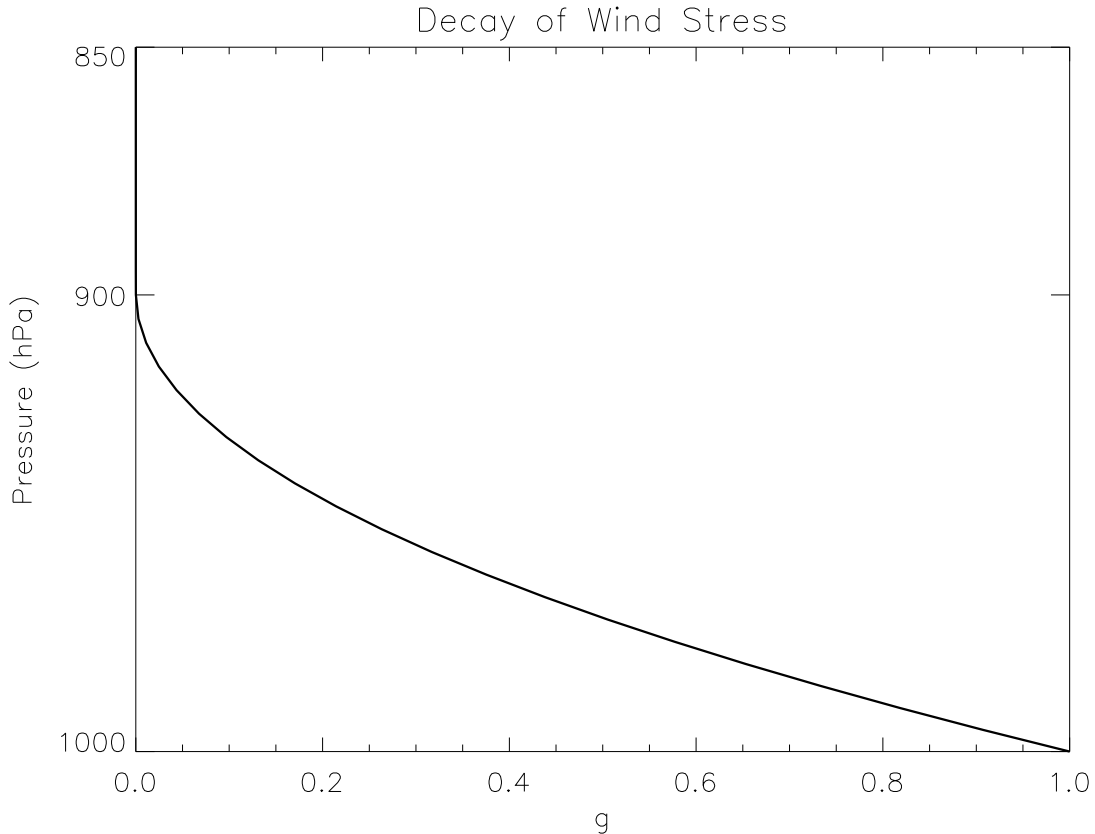


Figure 3.1: Plot the function g , which describes the decay of the effects of the surface wind stress through the boundary layer (1000 hPa-900 hPa), and into the free atmosphere (above 900 hPa), where the effects of surface friction vanish.

$g''(p)$ remains positive, resulting in $\omega < 0$, or sinking motion. Thus, the positive curvature of the chosen $g(p)$ creates the proper sign of the Ekman pumping in both low and high pressure systems.

3.4 A Mid-Latitude Example

Before applying the global omega equation to the low-latitude problem of tropical cyclogenesis, a mid-latitude example will be given. The quasi-geostrophic omega equation is used extensively in the analysis of extratropical cyclones, and applying the global omega equation to such a system provides a means by which the performance of the technique can be judged. Martin (2006) examined two extratropical cyclones using an f -plane version of the quasi-geostrophic omega equation. One of the cases was a rapidly-deepening cyclone which occurred in the northeast Pacific Ocean on 6-8 October 2004. Using data from

the Global Forecast System (GFS) model on a $1^\circ \times 1^\circ$ grid, the quasi-geostrophic omega was calculated from the divergence of the geostrophic \mathbf{Q} using successive over-relaxation (SOR) over a domain covering the local region. The results from his 0000 UTC 7 October analysis are shown in Figure 3.2. A pronounced couplet of upward and downward vertical motion associated with the system can be seen south of Alaska, with the downward motion behind the low pressure extending to the northwest, past the Aleutian Islands. The maximum magnitudes of omega in the ascending air (9 dPa s^{-1}) were almost twice the magnitudes of the descending air (5 dPa s^{-1}). The solution to the global omega equation, also using $1^\circ \times 1^\circ$ GFS data for 0000 UTC 7 October (Fig. 3.3), was calculated according to the method presented in this chapter, with the forcing represented by the divergence of \mathbf{Q} , and without friction. The omega from the global balanced theory matches up remarkably well with that generated from the mid-latitude, quasi-geostrophic equations. The same pattern of upward and downward vertical motions is evident, with the maximum magnitudes of each matching those from Martin's calculations. The similarity of the two patterns of omega in this mid-latitude example lends credence to the quality of the solutions to the global omega equation, giving confidence to the results of the study of large-scale vertical motion as relating to tropical cyclogenesis, to be presented in the following chapter.

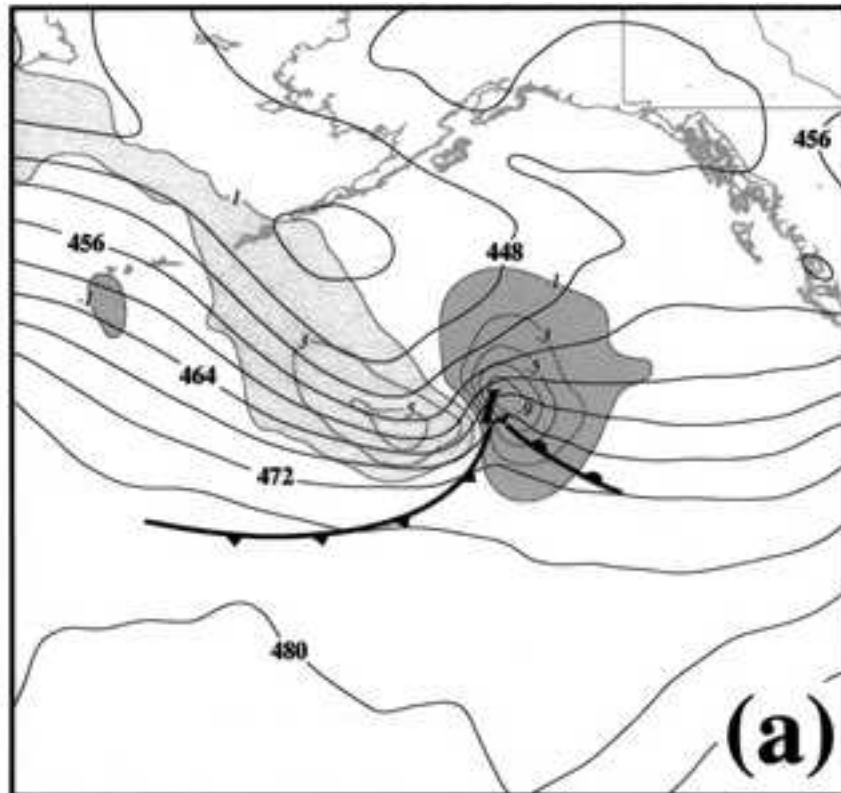


Figure 3.2: a) 700-mb ω calculated from the mid-latitude quasi-geostrophic equations using SOR, from Martin (2006). The 'L' marks the position of the surface low, and the fronts are drawn according to convention. ω is contoured every 2 dPa s⁻¹, starting at 1 and -1 dPa s⁻¹, with upward motions shaded in dark gray and downward motion shaded in light gray. The unshaded solid lines are the 900-500 hPa thickness, contoured every 4 dam. *Courtesy of the American Meteorological Society. Copyright 2006.*



Figure 3.3: 700-mb ω calculated from the global balance equations using the technique described in Chapter 3. The units of ω are dPa s^{-1} , with upward motions shaded in dark gray and downward motion shaded in light gray. Contour interval is 2 dPa s^{-1} , starting at 1 and -1 dPa s^{-1} .

Chapter 4

APPLICATION OF THE GLOBAL OMEGA EQUATION TO TROPICAL CYCLOGENESIS IN THE ATLANTIC OCEAN

4.1 Environmental Influences on Tropical Cyclogenesis

As a result of decades of study, various environmental conditions have emerged as conducive to tropical cyclogenesis. For example, warm sea surfaces were cited by Palmén (1948) as necessary for the development of tropical cyclones. Subsequent studies (e.g. Gray, 1968; Landsea et al., 1998; Gray, 2000) have confirmed this observation. The placement of the official Atlantic hurricane season within the year (June 1 to November 30, with the most active portion beginning in late August) also supports the need for ocean waters to be warmed throughout the summer before most tropical cyclones can form. In general, sea-surface temperatures warmer than 26 °C are required for the development and maintenance of a tropical cyclone.

Although warm sea-surfaces are critical to provide the sensible and latent heating required of tropical cyclones, the atmosphere also needs to be able to support the deep convection associated with these systems. In this regard, the low and middle troposphere needs to be sufficiently moist (Bister and Emanuel, 1997). The tropical atmosphere is usually associated with abundant moisture, but dry air can at times enter the lower latitudes, negatively impacting the development of tropical systems. Examples of sources of dry air include the Saharan air layer (Dunion and Velden, 2004) and intrusions of dry, mid-latitude air (Dunion, 2011).

In order for a tropical cyclone to develop within a moist airmass above a warm ocean surface, an initial disturbance is needed to provide the necessary vorticity upon which the vertical motions associated with

the deep convection act to stretch and intensify. Bracken and Bosart (2000) mention four initial disturbance types found in the Atlantic: African easterly waves, upper-level lows in the subtropics which develop toward the surface, the remnants of mesoscale convective systems, or old mid-latitude frontal boundaries which make their way into lower latitudes. Although these antecedents provide most of the vorticity, the vorticity of the Earth is also a factor, as tropical cyclones do not form equatorward of about 5° (Gray, 1968, 2000).

Excessive vertical shear hinders the formation of tropical cyclones, as it prevents the accumulation of heat and moisture in the core of the system. Measured as the vector difference of the winds at 850 and 200 hPa, vertical shear values above $10\text{--}15\text{ m s}^{-1}$ are generally regarded as disruptive to the development of a tropical cyclone (Musgrave et al., 2008). Although too much shear prohibits cyclogenesis, it is not necessarily true that an environment with zero shear provides a disturbance with the best chance of developing into a cyclone. In numerical simulations of Hurricane Gabrielle (2001), Musgrave et al. (2008) found that some vertical shear was beneficial to development. Bracken and Bosart (2000) also suggest that weak shear may in fact be necessary during the formation of a tropical cyclone, as it aids in the forcing of large-scale ascent.

4.2 Effects of Large-Scale Vertical Motion on Tropical Cyclogenesis

In this section, the large-scale vertical motion in the vicinity of a tropical disturbance will be considered as an additional environmental factor determining whether a disturbance will develop or dissipate. Perhaps the most common tool used to measure the large-scale vertical motion is the omega equation. Although usually applied in the midlatitudes, the results of the last chapter show that a global omega equation exists. Bracken and Bosart (2000) investigated the role of large-scale vertical motion on tropical cyclogenesis, but used a simplified version of the Sutcliffe-Trenberth (Sutcliffe, 1947; Trenberth, 1978) omega equation. In that version, omega is forced by the advection of vorticity by the thermal wind. Additionally, Bracken and Bosart (2000) did not solve the omega equation, but considered only the forcing for the omega. In the present work, omega itself will be computed according to the method discussed in Chapter 3.

In order to evaluate the usefulness of large-scale vertical motion in the forecasting of tropical cyclogenesis, composite disturbances will be created from developing disturbances and dissipating disturbances tracked over the Atlantic during the 2001-2009 hurricane seasons. Composite fields of height, wind, temper-

ature, relative humidity, and omega, will be created for 24, 18, 12, and 6 hours before either development or dissipation. In addition to compositing the disturbances according to whether they developed or dissipated, a stratification will be made according to the location within the Atlantic, as developing systems can exhibit differences according to where they form. Storms will be grouped according to whether they were located in the tropical Atlantic, the subtropical Atlantic, or the Gulf of Mexico. Thus six types of composites will be created: tropical Atlantic developing systems, tropical Atlantic dissipating systems, subtropical Atlantic developing systems, subtropical Atlantic dissipating systems, Gulf of Mexico developing systems, and Gulf of Mexico dissipating systems.

Dataset for Developing Systems

Information on the disturbances which developed into a tropical cyclone comes from the “decks” of the Automated Tropical Cyclone Forecasting System (ATCF) as described by Miller et al. (1990) and Sampson and Schrader (2000). During the 2001-2009 seasons, there were 154 tropical cyclones reported in the Atlantic Ocean. This number includes those cyclones with a subtropical designation (i.e. subtropical depressions and subtropical storms). Once a system becomes a depression or storm, its location and strength are closely monitored by the National Hurricane Center (NHC). Information about the system is ultimately recorded in the best track, or b deck of the ATCF, with information about the cyclone provided at 00, 06, 12, and 18 UTC. The focus of this work, however, is on systems before they underwent genesis. The locations of the systems are therefore needed at 24, 18, 12, and 6 hours before genesis.

For many tropical cyclones, the b deck contains information about the cyclone before the NHC designated it as a depression or storm, but the information is not as regular as the information available after cyclogenesis has occurred. For those cases for which best track data are not available, the a deck fixes are used, specifically the CARQ line. This line contains the location chosen by the NHC in order to run the numerical guidance for the disturbance. If the location of a system is not available on the a deck, the f deck of the ATCF is used. The f deck contains system location as determined by a variety of sources, such as satellite, aircraft, and radar. If gaps in a system’s location still exist, an attempt was made to fill in those points by interpolation or extrapolation using a least-squares fit to the known locations. In two cases, Tropi-

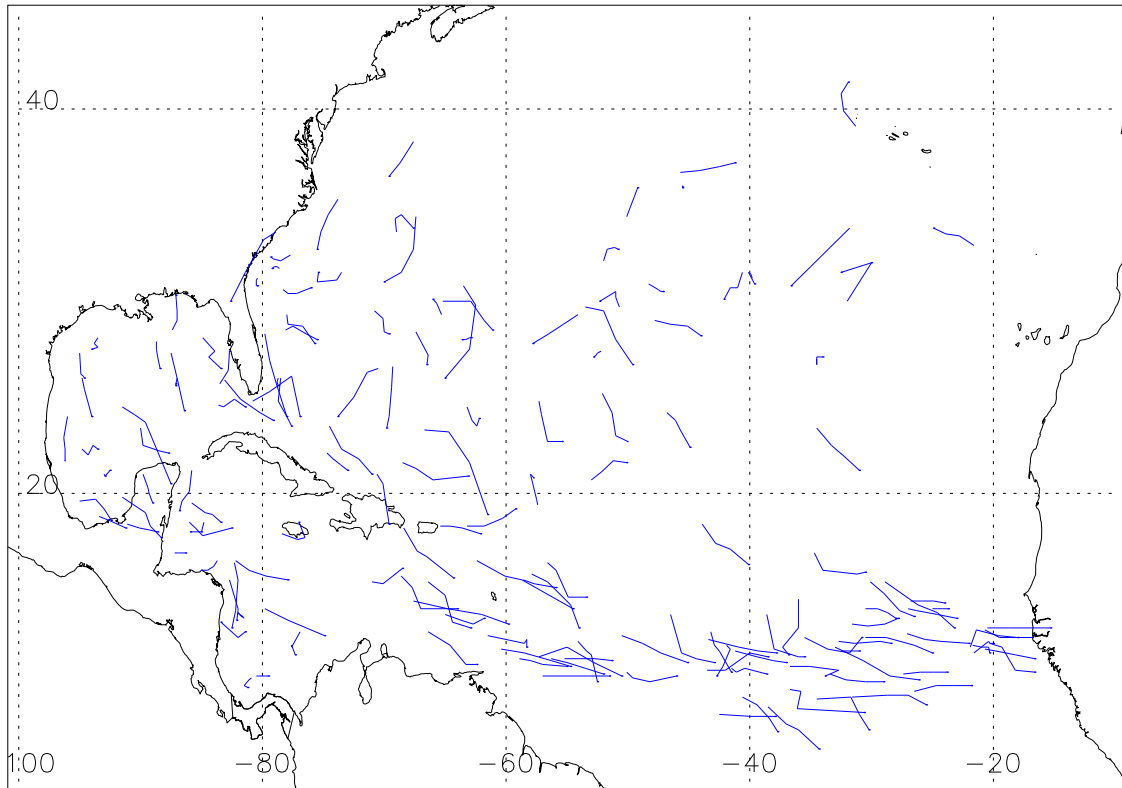


Figure 4.1: Tracks of the 154 tropical cyclones of the 2001-2009 seasons at 6, 12, 18, and 24 hours before genesis.

cal Storm Peter of 2003, and Tropical Depression 10 of 2004, none of the above methods was able to provide the necessary location information. The locations of the pre-cyclone disturbances were located using data from the National Centers for Environmental Prediction's Global Forecast System (GFS) analyses. The tracks of all 154 developing systems from 24 hours before development to 6 hours before development are plotted in Figure 4.1. The location of the tracks display the favored regions of development in the Atlantic, namely, the low latitudes west of Africa, the region extending northeast from the Bahamas, and the western Caribbean into the Gulf of Mexico. A similar grouping was found by Bracken and Bosart (2000).

Dataset for Dissipating Systems

For the disturbances which did not develop into a tropical cyclone, the locations come from a data set compiled by Cossuth et al. (2010). This data set contains all of the Dvorak satellite fixes recorded by the Tropical Analysis and Forecast Branch at the National Hurricane Center and the Central Pacific Hurricane Center in the 2001-2009 seasons, including the fixes for systems which did not develop into tropical cyclones. During those seasons, information on 100 non-developing systems was gathered. Only those disturbances lasting at least 24 hours were included. In preparing the data set, the first step was to determine a dissipation time. Analogous to the genesis time of the developing systems, the dissipation time was the point at which a disturbance would be considered to have begun the process of decay. The dissipation time is defined as 6 hours after the maximum current intensity (CI) number (Dvorak, 1975, 1984). If no single maximum CI number exists, the maximum which was latest in time was used. As with the developing systems, locations of the dissipating disturbances were found at 24, 18, 12, and 6 hours prior to dissipation. Gaps in the fixes were more frequent with this data set than with the data set for the developing systems. Unlike the three options for finding disturbance location directly from the ATCF for the developing systems, however, the data set for the dissipating systems contains the single Dvorak satellite fix option. Disturbance locations not found were filled in using interpolation or extrapolation using a least-squares fit to the locations retrieved from the Dvorak satellite fixes. For some cases, the GFS analyses again aided in locating the systems. The tracks of all 100 dissipating systems from 24 hours before dissipation to 6 hours before dissipation are plotted in Figure 4.2. The number of tracks which are entirely straight or straight along an appreciable portion is evidence of the greater number of gaps in the fixes for these systems as compared to the developing systems. The three regions of frequent development pointed out in conjunction with the tracks of the developing systems can also be seen in the tracks of the dissipating systems.

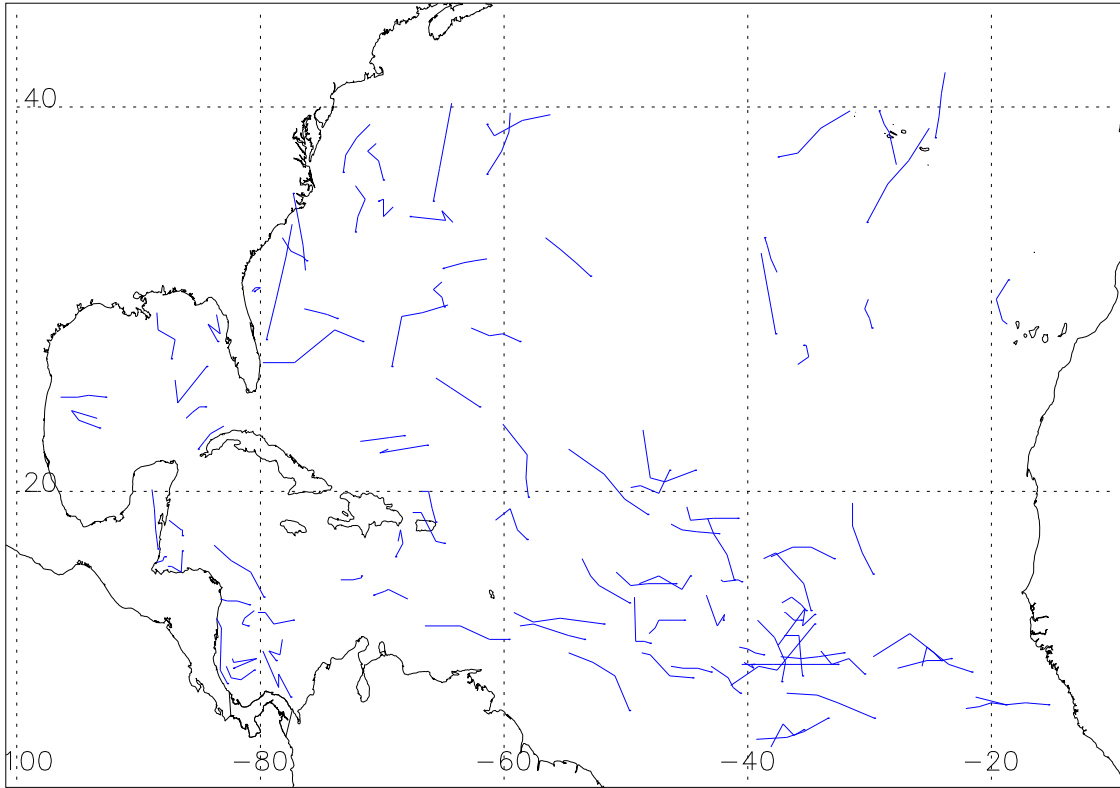


Figure 4.2: Tracks of the 100 dissipating disturbances of the 2001-2009 seasons at 6, 12, 18, and 24 hours before decay.

4.2.1 Datasets

The Calculation of Omega

The fields of omega are calculated using data from the GFS. The Regional and Mesoscale Meteorology Branch maintains an archive of GFS analyses of geopotential height, temperature, relative humidity, and the u- and v-components of the wind interpolated to a $2^\circ \times 2^\circ$ grid. In accordance with the recommendation of Phillips (1958) discussed in Chapter 2, the wind field was used to calculate the streamfunction, from which a balanced height field could be calculated according to the balance condition used in the creation of the global omega equation

$$\Phi(\lambda, \mu, p) - \bar{\Phi}(p) = 2\Omega\mu\psi(\lambda, \mu, p).$$

Thus the height field used will differ slightly from that stored in the GFS, but will have the proper relationship to the streamfunction such that the balance condition is satisfied. Because the temperature is related to the height field, a new temperature field consistent with the balance condition was also calculated using the hydrostatic relationship

$$T = -\frac{p}{R_d} \frac{\partial \Phi}{\partial p}.$$

As with the geopotential, this balanced temperature field differs only slightly from the original temperature field of the GFS.

Because the right-hand-side of the above equation vanishes for $\mu = 0$, $\Phi(\lambda, \mu, p) = \bar{\Phi}(p)$ at the equator, meaning the geopotential changes only with pressure along the equator. At each pressure level, $\bar{\Phi}(p)$ is given by the value of the zonal average geopotential as contained in the GFS data.

In order to isolate large-scale motions, a low-pass filter was applied to the streamfunction before the height field was computed. The filter is of the form discussed by Sardeshmukh and Hoskins (1984) and has a response function S_n given by:

$$S_n = \exp \left\{ - \left[\frac{n(n+1)}{n_0(n_0+1)} \right]^r \right\}, n \leq M.$$

In addition, only the first nine vertical modes were kept.

In solving the omega equation, the traditional form of the forcing was used. The **Q** form, which is exactly equal to the traditional form in the quasi-geostrophic framework, is not equal to the traditional form of the global omega equation. As shown in the previous chapter, the derivation of the **Q** form requires additional assumptions of a slowly-varying μ . In addition, because the computation of the omega equation uses the GFS analysis fields, the winds are (within the model atmosphere) without error. Thus there is no issue with calculating the forcing from the vorticity effect and the thermal effect, which can result in calculating small differences between two large numbers. In addition, the use of the traditional form of the omega equation allows the contribution to the total omega from the individual terms (vorticity, thermal, and friction) to be compared. Despite the potential drawbacks of looking at the individual components discussed in Chapter 1, this method can provide insight into the atmospheric processes important to an event such as tropical cyclogenesis. It has been used with more general forms of the omega equation in the midlatitudes

Table 4.1: The distribution of the 154 developing systems and the 100 dissipating systems among the three Atlantic subbasins.

	Tropics	Subtropics	Gulf of Mexico	Total
Developing	83	53	18	154
Dissipating	58	35	7	100

(DiMego and Bosart, 1982; Pauley and Nieman, 1992), Tropics (Baumhefner, 1968) and globally (Raisanen, 1995).

4.2.2 *Compositing Procedure*

As indicated by the tracks of both the developing and dissipating systems, certain regions in the Atlantic are particularly favorable for tropical cyclogenesis: the tropical Atlantic, the subtropical Atlantic, and the Gulf of Mexico. In order to examine the characteristics of the large-scale vertical motion typical for these genesis regions, composite analysis will be used. As discussed by Sinclair and Revell (2000), composite analysis does not capture the details of the individual members comprising the composite, but emphasizes the features common to all the members. Composite analysis is used throughout the atmospheric sciences, including tropical meteorology (e.g. McBride and Zehr, 1981; Bracken and Bosart, 2000).

The outlines of the three subbasins are given in Figure 4.3. Disturbances with an average latitude less than or equal to 20° N are included in the tropical Atlantic composite. Disturbances with an average latitude greater than 20° N are included in one of the other two subbasins according to average longitude: those with average longitude less than or equal to 81.5° W are included in the subtropical Atlantic composite and those with average longitude greater than 81.5° W are included in the Gulf of Mexico composite. The distribution of the 154 developing systems and the 100 dissipating systems are given in Table 4.1, which shows that for each of the two types (developing and dissipating), the tropical Atlantic produces the most systems, followed by the subtropical Atlantic, and with the Gulf of Mexico producing the fewest systems.

At each analysis time (24, 18, 12, 6 hours before development or dissipation, also denoted as -24, -18, -12, and -6 hours), the fields of height, temperature, relative humidity, u-wind component, and v-wind

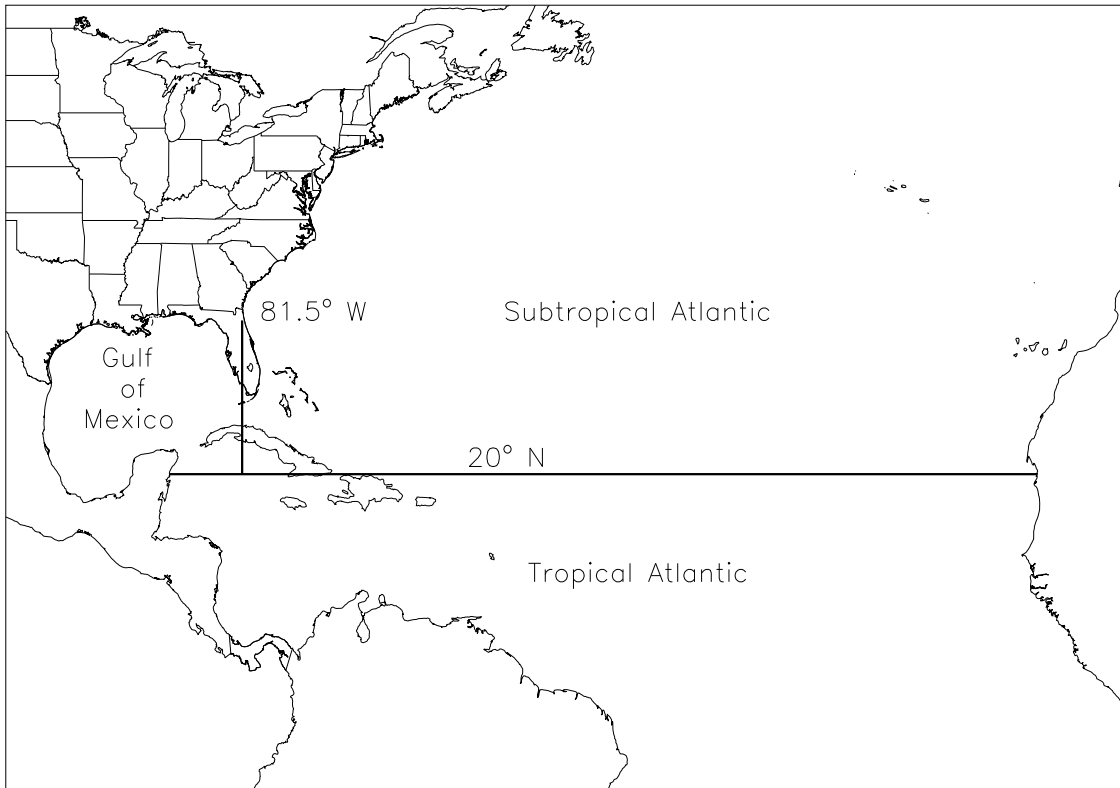


Figure 4.3: Map outlining the three subbasins: Tropical Atlantic, Subtropical Atlantic, and the Gulf of Mexico.

component obtained from the GFS analyses in a 40° longitude by 20° latitude box centered on the surface positions of the systems were used in the three subbasin composites. The composite fields were then placed on the sphere at the mean latitude and longitude associated with each category (e.g. tropical Atlantic, developing systems at -12 hours). The rest of the sphere was filled with a global composite consisting of the same times which went into the system composites. In creating the composite over the systems, an extra GFS grid point on each side was used, such that a smooth transition in the fields between the system and global composites could be obtained by successive passes of a 1-2-1 filter.

In compositing the fields of omega, two choices exist. The composite could come from solving the omega equation from the composite fields of height, temperature, and the u and v wind components. Alternatively, the omega fields from each member of the group could be averaged to create the composite

omega field. Even though the omega equation is a linear, partial differential equation, the forcing terms are nonlinear, so the two options will give different results. The second option will be used here, as the averaging involved in creating the composite developing and dissipating systems smooths out the features, weakening the forcing terms. In addition, solving the omega equation is similar to inverting a Laplacian operator, which has a smoothing effect itself. The end result is an omega field that does correspond exactly to the height field, but one in which potentially important features may have been smoothed away. In addition, preparing the composite omega field from the individual omega fields themselves allows for additional operations on the omega fields, such as significance testing, which will be examined at the end of this chapter.

4.3 Results

4.3.1 Tropical Atlantic Systems

Most Atlantic tropical cyclones initiate from easterly waves moving off of the coast of Africa near the Cape Verde Islands. The origins of these waves can often be traced as far east as Sudan and Ethiopia (Mekonnen et al., 2006). These systems constitute not only the majority of tropical cyclones in the Atlantic, but also the majority of major hurricanes (Category 3 and higher). Landsea (1993) reports that 80% of all major hurricanes in the Atlantic come from African easterly waves.

The tracks of the composite systems (Fig. 4.4) show the mean position of the disturbances at 24, 18, 12, and 6 hours before either development or dissipation. Although the path of the dissipating composite is to the west of the track of the developing composite, the tracks of the two composites are quite similar with a mean latitude of about 13°N and a mean longitude of about 52°W – roughly 750 km northeast of the coast of South America. Both are moving to the west-northwest, the developing composite at 11 kts and the dissipating composite at 10 kts.

The 850-200 hPa wind shear (vector difference) and the sea surface temperature (SST) experienced by the developing and dissipating composites are shown in Table 4.2. The wind shear values were calculated from GFS fields, using the u and v components averaged over a 4°x4° latitude-longitude box centered over the surface location. The SSTs were taken from Reynolds analysis (Reynolds and Smith, 1993) at the surface

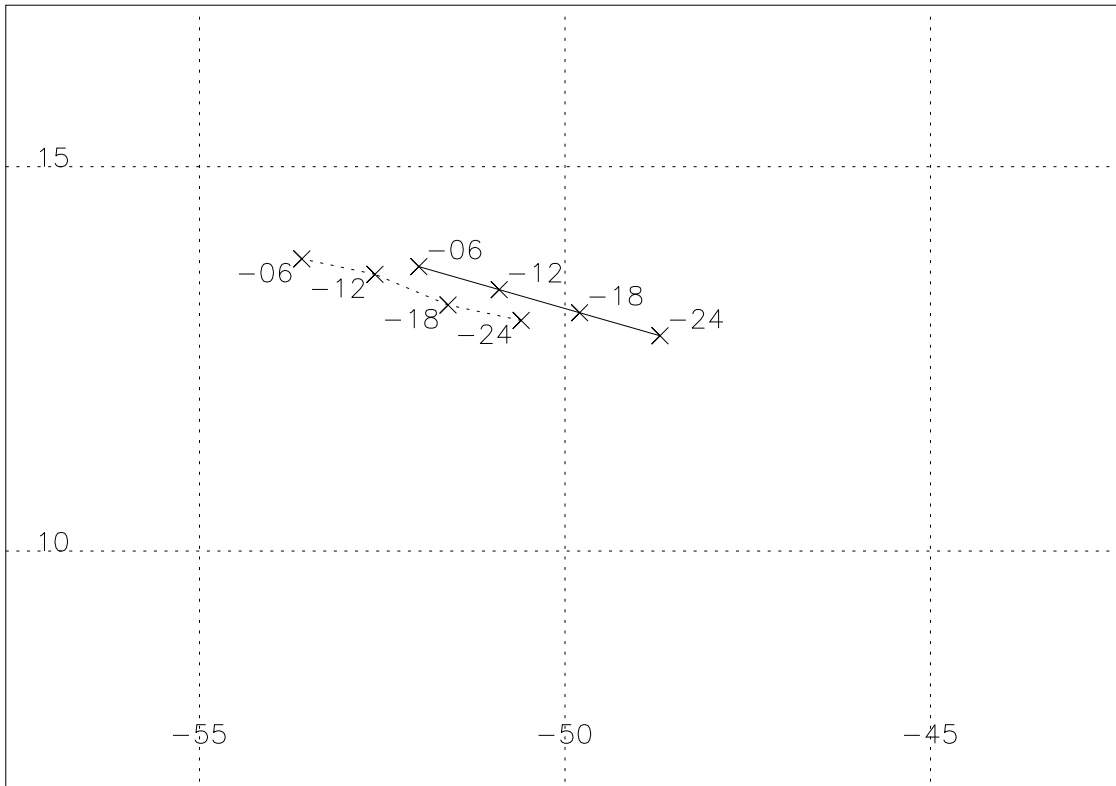


Figure 4.4: Location of the tropical Atlantic composite developing system (solid) and the composite dissipating system (dashed) at 24, 18, 12, and 6 hours before either genesis or dissipation.

location of the systems. The SST of the developing composites was at all times significantly¹ greater than the SST of the dissipating composite. In both cases, however, the temperatures were above 26 °C threshold. There also existed a difference in 850-200 hPa wind shear between the two composites. The developing systems experienced a 850-200 hPa shear just above 6 ms⁻¹ at all four times before development. The shear over the dissipating systems was higher, ranging from 8.4 ms⁻¹ at -24 hours to 8.8 ms⁻¹ at -6 hours. The differences between the shears were significant, although both means were below the 10–15 ms⁻¹ threshold suggested by Musgrave et al. (2008) as a range above which vertical wind shear becomes disruptive to the development of a tropical cyclone.

A time series of plan views of the composite 850 hPa height and omega shows the progression of

¹ In this paper, significance will be defined by the 95% level using a two-tailed Student's t-test

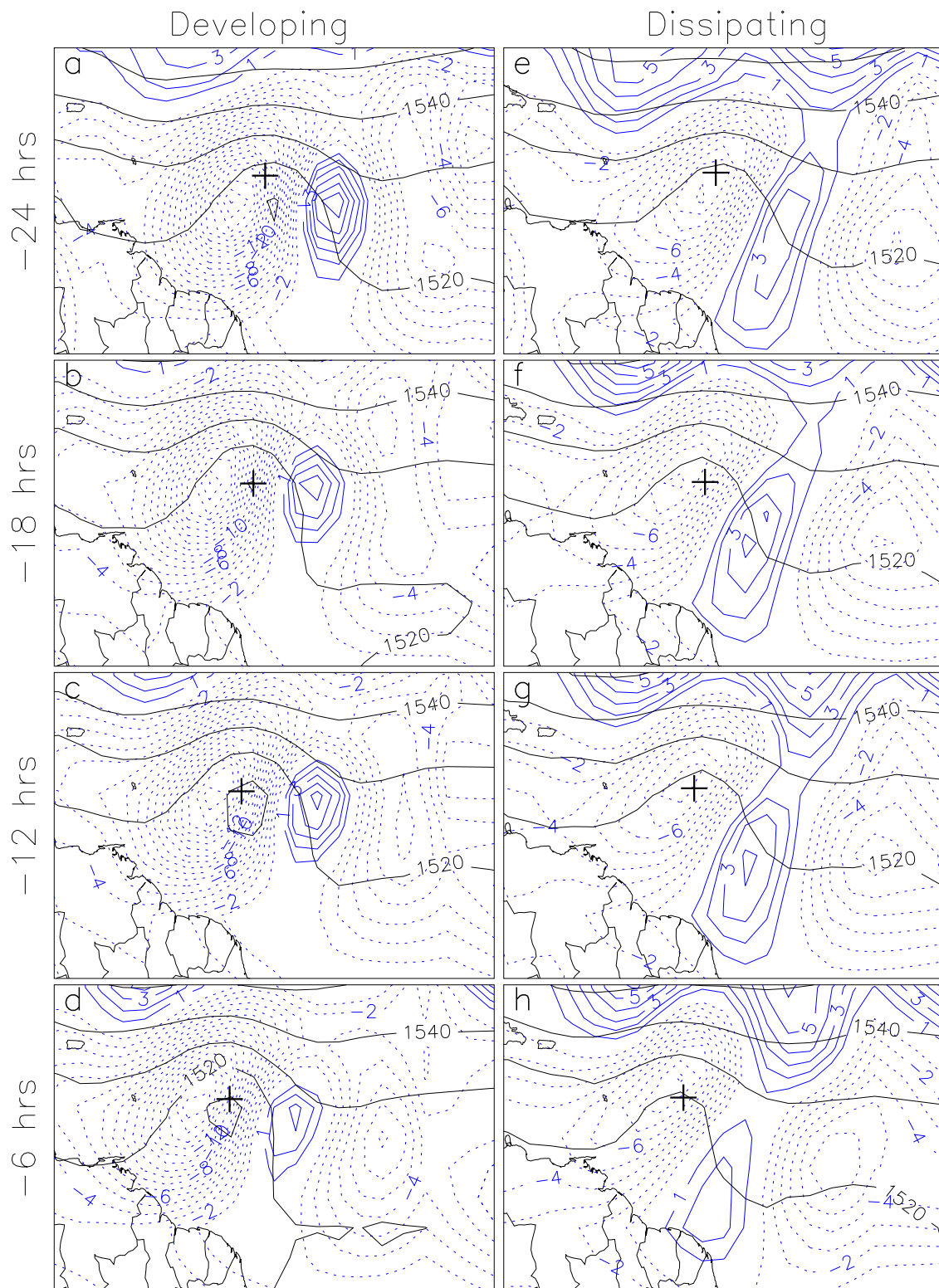


Figure 4.5: 850 hPa height (black) and omega (blue) for the developing and dissipating tropical Atlantic composites at 24, 18, 12, and 6 hours before either genesis or dissipation. The height field is contoured every 10 meters. The omega field is contoured every 1 hPa day⁻¹, with dashed contours indicating rising motion and solid contours indicating sinking motion. The zero contour is omitted, and the “+” indicates the surface position of the composite.

Table 4.2: The 850-200 hPa shear (ms^{-1}) and the SST of the Tropical developing and dissipating composites at 24, 18, 12, and 6 hours before development or dissipation. The shear calculations are using the winds averaged over a $4^\circ \times 4^\circ$ latitude-longitude box centered over the surface location, and the SSTs are taken at the surface location.

Time (hours)	Developing Systems		Dissipating Systems	
	Shear	SST	Shear	SST
-24	6.6	28.5	8.4	28.2
-18	6.2	28.5	8.6	28.2
-12	6.3	28.5	8.8	28.1
-6	6.2	28.5	8.8	28.1

the mean developing system (Fig. 4.5a-d) and the mean dissipating system (Fig. 4.5e-h). Both height composites show an 850-hPa trough progressing north and west, just as the plot of the mean locations indicates (4.4). The shape of the troughs are similar to the schematic of Frank (1969) of the low-level wind field found in easterly waves, and display the upshear tilt discussed by Reed et al. (1977). Such a pattern would be expected in the composites of tropical Atlantic disturbances, as the vast majority of disturbances in this subbasin are associated with easterly waves. The actual heights of both composites are similar as well, however, the trough of the developing system is much better defined in the sense of curvature of the height field, with a closed low developing at -12 hours. The greater curvature in the height field implies that the wave of the developing systems has a greater amount of low-level vorticity, one of the well-known ingredients necessary for the genesis of a tropical cyclone. The greater vigor of the composite wave associated with the developing systems is also seen in the accompanying omega field, produced from the solution of the global omega equation. The maximum magnitude in the area of rising motion to the west of the wave of the developing composite ($\sim 17 \text{ mb day}^{-1}$) is roughly twice the maximum magnitude of the rising motion of the dissipating composite ($\sim 9 \text{ mb day}^{-1}$). The developing composite also shows stronger maximum downward motion in the vicinity of the wave, (11 vs. 7 hPa day^{-1}), although the sinking motion of the composite dissipating system covers a larger area. The dipole of upward and downward motion seen in both composites is reminiscent of the rising and sinking motion ahead of and behind, respectively, of a midlatitude trough.

East-west cross sections through the composites provide confirmation of what is seen in the plan views, as well as reveal additional details of the two disturbances. Figure 4.6 shows the height anomaly (relative to the mean height at each level within the compositing domain) and omega through the developing composite (Fig. 4.6 a-d) and through the dissipating composite (Fig. 4.6 e-h) at the GFS latitude closest to the mean latitude of the composite disturbances. Confirming what the plan views showed, the composite perturbation height field of the developing systems indicates a more vigorous wave than that associated with the dissipating systems. At 24 and 18 hours before development, the minimum low-level height perturbation is -18 m. The low-level anomaly deepens by 4 meters, resulting in a minimum height anomaly of -22 m at 12 and 6 hours before genesis. In contrast, the negative low-level height anomaly of the dissipating composite fills over time. Between 24 and 12 hours prior to dissipation, the minimum height anomaly is -14 m; at 6 hours, the anomaly is -12 m. In addition to the stronger negative anomaly, the trough of the developing composite extends higher into the atmosphere, above 400 hPa. The composite wave of the dissipating system also extends above 400 hPa at -24 hours, but shrinks to below 400 hPa at -6 hours. Both composites also display a positive height anomaly at upper levels. An upper-level anticyclone, although not a dominant factor, is favorable to the development of disturbances (DeMaria and Kaplan, 2001), as its associated divergence allows a strong outflow at upper levels (Riehl, 1948). In this case, both the developing and dissipating composites show a strengthening of this feature with time. Also the upper-level anticyclone is displaced slightly to the east of the low-level center. In their study of developing and non-developing systems, McBride (1981) and McBride and Zehr (1981) composited Atlantic disturbances according to three categories, two non-developing — cloud clusters and wave trough clusters (or wave trough convection) and one developing — pre-hurricane cloud cluster. For the cloud cluster composite and the pre-hurricane composite, they also found that the upper anticyclone was displaced to the east. They measured the distance to be $\sim 3^\circ$ latitude. Their wave trough cluster composite showed no anticyclone. Also in agreement with McBride and Zehr (1981) is the greater upper-level horizontal shear associated with the developing systems, as can be inferred by the smaller spacing of the contours of perturbation height.

The pattern of omega in the vicinity of the wave for both composites is a four-cell pattern. The leading (western) edge of the wave is characterized by rising motion at lower levels and sinking motion at

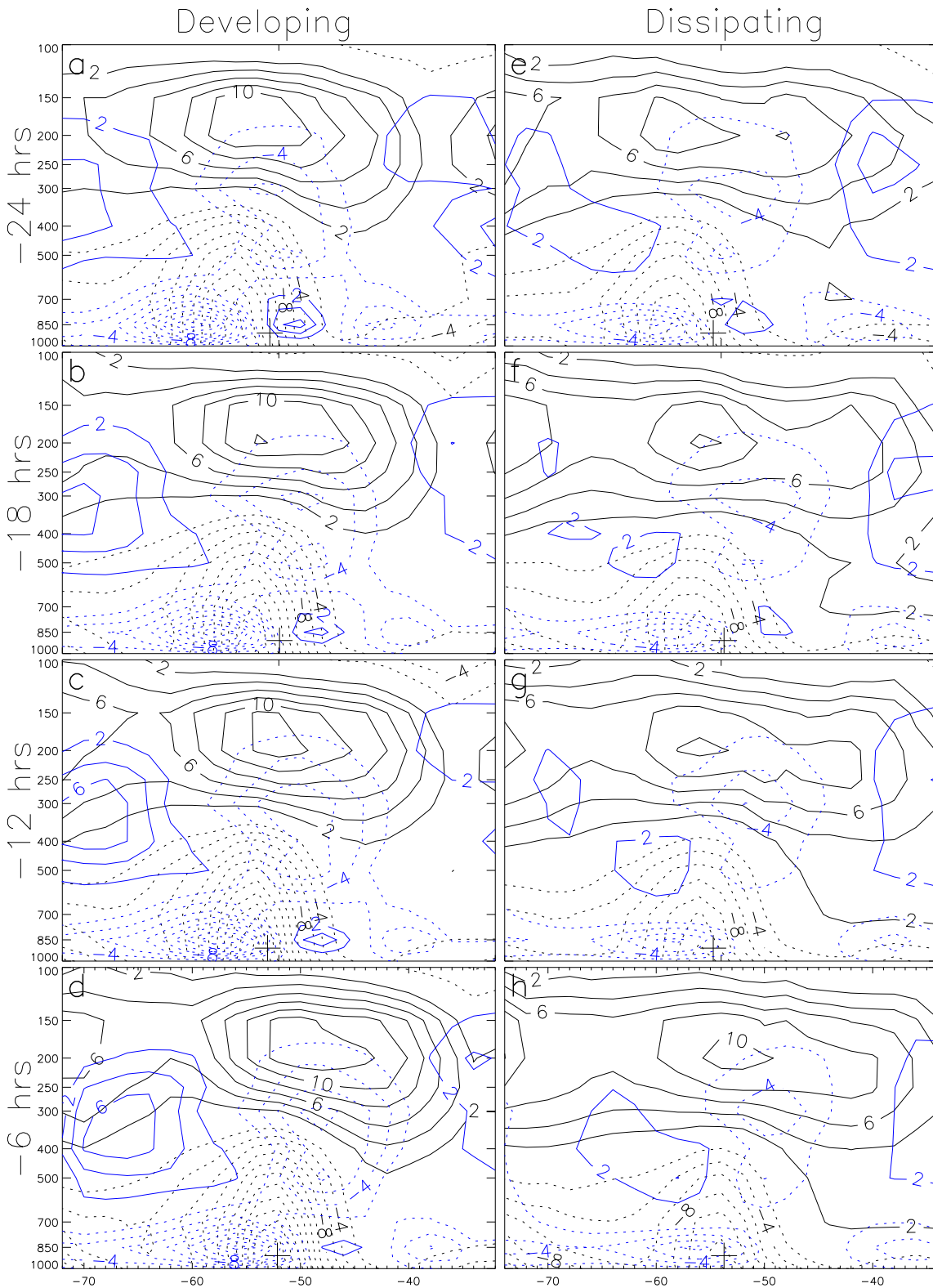


Figure 4.6: Cross section of height anomaly (black) and omega (blue) through the developing and dissipating composites at 24, 18, 12, and 6 hours before genesis or dissipation. The height anomaly is contoured every 2 meters and omega is contoured every 2 hPa day⁻¹. In both cases solid represents positive values and dashed represents negative values. The zero contour is omitted, and the “+” sign is placed at the longitude of the surface location of the composite disturbance.

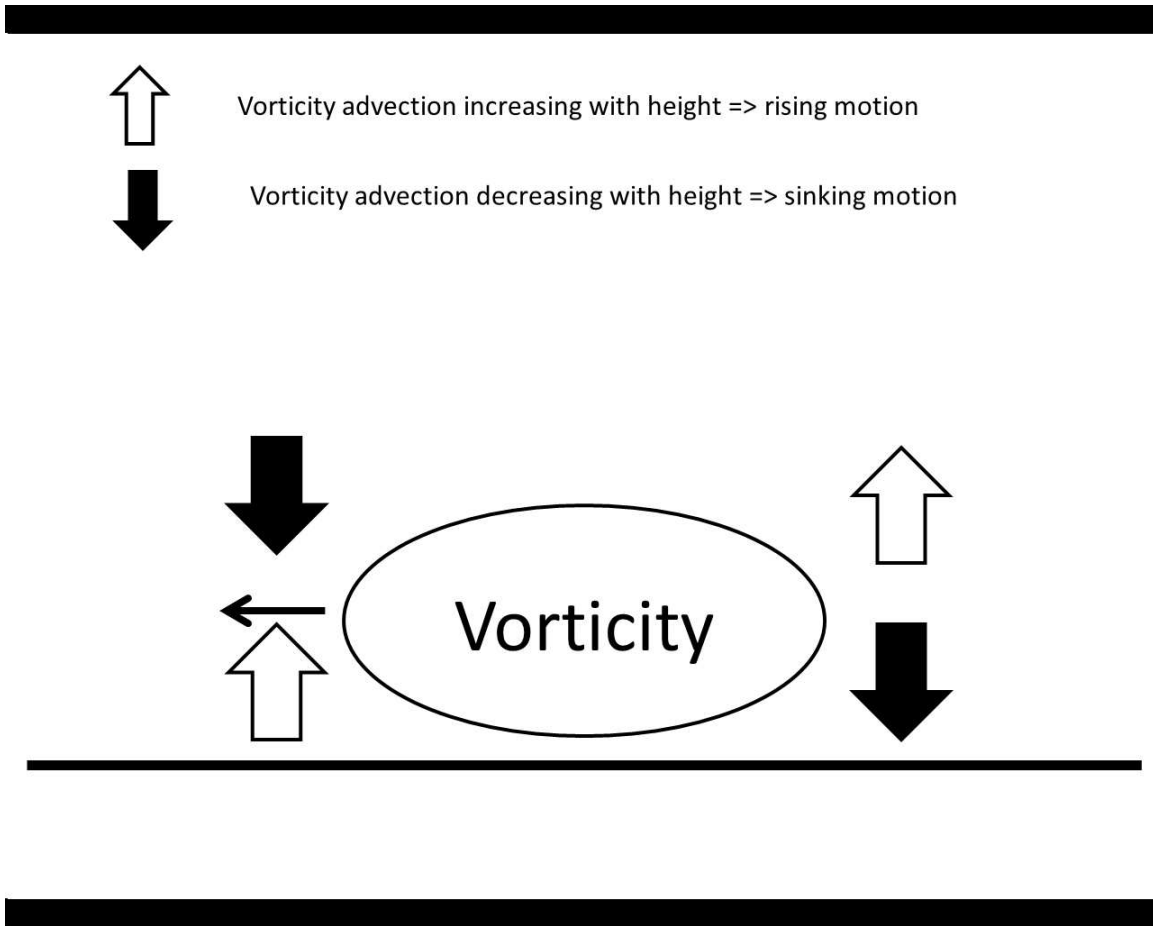


Figure 4.7: Vertical motions associated with the omega field forced by vorticity advection alone.

mid to upper levels. On the trailing (eastern) edge, the omega pattern is the opposite: rising motion at the top of the wave and sinking motion near the bottom. This pattern is consistent with the vertical motion which would exist in a westward-moving trough forced only by the vorticity term of the omega equation (Fig. 4.7). With advection of cyclonic vorticity increasing with height (decreasing with pressure) rising motion results, as seen at the lower levels of the wave. For advection of cyclonic vorticity decreasing with height, sinking motion results, as seen at the upper levels of the wave. This pattern is seen on the western edge of the wave. On the eastern edge of the wave, the opposite vorticity forcing is present, that is, cyclonic vorticity advection increases with height near the top of the wave, forcing rising motion. At the lower levels, cyclonic vorticity advection decreases with height, resulting in sinking motion. On both the western and the eastern edges of the wave, the transition between rising and sinking motion occurs near 600 hPa, a typical level for which

easterly waves have their maximum amplitude (Hopsch et al., 2010), again underscoring the importance of easterly waves in this subbasin of the Atlantic.

Interestingly, this four-celled pattern is also seen when viewing the distribution of vertical velocities associated with convection in tropical disturbances. Kiladis et al. (2009) present a conceptual model (reproduced here in modified form as Fig. 4.8) of convection associated with convectively coupled equatorial waves, which includes easterly waves. At the leading edge of the wave, the convective pattern consists of low-level rising motion situated underneath upper level subsidence. At the trailing edge, the convective motions continue at higher levels. Beneath this area of upward motion exists a region of sinking associated with the stratiform precipitation. In the case of easterly waves, the large-scale vertical motions are apparently in phase with the vertical motions produced by aggregate convection.

That the four-cell pattern of vertical velocity arises from the vorticity term can be confirmed by separating the forcing for the omega equation into individual terms. Since the omega equation is a linear partial differential equation, each forcing term may be considered separately, and the sum of the omega fields resulting from the individual forcing components will equal the total omega field resulting from including all of the forcing terms. Cross sections of the components of omega for the developing composite at -6 hours are shown in Figure 4.9. Panel a shows the total omega. Panel b shows the omega forced by vorticity effects, which includes not only the term $\frac{\partial}{\partial p} [2\Omega\mu\mathbf{v}_\psi \cdot \nabla (\zeta + 2\Omega\mu)]$, but also the lower boundary term, (3.12b), which is a vorticity advection. Panel c contains the omega resulting from the thermal effects, $-\nabla^2 \left[2\Omega\mu\mathbf{v}_\psi \cdot \nabla \left(\frac{\partial\psi}{\partial p} \right) \right]$, and Panel d the frictional effects. In comparing the four panels, the four-cell pattern seen in the total omega most resembles the omega forced by vorticity effects alone, although the rising motion at the low-levels of the western edge is not seen. It is in fact present, appearing if the contour interval is decreased to 0.25 hPa day⁻¹ (not shown). As important as the vorticity forcing is in determining the overall pattern of the total omega, it is clearly modified by the frictional forcing. In fact, frictional effects dominate the lower levels. The large contribution due to friction confirms the finding of Krishnamurti (1968a), who mentioned the importance, and possible dominance of frictional effects on the omega equation in the Tropics, where dynamical forcing can be weak. The temperature advection term (4.9 c) forces downward motion at lower levels on the eastern edge of the wave, and weak upward motion on the western

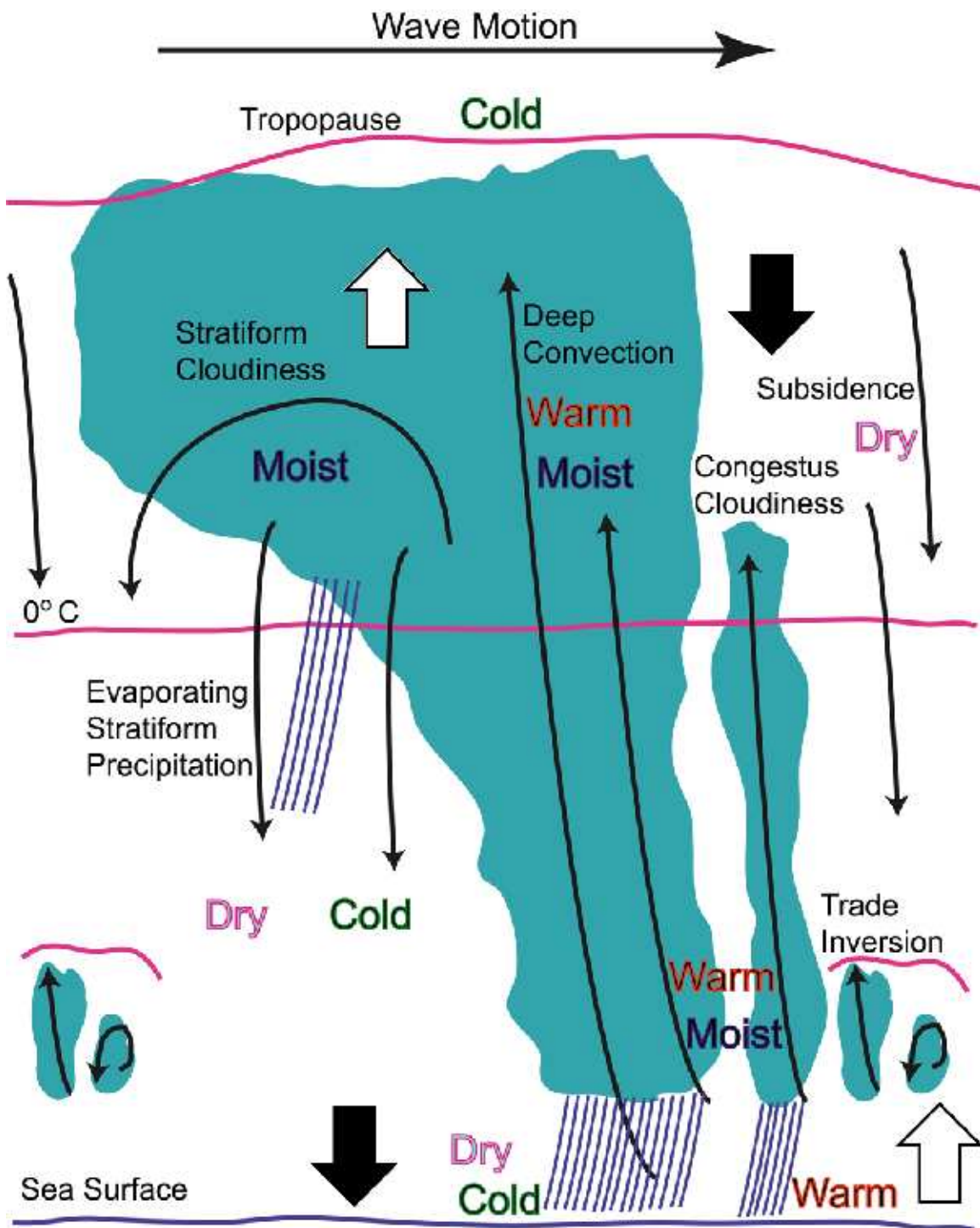


Figure 4.8: Vertical motions associated with convectively coupled equatorial waves as depicted by Kiladis et al. (2009). The wide arrows corresponding to the large-scale balanced motion attributed to vorticity advection (Fig. 4.7) have been added.

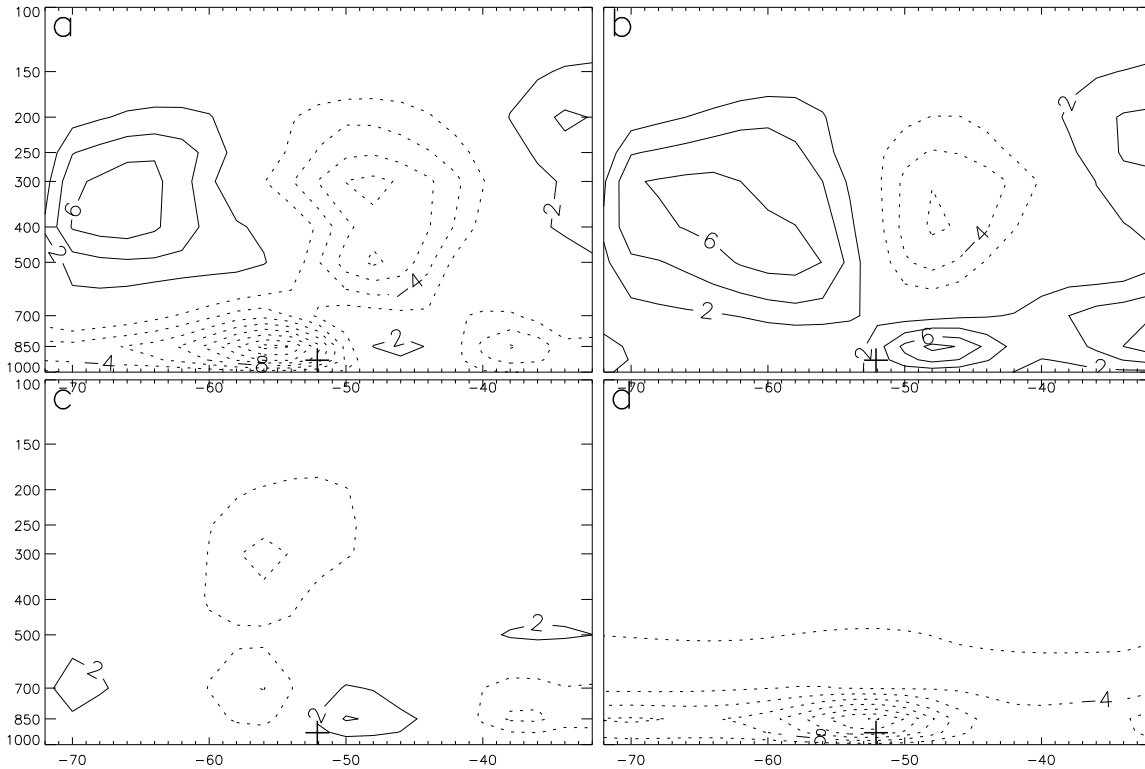


Figure 4.9: The contributions to the omega field for the tropical developing composite at 6 hours before development: a) total omega, b) vorticity effects, c) thermal effects d) friction effects. The omega field is contoured every 2 hPa day^{-1} , with dashed contours indicating rising motion and solid contours indicating sinking motion. The zero contour is omitted, and the “+” is located at the longitude of the surface location of the composite system.

edge at low levels.

The vertical motions due to the forcing components of the composite dissipating system (4.10) look similar, albeit weaker, to the corresponding components of the developing composite. The four-cell pattern is missing the sinking motion at low levels on the eastern edge of the wave, (4.10a), but its presence can be confirmed by looking at the omega resulting from the vorticity forcing terms (4.10b). The sinking motion is dominated by the lifting due to both frictional and thermal effects. The frictional effects are also primarily responsible for the low-level rising motion at the western edge of the wave. The thermal effects of the dissipating composite are weaker than in the developing composite on the western edge, but are stronger on the eastern edge.

Considering again the pattern of omega forced by vorticity of both composites, it is seen that the

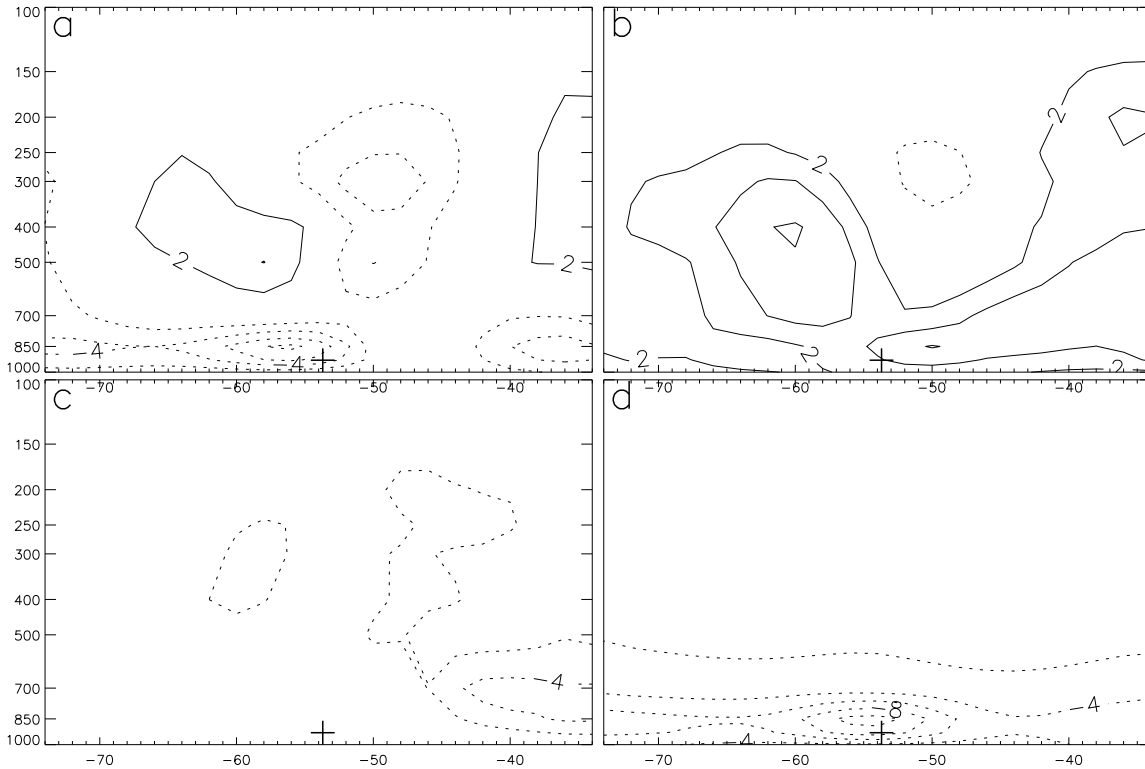


Figure 4.10: Same as 4.9, only for the dissipating composite.

rising motion at lower levels on the western edge is weaker than the sinking motion at the lower levels on the eastern edge of the wave. This asymmetry in ω is likely a consequence of the asymmetry in the perturbation height field of the wave itself. Looking at both Fig. (4.5) and Fig. (4.6), the contours of the perturbation height field are more closely packed on the eastern side of the wave than on the western side. Figure 1a of Reed et al. (1977) supports the existence of this asymmetry in that the strongest winds are seen on the eastern side of the wave. Since the height field is related to the vorticity field, a larger gradient of vorticity would be expected on the eastern side of the wave, likely resulting in a greater vorticity advection on the eastern side than on the western side. The top two panels of Fig. 4.11 show the perturbation height field as well as the vorticity advection by the balanced wind for both the developing composite and the dissipating composite at -6 hours. That the vorticity advection is greater on the eastern side for both the developing and dissipating composites is evident. Recall, however, that the forcing of the ω due to the vorticity effects is related to the vertical derivative of the vorticity advection. The bottom two panels of Fig.

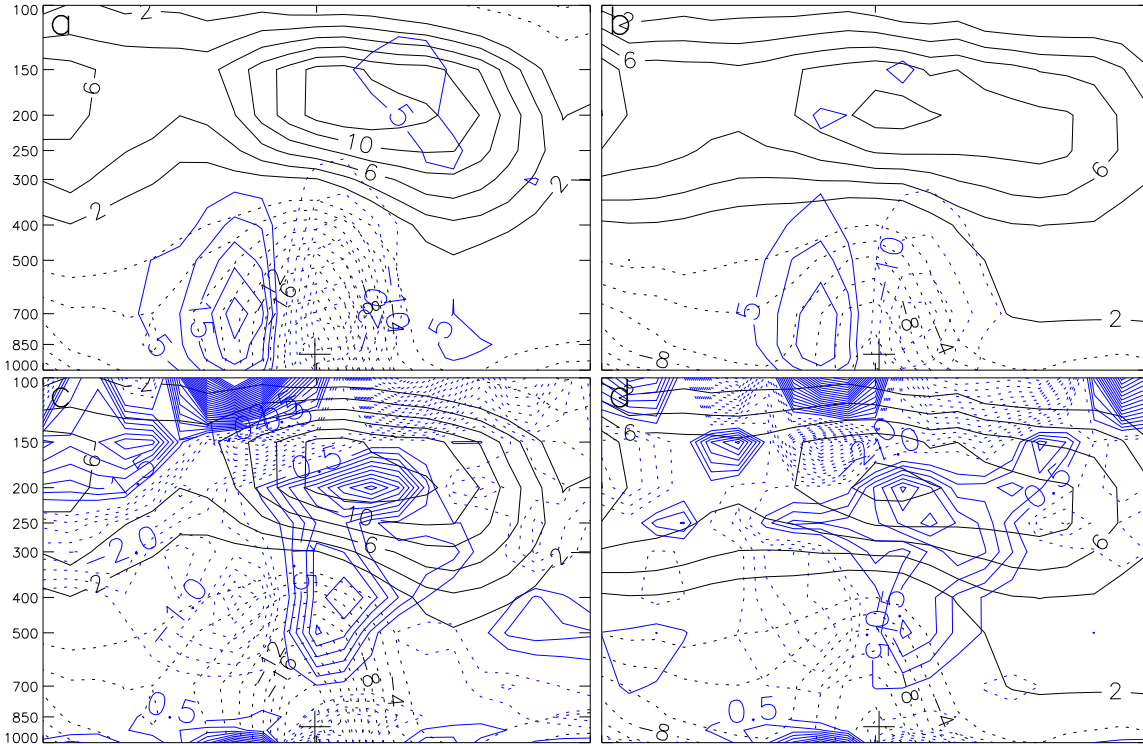


Figure 4.11: Perturbation height (black) and advection of the balanced vorticity by the balanced wind (blue) at -6 hours for: a) Developing composite and b) Dissipating composite. Perturbation height (black) and vorticity forcing for c) Developing composite and d) Dissipating composite. Perturbation height is contoured every 2 m, vorticity advection is contoured every $5 \times 10^{-11} \text{ s}^{-2}$, and vorticity forcing contoured every $0.5 \times 10^{-19} \text{ Pa}^{-1} \text{ s}^{-3}$. For all variables, solid contours denote positive values and dashed contours denote negative values. The zero contour is omitted, and the “+” is positioned at the surface longitude of the composite system.

4.11 show the forcing due to vorticity. The four-cell pattern, which was somewhat obscured in the omega field, is clearly evident in the forcing field for both composites. It is not clear, however, that the forcing on the eastern side at low levels is greater than on the western side. The pattern of the forcings is such, however, that upon solving the equation for omega, the low-level subsidence on the eastern edge of the wave is of greater magnitude than the low-level rising motion on the western edge.

The differences in the total omega fields and their components for the two composite systems can largely be attributed to the strength of the wave. This difference is particularly true for the vorticity and frictional effects — the stronger the wave, the more vorticity advection and greater Ekman pumping. The difference in the temperature effects, however, results not only from the flow associated with the distur-

bance, but also from the thermodynamic environment. A plan view of the 850-hPa heights and temperatures of the two composites six hours before development or dissipation reveals a different juxtaposition of the height and temperature fields between the two. In the developing composite, the thermal ridge to the east of the system is displaced somewhat to the north of the surface center, placing the temperature gradient within the circulation of the disturbance. In the dissipating system, the thermal ridge is farther south, essentially intersecting the surface position of the composite disturbance. This positioning results in the height contours and temperature contours to approximately parallel each other in the eastern region of the wave south of the thermal ridge. In the developing system, the height contours are at a greater angle to the temperature contours, resulting in greater cold-air advection, which is typically associated with sinking motion. The greater low-level sinking motion just to the east of the wave is in fact seen in the developing composite relative to the sinking composite as seen in Figures 4.9 c and 4.10 c. The existence of the thermal ridge not only affects the ω in the eastern portion of the disturbance, but is likely indicative of the presence of a Saharan Air Layer (SAL), a layer of warm air originating over the African continent. The SAL is also characterized by low relative humidities. The composite 850-500 hPa mean relative humidity plots 4.12 do show that the air to the west of the dissipating composite is a bit drier than the air to the west of the developing composite. In addition, the shape of the moisture ridge in the dissipating composite, and its alignment with respect to the ridge in height field appear to create a situation where the contours of the relative humidity are at a larger angle to the wind vectors, indicating greater dry air advection into the dissipating composite. The dry air of the SAL may therefore be a contributing factor to the dissipating systems' eventual demise. This suggestion is in agreement with other work regarding the interaction of an easterly wave with the SAL as an inhibitive factor to genesis (Dunion and Velden, 2004). In the case of the developing composite, the humidity contours are more parallel to the wind vectors, suggesting that the disturbance is protected from dry-air advection. The idea of an incipient disturbance being protected from the air of the environment, which may be hostile to the development of a tropical cyclone, forms the basis of the marsupial paradigm of tropical cyclogenesis (Dunkerton et al., 2009).

The omega pattern, although distinct, is quite weak, even for the developing composite in relation to the upward motion found to be necessary for genesis. According to McBride and Zehr (1981), 100 hPa

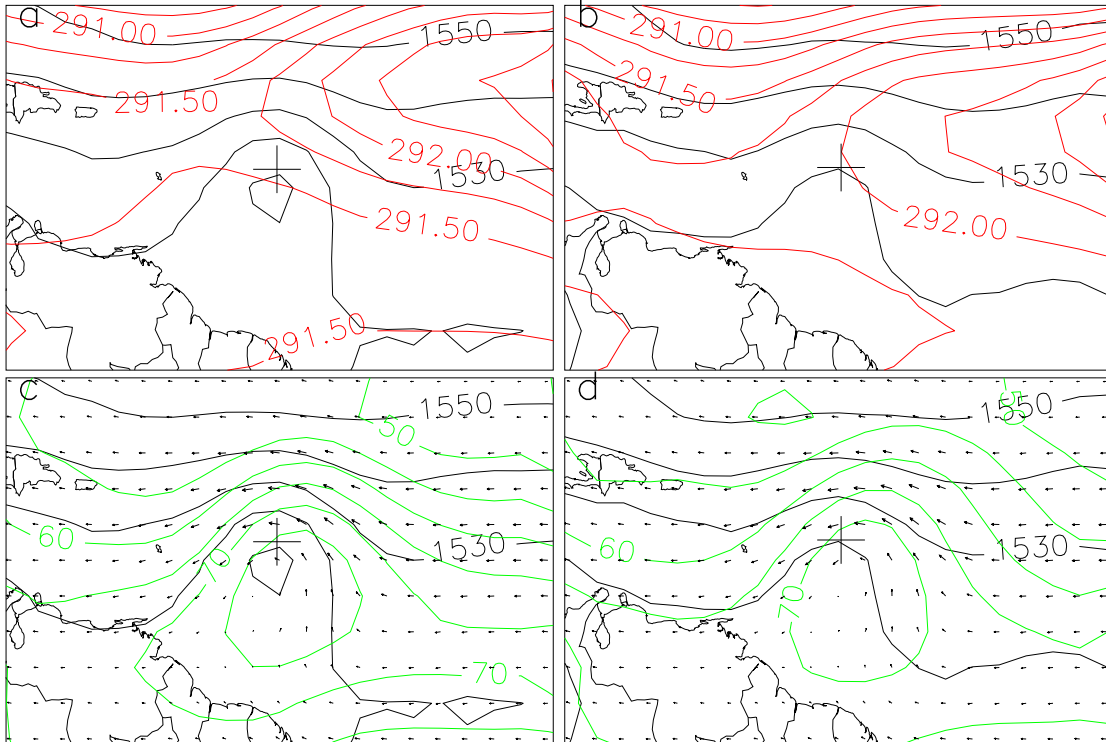


Figure 4.12: 850-hPa heights (black, m) and temperatures (red, K) at 6 hours before development or dissipation for a) the developing composite, b) the dissipating composite. 850-hPa heights, mean 850-500 hPa relative humidity (green, %), and 700-hPa GFS wind vectors at 6 hours before development or dissipation for c) the developing composite, and d) the dissipating composite. The “+” indicates the surface position of the composite.

day⁻¹ over an area of 4° radius is necessary for the development of a tropical disturbance into a tropical cyclone. The developing composite has a maximum of 7 hPa day⁻¹. This difference of more than an order of magnitude suggests that the large-scale vertical motion acts to condition the atmosphere to be more conducive to vertical convection. The role of large-scale vertical motion as a precursor, creating an environment suitable to sustaining vertical convection forced by smaller-scale processes was suggested by Doswell (1987) in a study of severe convection at midlatitudes. To investigate this possibility further, the divergence profile associated with the vertical motion of the composite systems was used to modify the vertical moisture profile of a typical tropical sounding to see if the developing composite would change the moisture profile in such a way as to make it more capable of sustaining deep convection than the composite of the dissipating system. For simplicity, the temperature profile was kept constant, but water vapor changes

Table 4.3: The CAPE, CIN, and LFC calculated from the 1-D cloud model using three different soundings, the Jordan sounding (Control), the Jordan sounding with the moisture profile altered by the divergence profile of the developing composite (Developing) and the dissipating composite (Dissipating).

	CAPE (J kg ⁻¹)	CIN (J kg ⁻¹)	LFC (m)
Control	231	25	1500
Developing	949	1	200
Dissipating	516	8	700

following a parcel will be assumed to obey the following conservation equation:

$$\frac{D(\ln \rho_v)}{Dt} = -\nabla \cdot \mathbf{v}$$

which, after performing the integration

$$\int_{\rho_{v,i}}^{\rho_{v,f}} d \ln \rho_v = - \int_{t_i}^{t_f} \nabla \cdot \mathbf{v} dt$$

gives

$$\rho_{v,f} = \rho_{v,i} e^{-(\bar{\nabla} \cdot \mathbf{v}) \Delta t}.$$

Using the mass continuity equation, the above equation may be written

$$\rho_{v,f} = \rho_{v,i} e^{\frac{\bar{\partial \omega}}{\partial p} \Delta t} \quad (4.1)$$

Applying (4.1) to each level of the sounding for each of the composite systems gives the change in water vapor density. For this experiment, the profile used was the Jordan mean sounding (Jordan, 1958), and the divergence was applied for 1 day, or about one quarter the typical period of an easterly wave (Burpee, 1972), for the developing composite and the dissipating composite. The modified moisture profiles were used along with the temperature profile of the unmodified mean Jordan sounding (control) in a one-dimensional entraining cloud model (DeMaria, 2009), and three convective parameters, convective available potential energy (CAPE), convective inhibition (CIN), and the level of free convection (LFC), were compared. The results are given in Table 4.3, which also gives the CAPE, CIN, and the LFC for the unmodified Jordan mean sounding.

The vertical profile of the divergence of both the developing composite and the dissipating composite create an atmosphere more conducive to convection than the original sounding, that is, they each increase

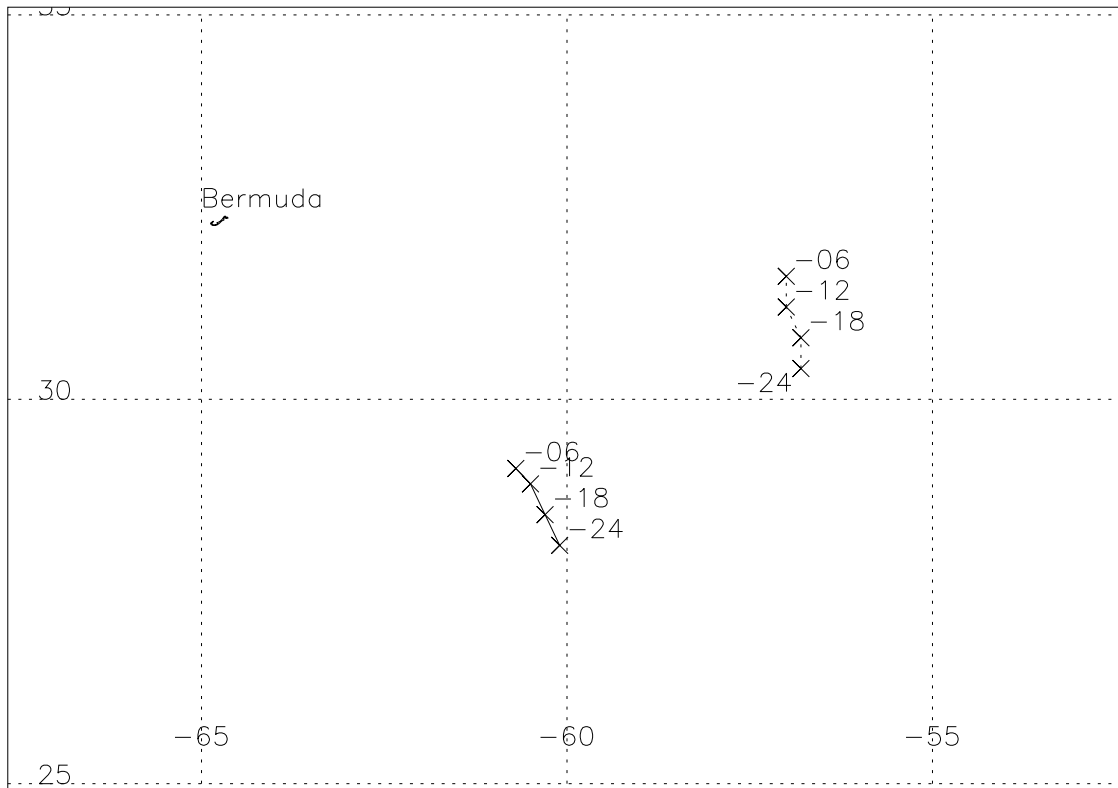


Figure 4.13: Same as 4.4, but for the subtropical Atlantic composites.

the CAPE, and decrease both the CIN and the LFC. The changes associated with the developing composite, however, create the atmosphere which is most able to support deep convection, by improving the three parameters by at least a factor of two over the dissipating composite.

4.3.2 *Subtropical Atlantic Systems*

Of all the ocean basins which produce tropical cyclones, the northwest Pacific and the north Atlantic are unique in that the poleward extent of the active waters reaches to around 30°N. Frank (1987) connects this poleward extent of tropical cyclone activity to the poleward extent of warm waters on the western side of the ocean basins, the so-called western boundary currents (Munk, 1950)—the Kuroshio Current in the Pacific and the Gulf Stream in the Atlantic. Because of this extratropical extent of warm waters, disturbances in these regions can be influenced by midlatitude components, most notably, upper-level troughs.

Table 4.4: As in Table 4.2, but for the Subtropical systems.

Time (hours)	Developing Systems		Dissipating Systems	
	Shear	SST	Shear	SST
-24	9.8	27.1	12.2	25.8
-18	9.1	27.1	12.1	25.7
-12	9.0	27.1	11.3	25.6
-6	7.9	27.0	11.5	25.4

The tracks of the composite systems in the subtropical Atlantic are given in Fig. 4.13. The track of the developing composite is roughly 700 km to the southeast of Bermuda and the dissipating roughly 800 km to the east southeast of Bermuda. Both composite disturbances move generally to the north. Comparing Fig. 4.13 with Fig. 4.4, the track of the composite storms in the Tropics, a greater separation between the two composite storms in the Subtropics is evident. In fact, for all four times, the mean latitude of the dissipating systems is significantly farther north than the mean latitude of the developing systems. In addition, the mean distance travelled from -24 to -6 hours by the dissipating systems (386 km) is significantly greater than the mean distance travelled by the developing systems (281 km). Of the three Atlantic subbasins considered in this work, only the Subtropics shows a significant difference in mean latitude and mean distance travelled between the developing and dissipating disturbances. The difference in position and distance travelled are particularly important in this region, as even though the Gulfstream brings warm waters poleward on the western edge of the Atlantic basin, further to the center of the ocean the sea surface temperatures at these latitudes are not conducive to the development of tropical cyclones. That the more northeast position of the dissipating composite puts it farther away from the warm Gulfstream waters is seen in the mean SST of 25 – 26 °C, compared to the mean SST of 27 °C of the developing composite (Table 4.4). That 1 – 2 °C difference is not only significant in a statistical sense, but also in a physical sense, in that SSTs lower than 26 °C are, in general, not capable of supporting a tropical cyclone.

The proximity of the disturbances to midlatitude troughs in the subtropical Atlantic suggests that these systems will usually form or dissipate under the influence of greater shear than the disturbances in the Tropics. Table 4.4 also presents the mean 200-850 hPa shear in a 4° latitude x 4° longitude area over

both the developing and dissipating systems. Although both means decrease with time, it is clear that the developing systems experience less shear than the dissipating systems. The differences between the means are all significant except at -24 hours. In addition, the mean wind shear of the dissipating systems is within the 10–15 m s^{-1} range mentioned previously, above which the vertical wind shear is considered unfavorable for development. For the developing disturbances, the mean shear is below this range for all times, and in particular at 6 hours before development.

As in the tropical Atlantic subbasin, the composites of the developing and dissipating systems in the subtropical Atlantic subbasin do show similarities, but also differences during the time leading up to development or dissipation. In plan view the 850-hPa height and omega fields of the developing composite (4.14a-d) shows a closed low deepening by 20 m, from 1520 m to 1500 m, during the 18 hours spanned by the figure. The omega field shows a distinct couplet, with rising motion over and to the east of the low, and sinking motion to the west, as would be expected in a midlatitude low. The couplet is asymmetrical, with the rising portion being the more intense by a factor of two to four. The subsident portion weakens with time, beginning with a maximum sinking of 12 hPa day^{-1} and ending with a sinking of 8 hPa day^{-1} . The ascending portion remains essentially the same, starting and ending at -24 hPa day^{-1} with a decrease to -28 hPa day^{-1} at 18 hours before development.

Similar to the developing composite, the closed 850-hPa low of the dissipating composite deepens with time, in this case by 10 m, from 1510 m to 1500 m (4.14e-h). Also similar is the asymmetric couplet of the omega field, again with the rising branch stronger than the sinking branch by a factor of two to four. The strength of the sinking branch remains at 8 hPa day^{-1} throughout the time period. The ascending branch of the omega field strengthens with time, at 24 hours before development the maximum rising motion is -28 hPa day^{-1} , and at 6 hours before development the value is -32 hPa day^{-1} . Whereas the two composites have similar magnitudes of the height field, and the rising and sinking branches of the omega fields, the shape of the fields is slightly different. Both the height field and the rising branch of the omega field in the developing composite are more circular than their counterparts in the dissipating composite, where southwestward extensions in the height and omega field are present. These extensions take on the appearance of an extratropical wave. In particular, the omega field of the dissipating composite looks similar to the 700-

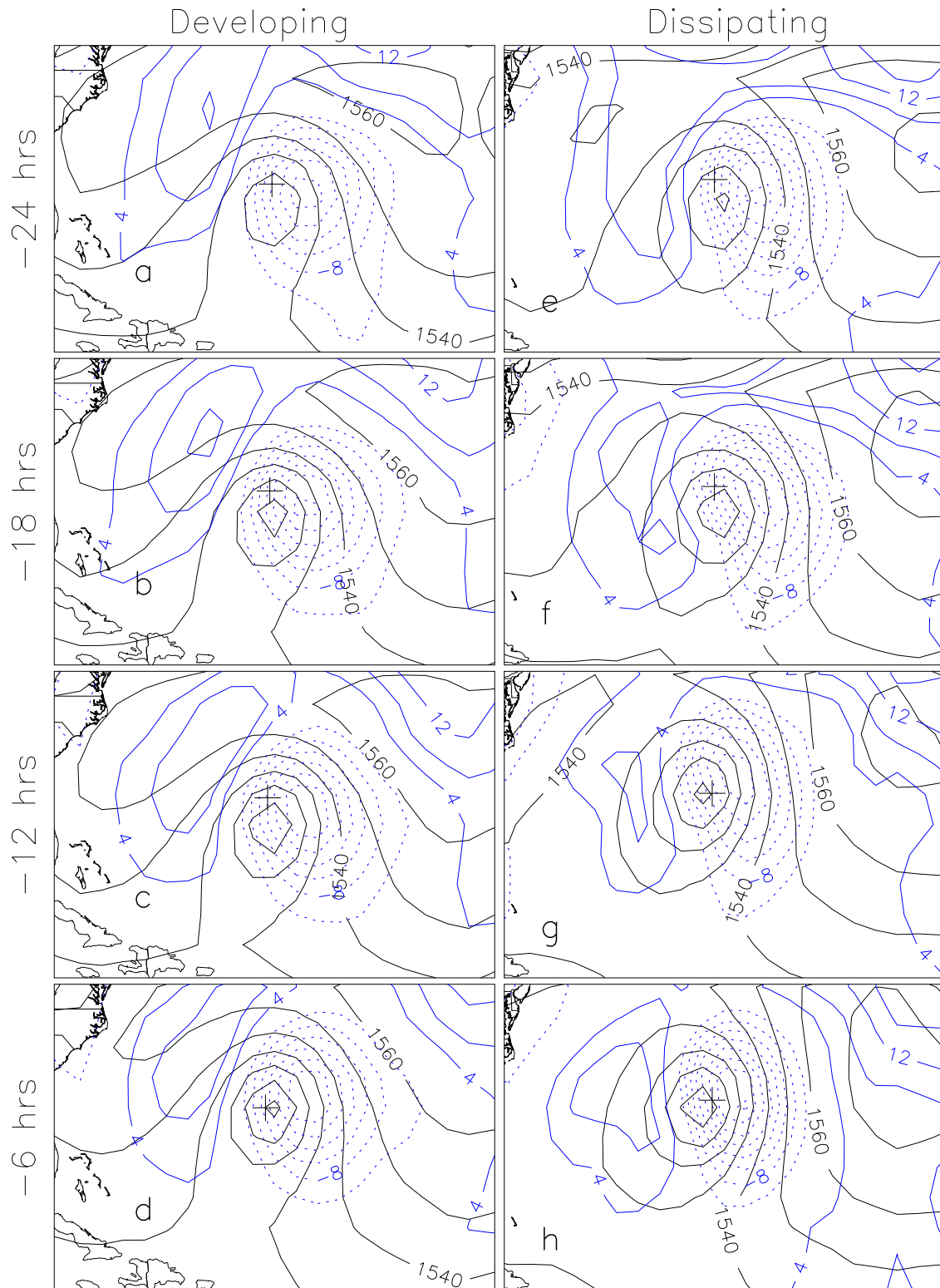


Figure 4.14: 850 hPa height (black) and omega (blue) for the developing and dissipating subtropical Atlantic composites at 24, 18, 12, and 6 hours before either genesis or dissipation. The height field is contoured every 10 meters. The omega field is contoured every 4 hPa day⁻¹, with dashed contours indicating rising motion and solid contours indicating sinking motion. The zero contour is omitted, and the “+” indicates the surface position of the composite.

hPa omega field of the midlatitude example given in the last chapter (Figs. 3.2 and 3.3). Also, whereas the sinking branch in the omega field is offset to the north with respect to the rising branch in the developing composite, the sinking branch in the dissipating composite wraps around to the southeast, coming close to the southwestward extension of the rising motion mentioned earlier. This pattern of rising and sinking motion is in alignment with the trough in the height field, again resulting in the appearance of a cold front.

The perturbation height field seen in east-west cross sections (Fig.4.15) through the disturbances (at the GFS latitude closest to the disturbance latitude) reveals the midlatitude influence in the development of tropical cyclones in the Subtropical Atlantic. Here the low at the surface continues all the way to 100 hPa for both the developing and the dissipating composites. Recall that in the Tropics, the pattern of perturbation height was a high at upper levels over the lower-level low (Fig.4.6).

The pattern of omega seen in the cross section of the two subtropical composites differs greatly from that seen in the tropical composites (Fig.4.6). Instead of a 4-cell pattern, the omega field is dominated by a rising branch to the east of the low and a sinking branch to the west. As seen in the 850-hPa plan view, the rising branch is more vigorous than the sinking branch for both composites. Within the rising branch there are likely two maxima of -24 to -28 hPa day⁻¹, one in the middle levels (500 hPa to 300 hPa) and one at lower levels (850 mb). At some times the maxima are clearly seen, such as at -18 hours in both the developing and dissipating composite (Fig.4.15b and f). At others, the two maxima need to be inferred by noting the shape of the contours of omega, and by recognizing that the contour interval of 4 hPa day⁻¹ may not be sufficient to capture both maxima. When the contour interval is increased to 2 hPa day⁻¹ (not shown) the two maxima are in fact better resolved. The pattern within the sinking branch is better described as consisting of an elongated maximum of 14 to 20 hPa day⁻¹, extending from 700 hPa to 250 hPa.

Splitting the omega into its vorticity, thermal, and frictional components for the developing composite (Fig.4.16) and the dissipating composite (Fig.4.17) at -6 hours provides additional insight. First note the similarity in both magnitude and shape of the omega fields produced by the vorticity term (Fig.4.16 b and Fig.4.17 b). Both composites have an ascending branch with a maximum of ascent of -16 hPa day⁻¹ at middle levels (500 hPa - 200 hPa). The descending branches are likewise similar with a broad maximum of descent of 8 hPa day⁻¹ at a slightly lower altitude (850 hPa - 300 hPa). The omega forced by friction is also

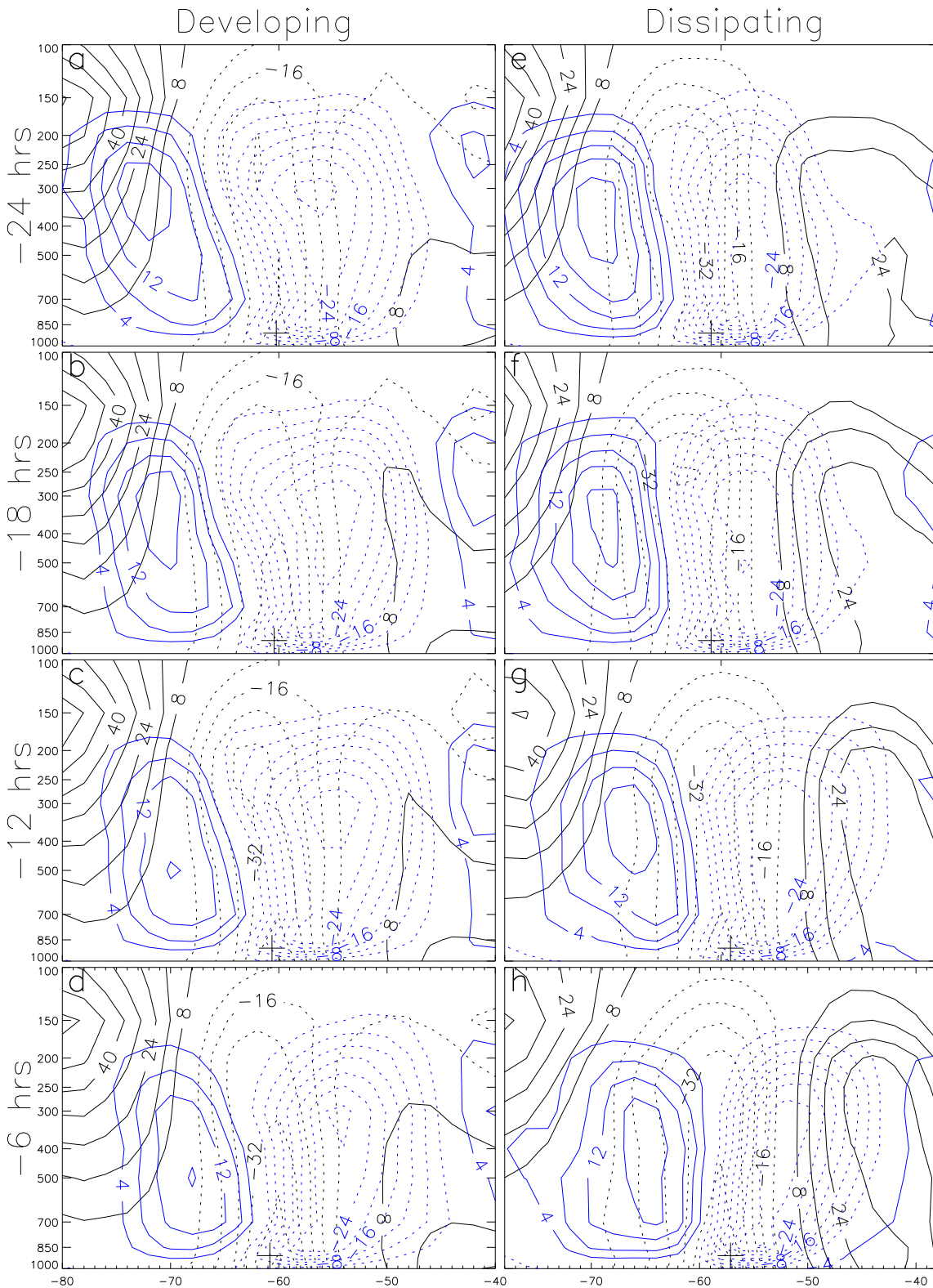


Figure 4.15: Cross section of height anomaly (black) and omega (blue) through the Subtropical developing and dissipating composites at 24, 18, 12, and 6 hours before genesis or dissipation. The height anomaly is contoured every 8 meters and omega is contoured every 4 hPa day⁻¹. In both cases solid represents positive values and dashed represents negative values. The zero contour is omitted, and the “+” is located at the longitude of the surface location of the composite system.

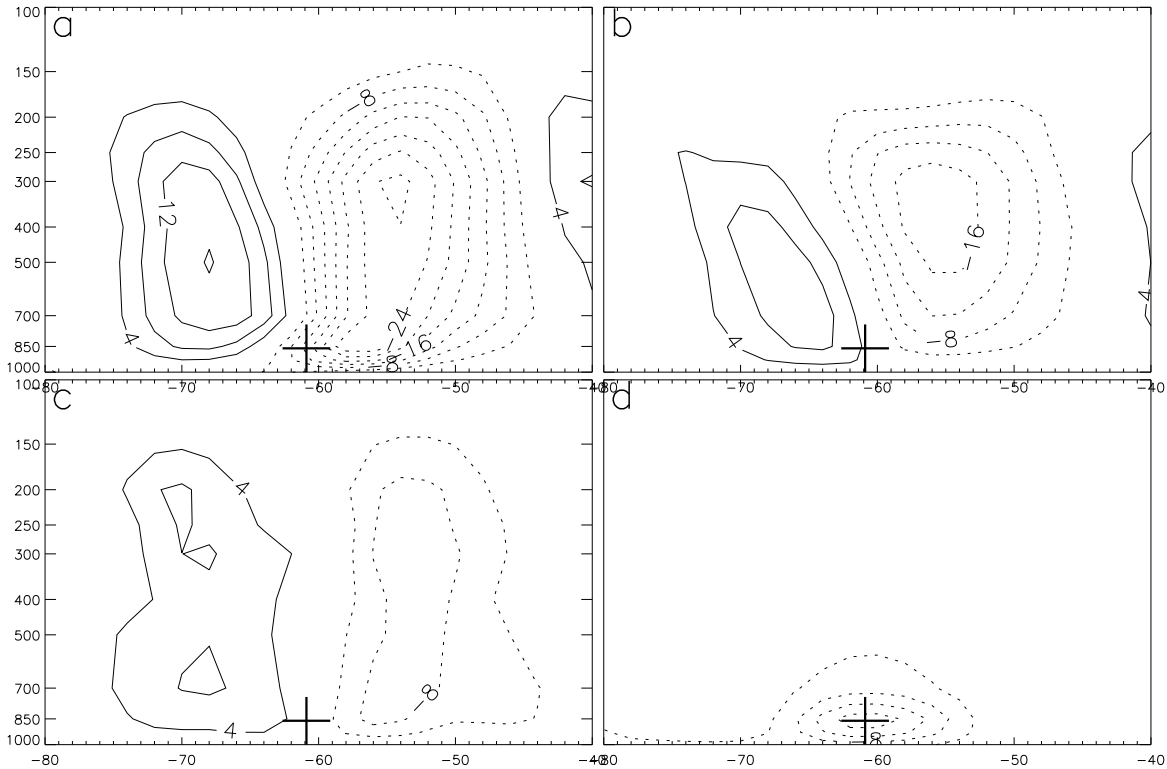


Figure 4.16: The contributions to the omega field for the subtropical developing composite at 6 hours before development: a) total omega, b) vorticity effects, c) thermal effects d) friction effects. The omega field is contoured every 4 hPa day^{-1} , with dashed contours indicating rising motion and solid contours indicating sinking motion. The zero contour is omitted, and the “+” sign marks the surface longitude of the composite system.

similar between the two. Both are dominated by a single maximum of -16 hPa day^{-1} at 850 mb (Fig.4.16 d and Fig.4.17 d). In addition, the pattern of omega forced by thermal effects shows a hint of two maxima, one centered at 250 hPa and the other at 700 hPa. Therefore, the two maxima in the ascending branch to the east of the low noticed in the analysis of the cross section time series are due to a combination of the vorticity and the frictional effects, as well as the thermal effects. Fig. 4.16 and Fig. 4.17 also show the smaller impact that friction has relative to the vorticity and thermal forcing on systems in the Subtropics than in the Tropics (Fig.4.16 and Fig.4.16). Although still the largest contributor to ascent, $(-16 \text{ hPa day}^{-1})$ friction does not completely dominate the upward motion at low levels as in the Tropics.

Examination of other fields reveals the greater midlatitude nature of the dissipating composite. The 850-hPa height field (Fig.4.18) shows a deepening of both systems over the 18 hour time frame. A striking

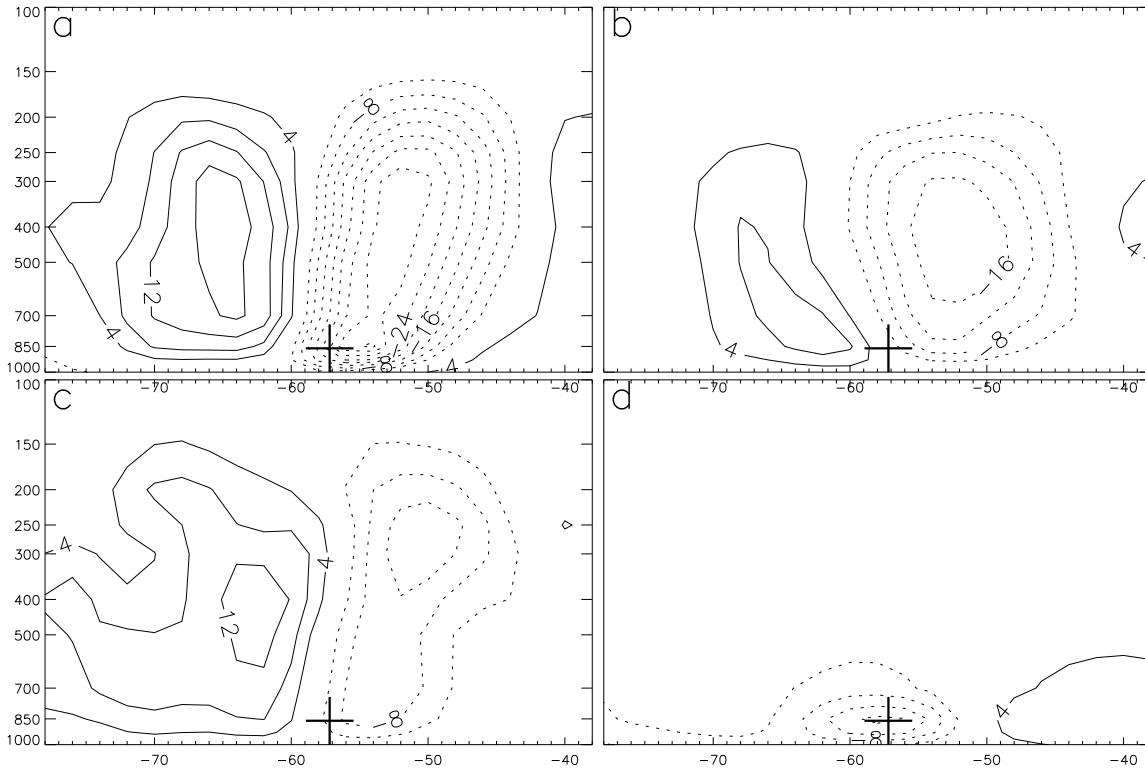


Figure 4.17: Same as 4.16, only for the dissipating composite.

difference, however, can be seen in the temperature field, where the contours in the developing composite run basically east to west with a signal of a thermal trough to the west of the low. The temperature field of the composite dissipating system is overall colder, but also displays an elongated "S" pattern, typical of that created by the warm and cold front of midlatitude systems. In addition, the temperature gradient is at all times larger in the dissipating composite than in the developing composite. By thermal wind considerations, this means that the vertical shear should also be greater for the dissipating systems, which would be consistent with their decay as excessive vertical wind shear is known to hinder tropical cyclogenesis. Measurements of the 850-200 hPa vertical wind shear confirm what the 850-hPa temperature gradient suggests (Table 4.4). Overall, the shear for the developing composite shows a slight decrease from 10 m s^{-1} to 8.6 m s^{-1} during the hours leading up to cyclogenesis. The shear for the dissipating composite stays basically the same throughout the period, with a small decrease at 12 hours before dissipation. The shear values are less for the developing systems, but also below the $10\text{--}15 \text{ m s}^{-1}$ value generally agreed upon as the cutoff value

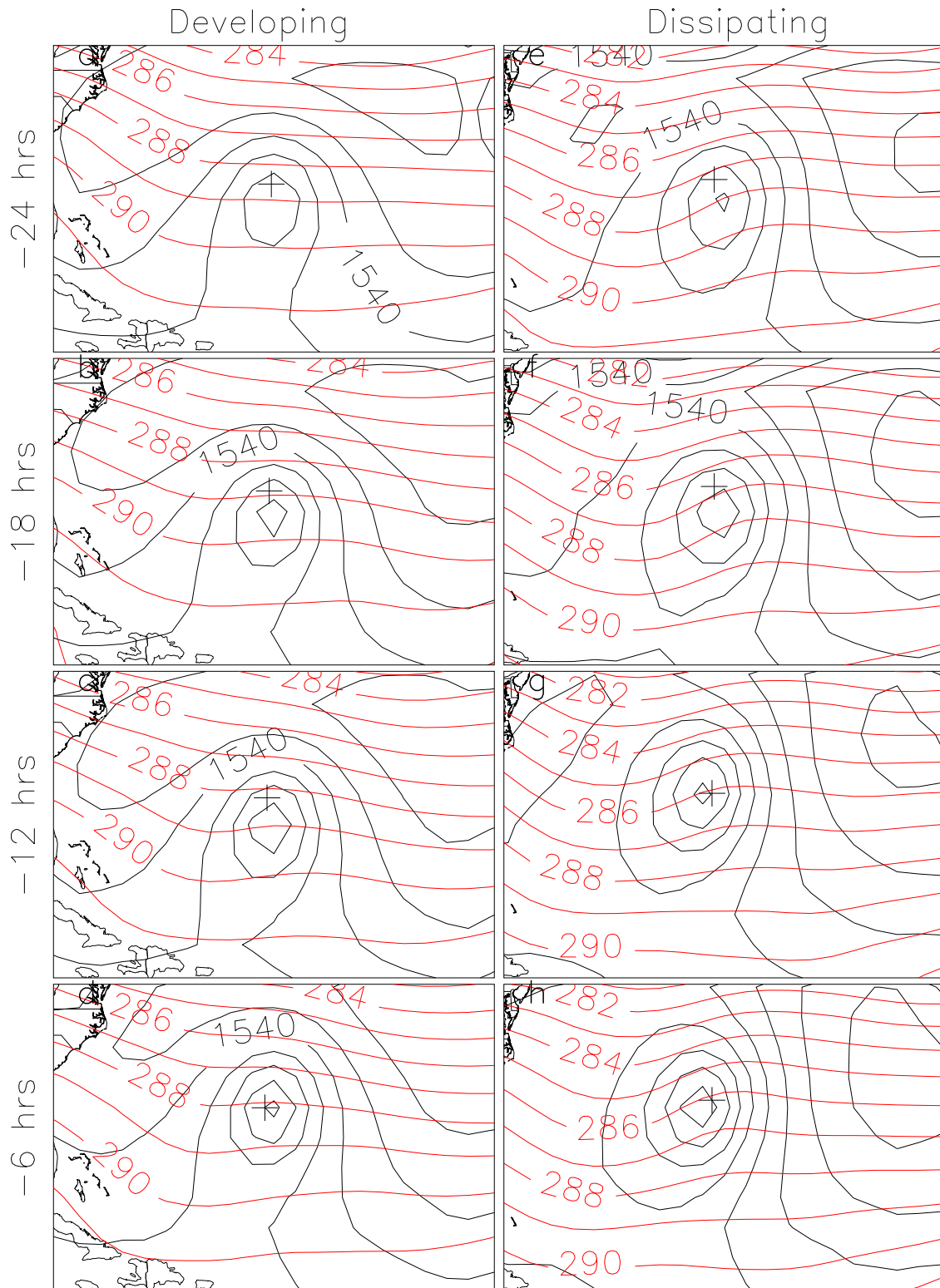


Figure 4.18: The 850-hPa height(black) and temperature(red) from the GFS analysis for the developing and dissipating composite at 24, 18, 12, and 6 hours before either development or dissipation. The height field is contoured every 10 m and the temperature field is contoured every 1 K. The “+” indicates the surface position of the composite.

Table 4.5: As in Table 4.2, but for the Gulf of Mexico systems.

Time (hours)	Developing Systems		Dissipating Systems	
	Shear	SST	Shear	SST
-24	7.6	29.5	8.1	28.7
-18	7.0	29.5	7.8	28.6
-12	7.5	29.4	7.3	28.5
-6	7.7	29.4	7.8	28.4

(DeMaria et al., 2001), above which genesis is unlikely. The shear of the composite dissipating systems, while not excessive, is within that cutoff range.

4.3.3 *Gulf of Mexico Systems*

The number of systems creating the Gulf of Mexico composites was much lower than the number going into making either the Tropical or Subtropical composites. Eighteen developing systems were used and seven dissipating systems were used. The conclusions drawn concerning the differences between composites with so few members should be viewed with some caution, but until the number of systems is increased, the analysis will proceed with what is available.

The tracks of the composite developing and dissipating disturbances show that both move to the northwest with time in the central Gulf of Mexico (4.19). The track of the developing composite was southwest of the track of the dissipating composite, but the difference in location was at no time statistically significant. Table 4.5 shows the vertical wind shear and SST for the Gulf of Mexico composites. The means of 850-200 hPa shear were not at any of the four times different by a statistically significant amount. For both systems, the mean vertical wind shear was 7–8 m s^{-1} , values not detrimental to development. The mean sea surface temperatures for the developing systems was about 29.5 °C, significantly warmer by about 1 °C than the sea surface temperature of the dissipating systems.

The composite 850-hPa height field is dominated in both cases by a trough in the central Gulf of Mexico (4.20). The trough of the dissipating composite is a bit deeper, with heights of 1500-1510 m near the center. The heights near the center of the developing composite are around 1520 m. The shapes of the

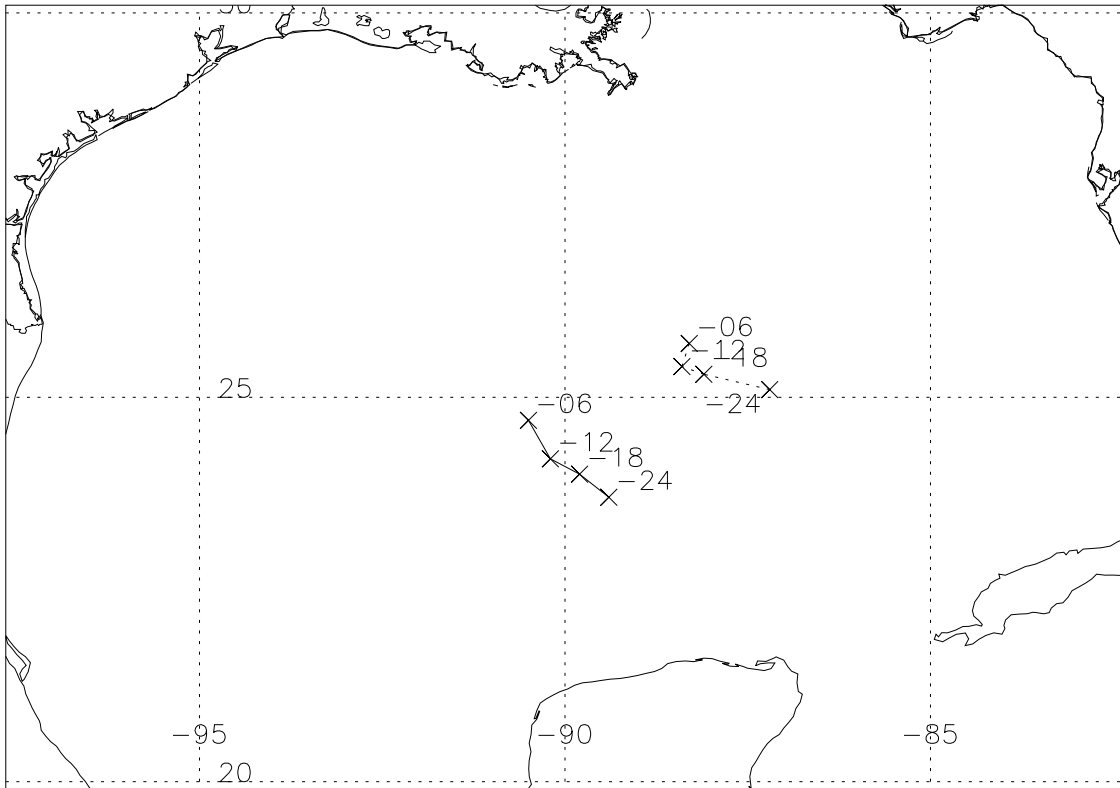


Figure 4.19: Same as 4.4, but for the Gulf of Mexico systems.

two composites are also different. Although both systems resemble the easterly wave of the Tropical disturbances, the developing composite has the more “inverted V” appearance, whereas the dissipating composite is more circular in shape, suggesting that genesis in the Gulf of Mexico is often associated with an easterly wave. Aiyyer and Molinari (2008) also found that most cyclogenesis events in the Gulf of Mexico were associated with an easterly wave, although their data set was considerably smaller, lasting only a few weeks during the 1998 season. Similar to the tropical composites, the configuration of the height field in the Gulf of Mexico also displays the asymmetric pattern of the height contours more closely packed on the eastern side of the wave than on the western side and upshear tilt.

The 850-hPa omega field for both systems is dominated by rising motion; no regions of descent are seen near either low. This is in sharp contrast with the Tropical and Subtropical cases, where a dipole of rising and sinking motion is seen. The maximum in the field of upward motion of the developing composite

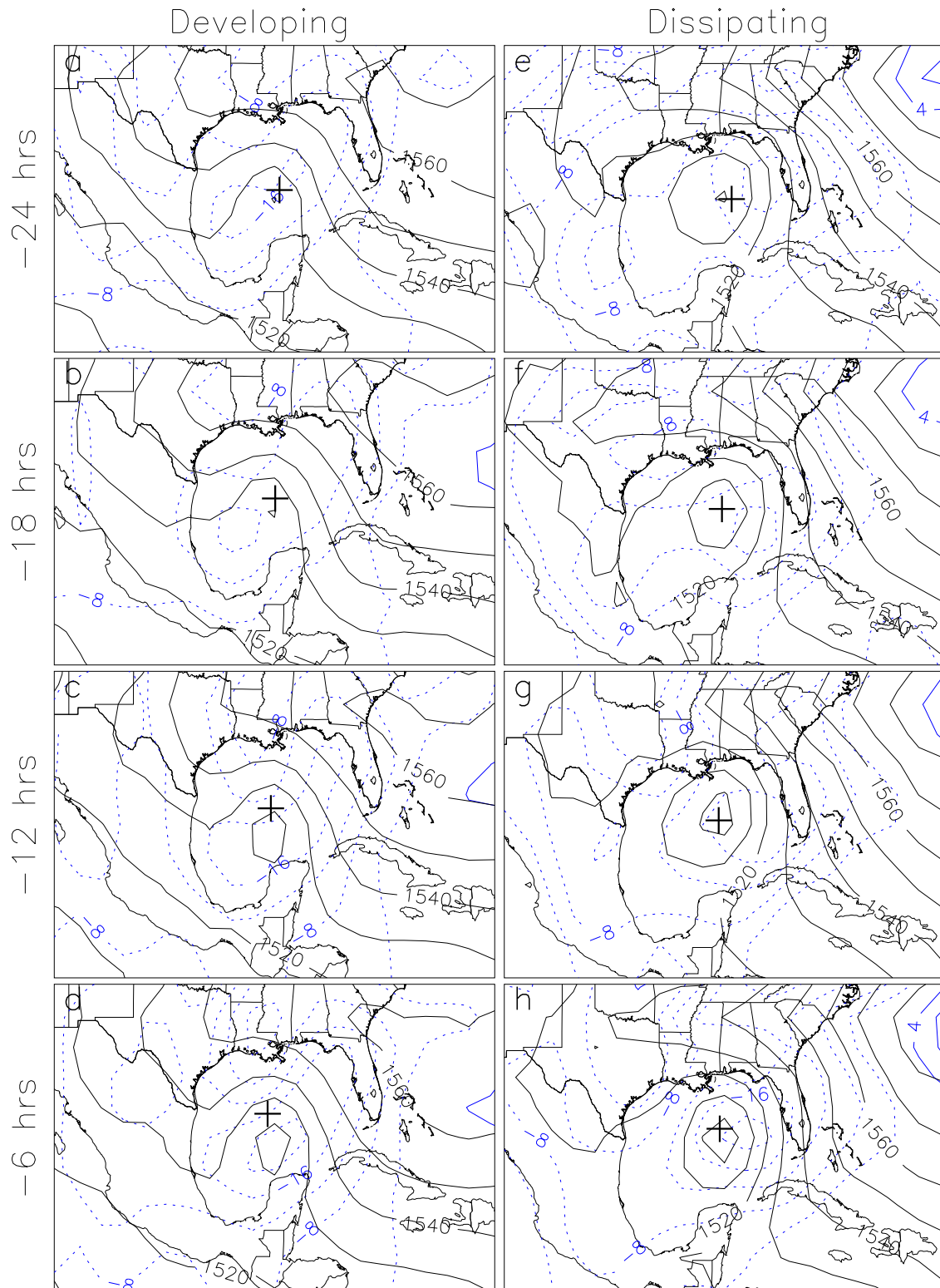


Figure 4.20: 850-hPa height (black) and omega (blue) for the developing and dissipating Gulf of Mexico composites at 24, 18, 12, and 6 hours before either genesis or dissipation. The height field is contoured every 10 meters. The omega field is contoured every 4 hPa day^{-1} , with dashed contours indicating rising motion and solid contours indicating sinking motion. The zero contour is omitted, and the “+” indicates the surface position of the composite.

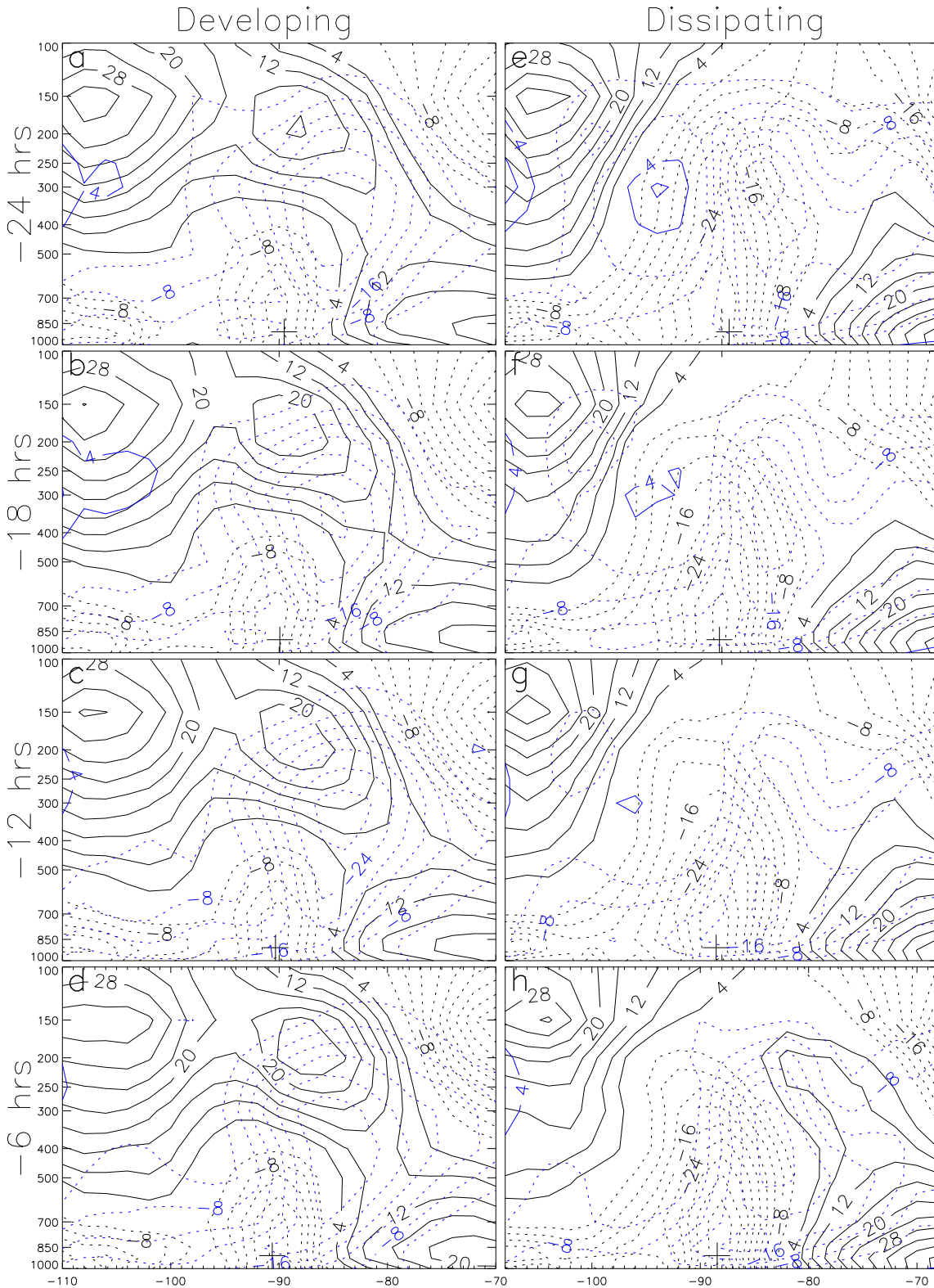


Figure 4.21: Cross section of height anomaly (black) and omega (blue) through the developing and dissipating composites at 24, 18, 12, and 6 hours before genesis or dissipation. The height anomaly is contoured every 8 meters and omega is contoured every 4 hPa day⁻¹. In both cases solid represents positive values and dashed represents negative values. The zero contour is omitted, and the “+” sign marks the surface longitude of the composite system.

is curved, beginning to the southwest of the system center and wrapping around to the east, and then to the northeast of the surface position. The strength of ascent increases from -16 hPa day^{-1} at -24 hours to -20 hPa day^{-1} at -6 hours. The maximum rising motion of the omega field of the dissipating composite is characterized by two centers. The stronger is located to the east of the surface low and strengthens from -16 hPa day^{-1} at -24 hours to -22 hPa day^{-1} at -6 hours. The weaker maxima is to the southwest. It begins at -12 hPa day^{-1} , strengthens to -14 hPa day^{-1} at -18 hours, and is not clearly evident at -6 hours, but the remaining values are between -10 and -12 hPa day^{-1} .

Distinct differences between the developing composite and the dissipating composite are also seen in the cross section through the center of the systems (4.21). The perturbation height field of the developing composite shows a structure similar to the both the developing and dissipating composite of the tropical systems (4.6), with the perturbation low at the surface laying below a perturbation high at upper levels, and with the perturbation high displaced somewhat to the east of the perturbation low. There is a difference, however, in the nature of this perturbation high and that seen in the composite of the developing tropical systems. The tropical high consisted of primarily of a single maximum, with a small secondary maximum to the west. In the Gulf of Mexico composite, the perturbation high consists of two maxima, with the western maxima ($\sim 32 \text{ m}$) stronger than the eastern maxima ($\sim 20 \text{ m}$). The composite of the dissipating systems, on the other hand, has a perturbation height field resembling that of both the developing and dissipating composites of the subtropical systems (4.15), with the perturbation low extending from the surface into the upper troposphere.

The main feature of the omega field of the developing system is a maximum of upward motion centered near 400 hPa and just to the east of the surface low. The strength of the maxima varies with time, starting at -26 hPa day^{-1} , strengthening to -28 hPa day^{-1} at -18 and -12 hours, and ending back at -26 hPa day^{-1} at -6 hours. There are three small regions of downward motion near the edges of the domain, the first at the western edge near 250 hPa , the second on the eastern edge at 200 hPa , and the third at the eastern edge at 850 hPa . The cross section of omega in the dissipating composite is also dominated by upward motion. The center of this upward motion is similar to that of the developing composite in that it is displaced to the east of the low. The magnitude of the ascent is also similar, starting and ending at -26 hPa day^{-1} . In

this case a weakening to -22 and -20 hPa day⁻¹ occurred at -18 and -12 hours, respectively. The level of the maximum upward motion was more variable in time in the dissipating composite as compared to the developing composite. This level began at 300 hPa at -24 hours, dropped to between 500 hPa and 700 hPa by -12 hours, and rose back to 400 hPa by -6 hours. The omega field also shows three areas of sinking motion. The first two are similar to those seen in the developing composite — one at upper levels on the west and one at lower levels on the east. The third is different, however, and is centered to the west of the surface center but does encroach appreciably into the perturbation low that defines the disturbance. At -24 hours it is a 8 hPa day⁻¹ maximum centered at 300 hPa. By -6 hours it weakened to -2 hPa day⁻¹ and lowered to between 300 hPa and 400 hPa. This region of subsidence is the most notable difference between the two composites in the cross section of omega. Insights into its origin can be found by looking at the component omega fields.

Examining the components which make up the rising portions of omega for the developing system at -6 hours, it can be seen that the vorticity effect plays the largest role, although both the thermal effect and the frictional effect also contribute to the upward motion. In this case, the thermal effects force rising motion only to the east of the low, whereas the frictional term forces rising motion to both the east and to the west with the ascending motion extending higher up to the west of the system. Downward motion is also forced by the vorticity and thermal effects. The thermal forcing results in two regions of downward motion on both sides of the upward motion. The effects of vorticity forcing are seen primarily along the western edge, although a small area of downward motion is seen at the surface, just below the primary region of upward motion.

The makeup of the dissipating composite at -6 hours is similar to that of the developing composite in that the vorticity forcing is responsible for the largest fraction of total rising omega, with contributions also from the thermal forcing and frictional forcing. Again, the thermal forcing results in upward motion primarily to the east of the surface low, and the frictional forcing to both sides, but to a greater depth on the western side. The primary source of the downward motion is the thermal effects acting just to the west of the system. A second area of thermally forced downward motion can be seen further to the east, beyond the region of ascent. The largest area of descent forced by the vorticity effects is seen on the western edge, with

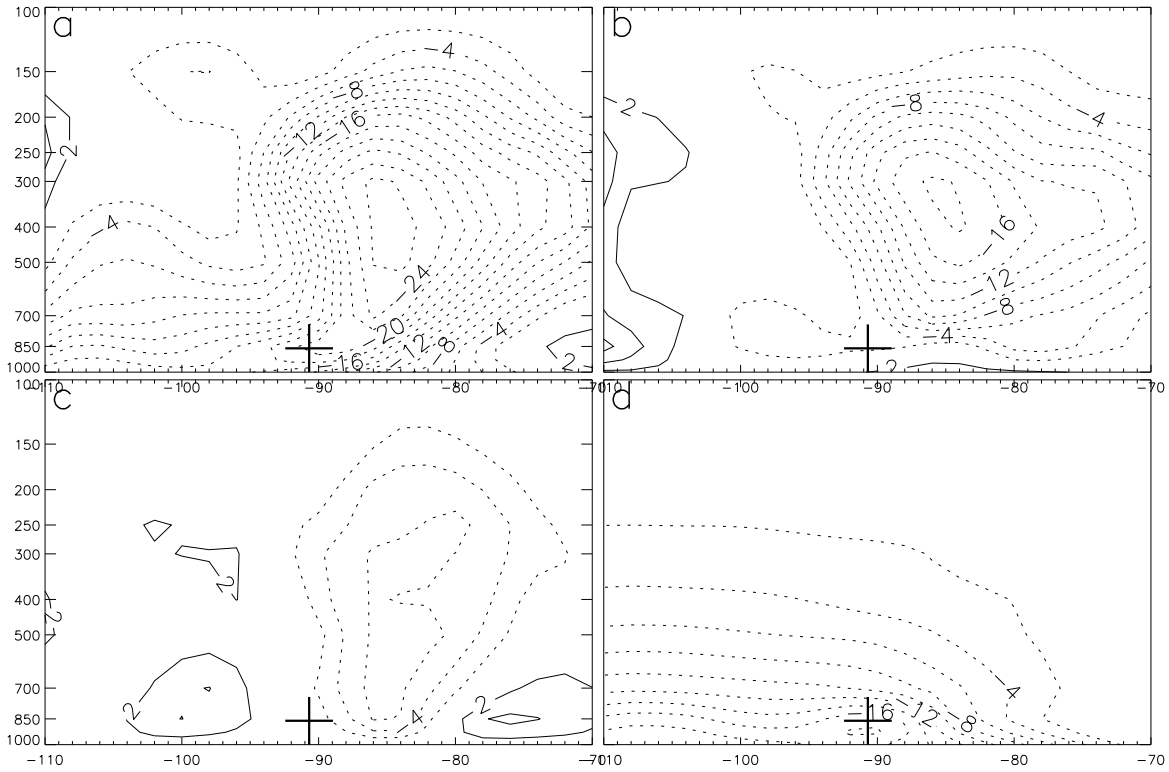


Figure 4.22: The contributions to the omega field for the Gulf of Mexico developing composite at 6 hours before development: a) total omega, b) vorticity effects, c) thermal effects d) friction effects. The omega field is contoured every 2 hPa day⁻¹, with dashed contours indicating rising motion and solid contours indicating sinking motion. The zero contour is omitted, and the “+” sign marks the surface longitude of the composite system.

an additional small area to the west of the low, near 500 hPa.

The downward motion over and to the west of the low, which is seen to be the primary distinguishing characteristic between the developing and the dissipating composites, is primarily the result of thermal forcing which is active in the middle to upper troposphere. The different configuration of the height fields and their interaction with the temperature fields illustrates this effect. As an example, Fig 4.24 shows the 250-hPa height, temperature, and thermal forcing for omega at -6 hours. The low-level center of the developing composite is located on the western periphery of a ridge in both the height field and the temperature field. The forcing for vertical motion is minimal, as the height field and the temperature field are essentially parallel, implying little warm air advection. In contrast, the height field of the dissipating composite is characterized by a trough, the height contours of which cross the temperature contours such that cold air

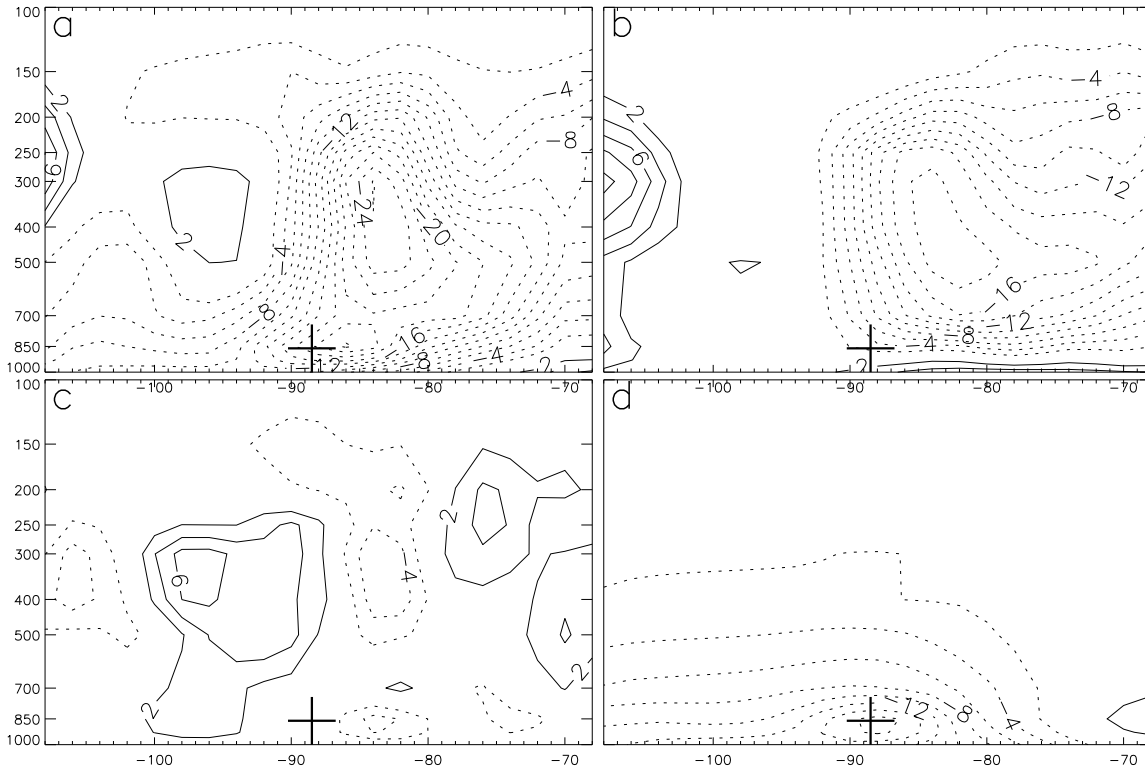


Figure 4.23: Same as 4.22, only for the dissipating composite.

advection dominates the western side of the trough and warm air advection is typical on the eastern side of the trough. Cold air advection is typically associated with descent and warm air advection with ascent, thus the sinking to the west and the rising to the east is the typical pattern seen in middle latitude troughs. In this instance, the forcing for sinking motion extends to the east such that a portion is over the surface low, just as was seen in the cross section.

Looking again at the component of omega due to the frictional forcing (Figs. 4.22d and 4.23d), it is seen that the effect of friction on the large-scale vertical velocity reaches quite a distance into the troposphere, up to 300 hPa in the dissipating composite and up to 250 hPa in the developing composite. This vertical extent exceeds that of the omega due to frictional effects in the Tropics (Figs. 4.9 d and 4.10 d) and the Subtropics (Figs. 4.16 d and 4.17 d). To understand why, consider an alternate set up to solving the omega equation than is used in this work. In the solution of the omega equation used here, the effect of friction is written as a forcing of the omega equation, i.e. a term on the right hand side of the equation. An

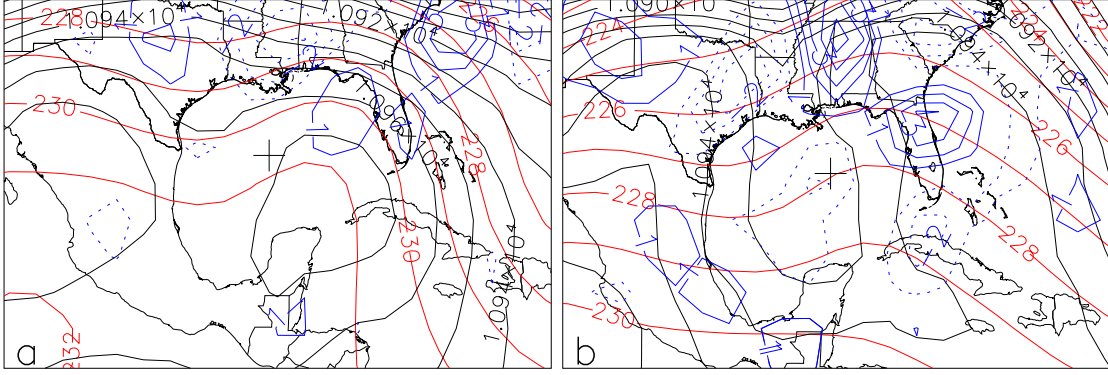


Figure 4.24: 250-hPa heights (black, m), temperature (red K), and thermal forcing for omega (blue,) for a) developing and b) dissipating composites at -6 hours. The height field is contoured every 10 m, the temperature field every 1 K, and the forcing field every $1 \times 10^{-18} \text{Pa}^{-1} \text{s}^{-3}$. The “+” indicates the surface position of the composite.

alternate approach is to compute omega at the top of the boundary layer and use that as the lower boundary condition on the solution of omega in the free atmosphere, where frictional effects are ignored. If the second method is used, the omega equation due to frictional effects in the free atmosphere is

$$\frac{R\bar{\Gamma}}{p^2} \nabla^2 \omega + 4\Omega^2 \mu^2 \frac{\partial^2 \omega}{\partial p^2} = 0.$$

Neglecting for the moment that $\mu = 0$ at the equator, the equation may be written

$$\frac{R\bar{\Gamma}}{4\Omega^2 \mu^2 p^2} \nabla^2 \omega + \frac{\partial^2 \omega}{\partial p^2} = 0.$$

Now, assuming a solution of the form $\omega(\lambda, \mu, p) = w(p) e^{i(kx+ly)}$ the equation may be written

$$\frac{d^2 w(p)}{dp^2} = (k^2 + l^2) \frac{R\bar{\Gamma}}{4\Omega^2 \mu^2 p^2} w(p).$$

Without solving the equation, some of its characteristics may be determined by noting the behavior of $\frac{d^2 w(p)}{dp^2}$ as the length scale, given by the quantity $(k^2 + l^2)$, varies. For small scales, $(k^2 + l^2)$ is large resulting in a large value for $\frac{d^2 w(p)}{dp^2}$. The second derivative is related to the curvature of a function, so for this case $w(p)$ has a large curvature. Because $w(p) = 0$ at the top of the atmosphere, this means that the magnitude of $w(p)$ decreases quickly away from the boundary layer. On the other hand, for large scales, $(k^2 + l^2)$ and $\frac{d^2 w(p)}{dp^2}$ are small, resulting in a small curvature of $w(p)$, so that its magnitude will decrease slowly with pressure, allowing it to penetrate farther into the tropopause. In this work the top of the boundary layer is

assumed to be 900 hPa. Looking at that level in the cross sections of omega force by friction, it is clear that the omega in the Gulf of Mexico composite has the largest horizontal scale, and therefore will penetrate to a greater altitude than the omega seen in the Tropics and Subtropics. It is necessary to point out that the above discussion is a mathematical argument used to explain the characteristics of the omega forced by friction within the GFS model. The cross section of the Gulf of Mexico composite does extend onto land where the interpretation of the meteorological fields is complicated by the fact that several pressure levels may be under ground. The composites of the Tropical and Subtropical systems contain very few land masses, so the effects of friction are likely to be more accurately depicted in the GFS fields.

4.4 Significance Testing

In reviewing the composites plots in the three Atlantic subbasins, distinct differences appear in the omega field between the developing and the dissipating composites. These differences are consistent with the behavior of other fields, and are supported by forecaster experience. That is, the differences between the two composites of omega are visually distinct. Additional computations are needed, however, to determine if the differences of the composite fields are statistically significant. To perform this computation, a Student's t-test was performed on the omega fields which composed the composites. The three plots to follow show the cross section of omega through the center of the developing composites in the three subbasins at -24, -18, -12, and -6 hours. Areas for which the developing composite had a significantly smaller omega (greater rising motion) are shaded in light gray, and areas for which the developing composite had a significantly larger omega (greater sinking motion) are shaded in dark gray.

In the Tropics the greater rising motion of the developing composite at the low levels of the leading (western) portion of the wave, evident in previous plots, is seen to be significant from 1000 hPa to above 700 hPa. This signal is evident at all four times and underscores the differences seen in the two composite omega fields for the tropical disturbances (Fig. 4.25). In the Subtropics the omega patterns showed that the rising and sinking branches of the omega field in the dissipating composite were of similar magnitude to the developing composite. This similarity was confirmed by the difference of means tests (Fig. 4.26). There is a small area of significantly greater upward motion of the developing composite at -18 hours in

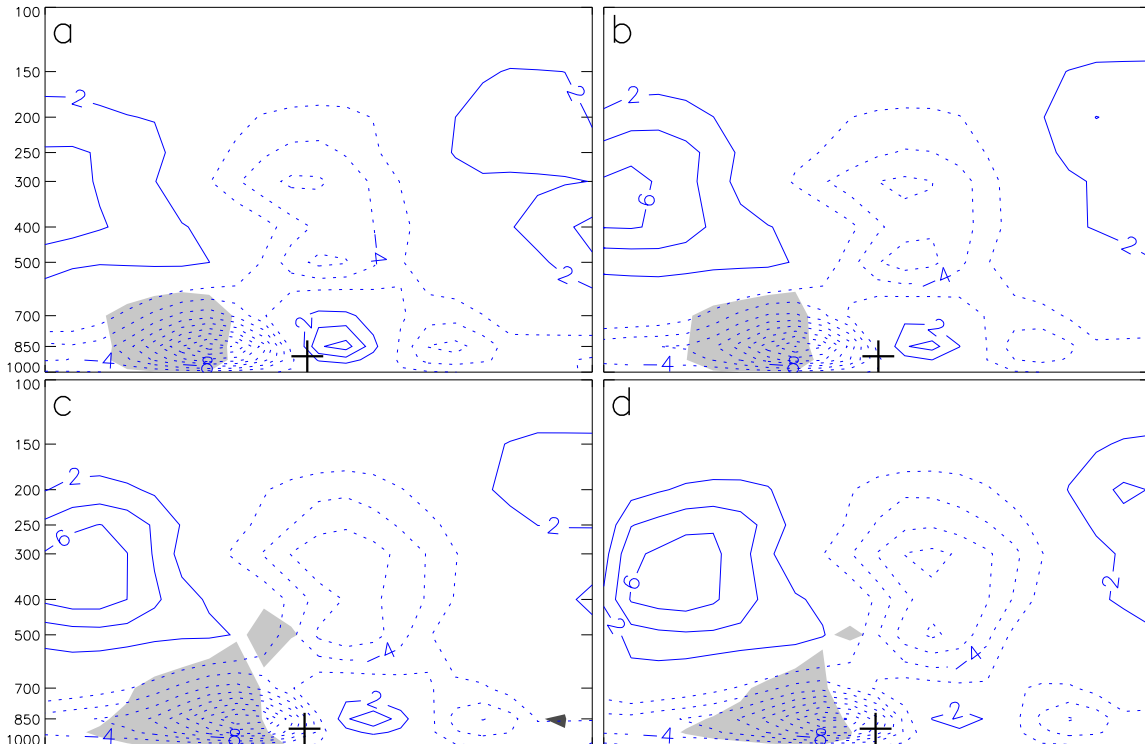


Figure 4.25: Cross sections of omega at a) -24 hours, b) -18 hours, c) -12 hours, d) -6 hours for the tropical developing composite. Areas where the developing composite has significantly greater rising motion are shaded light gray and areas where the developing composite has significantly greater sinking motion are shaded dark gray. Omega is contoured every 2 hPa day^{-1} with dashed contours indicating rising motion and solid contours indicating sinking motion. The “+” sign marks the surface longitude of the composite system.

the 200-hPa to 150-hPa layer, and a larger area near the surface at the eastern edge of the cross section at -6 hours, but these lack the areal coverage and temporal continuity seen in the statistical differences of the tropical systems. Apparently, the magnitude of omega is not as important as the midlatitude nature of the dissipating composite, with its higher shear and its northward movement into cooler waters. As has been seen in other analyses, the Gulf of Mexico case (Fig. 4.27) lies somewhere between the tropical and subtropical systems. Here, the developing composite shows some significantly greater upward motions around 300 hPa over the center of the composite at -18 hours and -12 hours. This area is likely in response to the enhanced downward motion at the rear of the upper-level trough mentioned in the discussion of the dissipating composite. A second area appears at -12 hours and likely reflects the generally broader area of

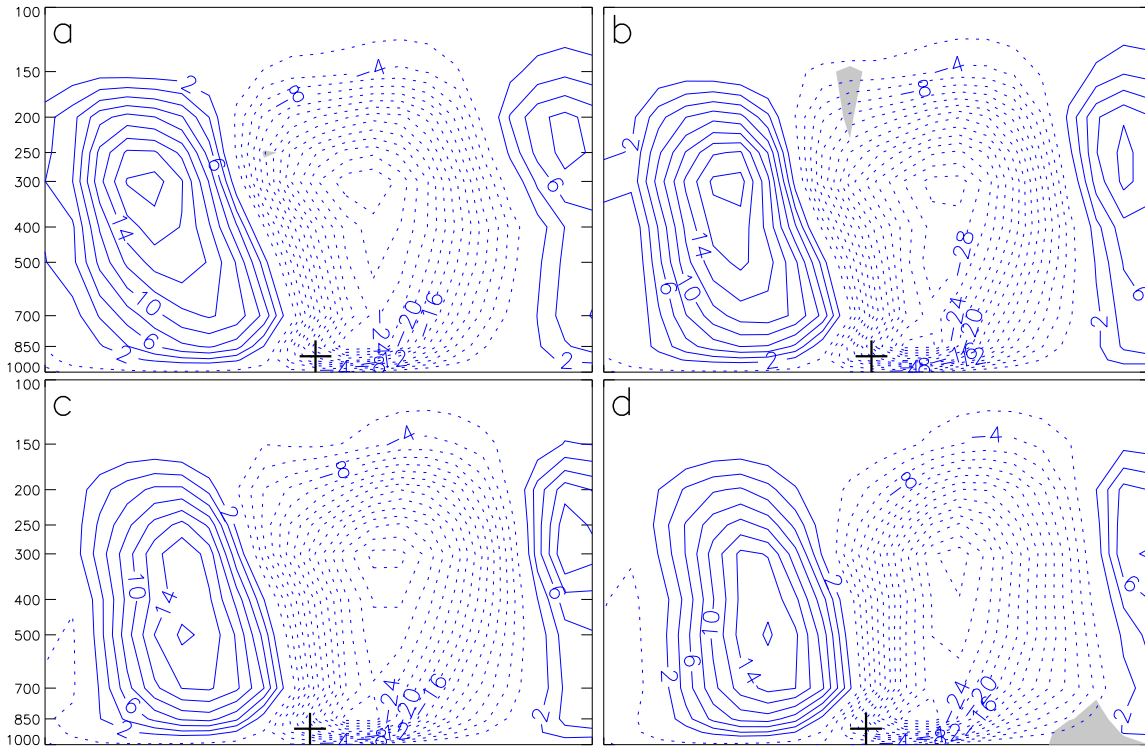


Figure 4.26: Same as Figure 4.25 but for the subtropical developing composite.

rising motion associated with the developing composite evident at -6 hours (Figs. 4.22 and 4.23). Although these areas of significantly different ascent are larger than those seen in the Subtropics (4.26), they lack the clear temporal consistency seen in the Tropics (4.25).

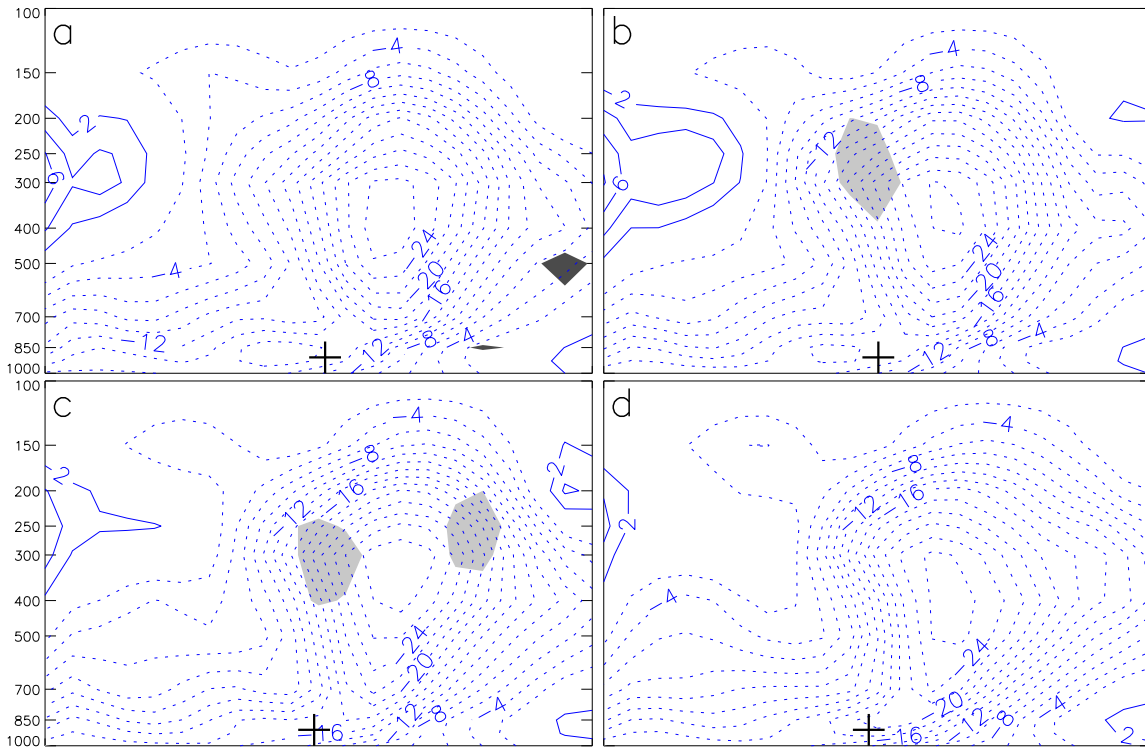


Figure 4.27: Same as Figure 4.25 but for the Gulf of Mexico developing composite.

Chapter 5

THE USE OF THE GLOBAL OMEGA AS A PREDICTOR OF TROPICAL CYCLOGENESIS IN THE ATLANTIC

To further examine the utility of the global omega equation in analyzing tropical cyclones, its quantitative performance as a discriminator in a tropical cyclogenesis product was measured. The product used is the Tropical Cyclone Formation Probability Guidance Product, or simply, the genesis product. It was developed at the Cooperative Institute for Research in the Atmosphere at Colorado State University and was transitioned to operations at the National Environmental Satellite, Data and Information Service of the National Oceanic and Atmospheric Administration. The product is a 24-hour forecast of the probability of tropical cyclogenesis in 5° latitude x 5° longitude boxes (Schumacher et al., 2009). The analysis uses a variety of input parameters in a two-step process to determine the probability of tropical cyclogenesis. The parameters are first screened to remove those points which are in an environment that is hostile to the formation of tropical cyclones. In the second step, the screened dataset is used in a linear discriminant analysis (LDA), the results of which are used to develop the probabilities of tropical cyclone formation. Seven variables are used in the linear discriminant analysis. They are climatology, 850-hPa circulation, 850-hPa divergence, the distance to any existing tropical cyclone, the vertical wind shear between 850 hPa and 200 hPa, the percent of satellite pixels less than -40° C in the water vapor ($6.7\mu m$) band, and the percentage of the analysis box which contains land. The first three—climatology, 850-hPa circulation, and the distance to any existing tropical cyclone— were found to be the largest contributors to a high probability of the formation of a tropical cyclone.

The results of the significance tests in the previous chapter were used as a guide for how to include

the global omega into the genesis product. The subtropical systems did not show any persistent areas of significantly different means. In the Gulf of Mexico, an area of significantly greater rising motion in the developing composite was seen around 300 hPa, but lasted for only two time periods. The greatest statistically significant signal was seen in the Tropics. At the leading edge of the wave from 1000 hPa to 700 hPa, the developing composite showed greater upward motion than the dissipating composite. This region existed at all four times examined. For this reason, the 850-hPa omega field was chosen as the additional input into the genesis product. In addition to having the most robust signal of statistical significance, the tropical subbasin contained most of the disturbances, with 54% of the developing and 58% of the dissipating disturbances developing in that region. The specific level of 850 hPa was chosen because it is a level frequently used for tropical analysis, and it is located near the center of the region of statistical significance.

To determine the impact that the inclusion of omega has on the probability forecast, the Brier skill score (BSS) of the forecast without omega is compared to the BSS of the forecast which includes omega as a discriminant. The BSS, as discussed by Schumacher et al. (2009), is “a measure of the improvement of a probabilistic forecast over the reference forecast and can range from $-\infty$ to 1”. A BSS of zero means the forecast probability has no skill with respect to the reference forecast. Positive numbers indicate skill with respect to the reference forecast, with 1 being a perfect score. The reference forecast used in Schumacher et al. (2009) and here is the climatological formation probability. The comparison will include the Atlantic Ocean as a whole, as well as the subregions defined by Schumacher et al. (2009). They divided the Atlantic into 5 subbasins (Figure 5.1) instead of the three used in Chapter 4 (Figure 4.3). In addition to showing the BSS results, the percent change of the BSS when the global omega is included from when it is omitted is also presented. In order to get a large enough sample for the analysis to work properly, the sample for the genesis product analysis included the years 1995-2009.

Although small, the BSSs of the forecasts without as well as with 850-hPa omega are positive, indicating skill with respect to climatology (Table 5.1). For the Atlantic Ocean as a whole, including the 850-hPa omega as an eighth discriminator improves the performance of the genesis product by 1.1% . By subbasin, the inclusion of the large-scale vertical motion at 850 hPa has a positive impact in the prediction of the probability of tropical cyclogenesis in the tropical Atlantic and the Caribbean, with an increase in

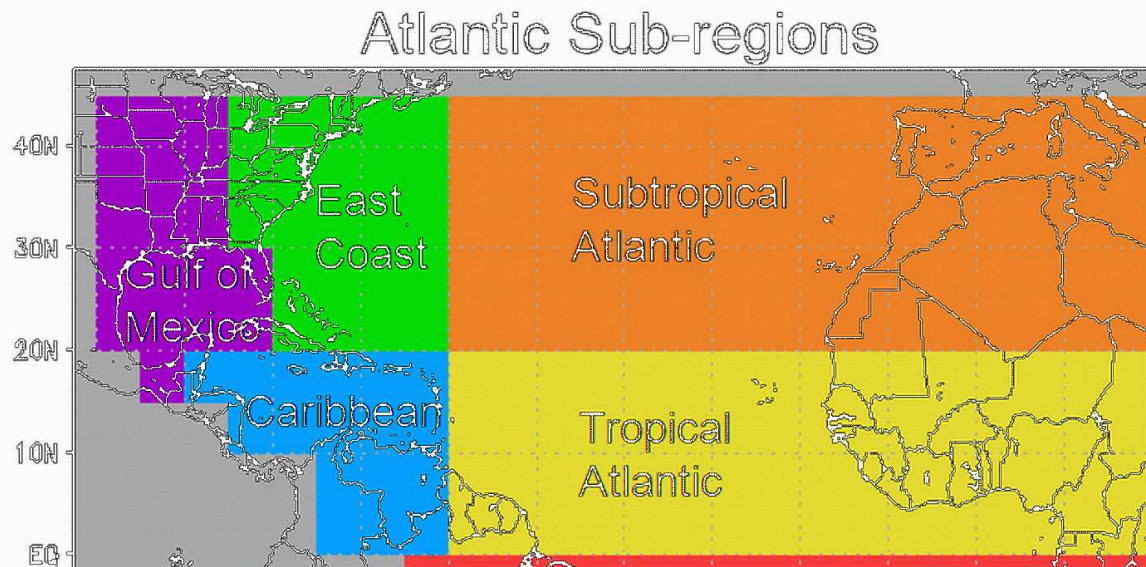


Figure 5.1: The five subregions of the Atlantic used in Schumacher et al. (2009).

BSS by 1.5% and 4.9% respectively. The combination of the tropical Atlantic and the Caribbean subbasins of Schumacher et al. (2009) is roughly equivalent to the tropical Atlantic subbasin as defined in this work. In the subtropical Atlantic, the inclusion of the 850-hPa omega acts to slightly degrade the performance of the genesis parameter (-0.8%), but in the East Coast subbasin, the impact is again positive at 2.9% improvement over the product without the 850-hPa omega. These two subbasins combine to approximately form the subtropical Atlantic subbasin defined in this work. Finally, in the Gulf of Mexico, the low-level, large-scale vertical motion improves the performance of the genesis product by 5.8%.

Although including the 850-hPa omega does result in a positive impact on the genesis parameter overall, further examination into the results of the linear discriminant analysis do show some inconsistencies with the results of Chapter 4. The LDA computes normalized coefficients, the magnitudes of which indicate the relative importance of the discriminants. The sign of the coefficient also provides a check on the physical basis of the discriminants' relation to cyclogenesis. For example, the LDA for the Atlantic as a whole produced the normalized coefficients listed in Table 5.2. As indicated above, the three largest contributors are climatology, 850-hPa circulation, and the distance to any existing tropical cyclone. This ranking is clear when looking at the respective magnitudes of their coefficients, 1.62, 1.38, and 0.69. In terms of physical

Table 5.1: Comparison of the Brier skill score for the forecast probability without 850-hPa omega and with 850-hPa omega as a discriminant. The third line shows the percent change when the 850-hPa omega is included. The results are given for the Atlantic Ocean as a whole and for each subbasin. The abbreviations are ATL=entire Atlantic, TAT=tropical Atlantic CAR=Caribbean, SAT=subtropical Atlantic, ECO=East Coast, GOM=Gulf of Mexico.

	ATL	TAT	CAR	SAT	ECO	GOM
without 850-hPa omega	0.01754	0.01964	0.03855	0.01164	0.02306	0.06382
with 850-hPa omega	0.01773	0.01994	0.04045	0.01232	0.02374	0.06330
% change	+1.1	+1.5	+4.9	-0.8	+2.9	+5.8

reasoning, consider the sign of the coefficient for the 850-hPa circulation. Because it is positive, it would be expected that the greater the circulation, the greater the probability of genesis. On the other hand, a negative coefficient such as the 850-hPa divergence implies that the lower the divergence (or greater convergence), the greater the probability of genesis. Both of these examples are consistent with a physical understanding of tropical cyclogenesis.

When viewing the 850-hPa omega under consideration of the two properties of the normalized coefficients, it is seen that the large-scale motion is only ahead of the percent land coverage in importance among the seven discriminants. Additionally, the sign of the coefficient suggests that the greater the omega, the greater the chance of genesis, which means that genesis is favored in sinking environments. This result is in contrast with the reasoning behind using the 850-hPa omega in the genesis product. That is, there was found to be a significantly greater upward motion in the developing systems than the dissipating systems in the tropics, the region in which most of the disturbances were found. This non-intuitive result could be the result of a strong correlation between the 850-hPa omega and another discriminant, but that was not found. The correct sign for the normalized coefficient for the 850-hPa omega was produces, however, when only it and the climatology term were considered in the LDA. It is assumed, therefore, that something about the LDA is generating a result which contradicts physical reasoning. To be sure, the behavior of the 850-hPa omega is unexpected. It is however, not the only discriminant which has a normalized coefficient which is inconsistent with physical reasoning. In the study of Schumacher et al. (2009), both the cloud-cleared water vapor brightness temperature, as well as the vertical instability displayed this inconsistency (Shumacher,

Table 5.2: Normalized coefficients of the LDA listed in order of decreasing magnitude. The abbreviations are: CPRB=climatological formation probability, CIRC=850-hPa circulation, DNST=distance to any existing tropical cyclone, PCCD=percentage of cold pixel coverage, VSHR=850–200-hPa vertical wind shear, HDIV=850-hPa horizontal divergence, QGOM=850-hPa omega, and PLND=percent land coverage.

Discriminant	CPRB	CIRC	DNST	PCCD	VSHR	HDIV	QGOM	PLND
Normalized coefficient	1.62	1.38	0.69	0.63	-0.29	-0.18	0.17	-0.12

personal communication).

Although the 850-hPa omega did improve the overall performance of the genesis product, it is not recommended as an additional parameter in the probability forecast, due to the uncertain nature of the relationship between the sign of the normalized coefficient and physical reasoning. Also, the LDA analysis found it to be one of the least significant contributors. Finally, unless the genesis product were to be run on a subbasin basis, it is probably not advisable to include as a discriminant a parameter for which physical reasoning suggests differing relationships to tropical cyclone formation depending on location within an ocean basin.

Chapter 6

CONCLUSION

The quasi-geostrophic system of equations, along with its associated omega equation have seen much use since their development in the middle of the 20th century. The quasi-geostrophic system was derived out of the need for a system of equations which was simple enough to be run on the early computers, yet retained enough of the complexity of the primitive equations to be useful in advancing the understanding of the large-scale motions of the atmosphere. The quasi-geostrophic equations continue to be used in research, and are a mainstay in modern education in the atmospheric and oceanic sciences.

Although its use is ubiquitous in the study of middle latitude flows such as the movement of upper-level troughs and ridges, along with their associated midlatitude cyclones, it has seen little use in the Tropics where the assumption of geostrophic balance is not as valid. In this work, a balanced system of equations valid over the whole sphere has been derived. In the derivation, three key steps were taken. First the horizontal wind was decomposed into a nondivergent and an irrotational component instead of the geostrophic and ageostrophic components as used in quasi-geostrophic theory. Second, the Coriolis parameter is assumed to be slowly varying with respect to the latitudinal variation of streamfunction defining the nondivergent flow. This assumption leads to a balance given by $2\Omega\mu\psi(\lambda, \mu, p) = \Phi(\lambda, \mu, p) - \bar{\Phi}(p)$. Third, when creating the atmosphere which contains a balance between the wind and mass fields, it is necessary to begin by defining the streamfunction of the wind, and then compute the mass field in balance with it. From the balance condition, it can be seen that this method is the only way to avoid a discontinuity at the equator. Furthermore, Phillips (1958) found in the geostrophic context that it is more accurate to begin with a wind field and from there compute the balanced mass field, than to begin with a mass field and from it compute

the balanced wind field. With these three steps, the derivation of a balanced system of equations valid for the whole sphere proceeds in a manner similar to that used to derive the quasi-geostrophic set of equations. Not surprisingly, the resulting set of equations is essentially the same in appearance as the quasi-geostrophic equations.

From this new set of equations, the derivation of an omega equation again follows just as in the quasi-geostrophic case. The omega equation takes the form

$$\begin{aligned} \frac{R\bar{\Gamma}}{p^2} \nabla^2 \omega + 4\Omega^2 \mu^2 \frac{\partial^2 \omega}{\partial p^2} &= \frac{\partial}{\partial p} [2\Omega \mu \mathbf{v}_\psi \cdot \nabla (\zeta + 2\Omega \mu)] \\ &- \nabla^2 \left[2\Omega \mu \mathbf{v}_\psi \cdot \nabla \left(\frac{\partial \psi}{\partial p} \right) \right] - \frac{\partial}{\partial p} (2\Omega \mu \mathbf{k} \cdot \nabla \times \mathbf{F}). \end{aligned}$$

That is, the large-scale vertical motion associated with this balanced system of equations is forced by the vertical derivative of vorticity advection by the nondivergent wind and the Laplacian of the advection of the temperature by the nondivergent wind. It is similar to the quasi-geostrophic omega equation except that horizontal advectons are accomplished by the non-divergent wind instead of the geostrophic wind, and that the Coriolis parameter is allowed its full variation. This variation is assumed to be slow with respect to the variation of the streamfunction, however, meaning that the approximation breaks down as the meridional variations of the streamfunction decrease (sectoral harmonics). In this formulation the frictional force was retained, using the results of Krishnamurti (1968a), who noted that because the dynamical forcing in the Tropics is weaker than in midlatitudes, the frictional force may approach, if not exceed, the magnitude of the dynamical forcing in the omega equation. In addition to this “traditional” form of the omega equation, a \mathbf{Q} form of the omega equation may be derived. Here there is a slight departure from the standard f -plane derivation of the \mathbf{Q} form of the omega equation. Further use of the approximation of the slowly-varying μ is necessary, and as a result, the traditional form of the omega equation was used for the rest of the study. The traditional form has its drawbacks, too. Care must be taken not to draw too many conclusions from examining the omega resulting from the vorticity forcing or the thermal forcing alone, as they have a mutual term which cancels upon their summation. Using those terms in isolation as a means of searching for the processes responsible for the vertical motions of a system, and not to make calculations of the vertical motions themselves, can still provide insight into the workings of the atmosphere. In order to solve the

omega equation over the entire sphere, it was transformed using normal modes in the vertical and spherical harmonics in the horizontal. This transformation results in a system of equations for each vertical and zonal mode which is then solved to get the spherical harmonic coefficients. The inverse Legendre, Fourier, and vertical normal mode transfers are then performed to arrive at the solution in physical space.

The equations constituting the balanced system derived in this work, and their associated omega equation represent a new tool in the study of the atmosphere. In particular, the large-scale motion associated with tropical disturbances can be studied with the globally-valid omega equation in a manner similar to which the large-scale vertical motions of midlatitude weather systems have been extensively examined using the quasi-geostrophic equations. The role of synoptic-scale forcing in relation to tropical cyclogenesis mirrors the role that Doswell (1987) suggested for synoptic-scale forcing of deep midlatitude convection. That is, it is not vigorous enough to account for the magnitudes of the vertical motion observed in tropical cyclones, but rather acts to condition the atmosphere by reducing the static stability, making the atmosphere more conducive to the deep, moist convection necessary to form and sustain a tropical cyclone.

In applying the global omega equation to tropical cyclogenesis, the Atlantic Ocean was chosen as the basin of study. Data for the 154 named storms of the 2001-2009 Atlantic seasons were collected from the NHC archives. Composite systems, composed of the disturbances associated with the named storms at 24, 18, 12, and 6 hours before genesis, were created using the fields of height, temperature, the u- and v-wind components, relative humidity, and omega. Composite systems of those disturbances which eventually dissipated were also created, again for 24, 18, 12, and 6 hours before dissipation. For these systems, a dataset consisting of Dvorak satellite fixes compiled at Florida State University was used. Because genesis displays different characteristics depending on where in the Atlantic a cyclone forms, the composites were created according to the subbasin in which the disturbance was found. Three subbasins were used — the tropical Atlantic, the subtropical Atlantic, and the Gulf of Mexico. As hypothesized, the composite systems did show different characteristics according to the different subbasins.

The tropical Atlantic subbasin contained the largest fraction of both developing systems (83) and dissipating systems (58). Both composites displayed a structure in the height field characteristic of a tropical wave, with a ridge above an inverted-V trough at low levels. The trough showed the upshear tilt noted by

Reed et al. (1977). Some differences between the two composites were seen already in the conventional measures of cyclogenesis potential. First the height field of the developing composite was characterized by greater (in magnitude) negative height anomalies than the dissipating composite, indicating a stronger wave. The SSTs were different statistically, but only by 0.3-0.4°C. The 850-200 hPa shear was also less in the developing composite by a statistically significant value of more than 2 ms⁻¹. Rising motion was seen ahead of both composites at low levels, which upon looking at the omega for the individual forcing terms (vorticity, thermal, and friction), the frictional effect was seen to dominate, although the four-celled pattern of omega associated with the vorticity forcing was also evident and was the primary contributor to the pattern of omega at mid and upper levels. The vertical motion at the mid and upper levels was, however, noticeably weaker than at low levels. Differences in the forcing due to the thermal term appear to be associated with the different alignment of the low-level height and temperature fields, with the dissipating composite suggesting a greater interaction of the warm air of the Saharan Air Layer with the wave. This interaction was also seen in the relative humidity composite suggesting that dry air was also a likely factor in its demise. The tropical Atlantic composites were also used to demonstrate the indirect role that large-scale vertical motions have in the tropical cyclogenesis process. By applying the vertical divergence profile of each composite to a typical tropical sounding, it was shown that the flow of the developing composite was able to create greater instability by moistening the sounding than the dissipating composite, as seen in the greater CAPE values as well as lower numbers for the CIN and LFC.

Fifty-three disturbances went into the developing composite and 35 disturbances went into the dissipating composite of the subtropical Atlantic. Both the developing composite and dissipating composites in the Subtropics were characterized by a trough existing not only at low levels, but throughout the troposphere. It was seen that the height and temperature fields of the dissipating composite were much more reminiscent of a midlatitude low, with the composite upper-level trough acquiring an increasingly negative tilt with time, and a low-level temperature and omega field indicative of a cold front. In contrast, the upper-level trough of the developing composite was more closed and cutoff in appearance. In spite of these differences, both the developing and dissipating systems produced vertical motions throughout the depth of the troposphere, with all three components (vorticity, thermal, and frictional) contributing. The dissipating composite, however,

was further north and east, placed over significantly cooler water to the east of the Gulf Stream. It was also in significantly greater shear, with values approaching those generally considered to be disruptive to genesis. In addition, the low-level center of the composite dissipating disturbance travelled a greater distance than the low-level center of the developing composite. The direction of this motion was to the northeast, toward cooler waters. On the other hand, the developing composite existed over 27°C waters and under the influence of less shear (10 ms⁻¹ at -24 hours and dropping to 8 ms⁻¹ by -6 hours). Also, its more stationary nature was conducive to concentrating the convection in a localized area, ultimately resulting in the formation of a tropical cyclone.

Of the three subbasins, the Gulf of Mexico had the fewest of both the developing systems (18) and dissipating systems (7). These numbers are lower than would be desired, but composites were created nevertheless. The composites contained some characteristics of both the Tropical disturbances and the Subtropical disturbances. At low levels, the height fields of both systems had the appearance of an easterly wave, with the developing composite displaying a more traditional inverted-V shape. The height field of the developing composite was characterized by a ridge in the upper troposphere, just as in the developing composite of the tropical subbasin. The negative height anomaly of the dissipating composite extended to the upper levels, just as in the developing and dissipating composites of the Subtropics. The omega field at lower levels for both composites was dominated by rising motion. At upper-levels, however, the dissipating composite showed some descending motion associated with the upper trough. This region of descent extended into the negative height anomaly defining the system. There existed no significant differences in the 850-200 hPa shear, but the developing composites were over water which was about 1°C warmer than the dissipating composite.

In all three regions, the magnitude of the vertical velocities was roughly an order of magnitude too weak compared to the 100 hPa day⁻¹ suggested by (McBride and Zehr, 1981) as necessary for the formation of a tropical cyclone. It is apparent, then, that the role which large-scale vertical velocities play in the formation of tropical cyclones is one of conditioning the atmosphere. Bracken and Bosart (2000) also came to this conclusion by examining the forcing for vertical motions over tropical disturbances using a much simplified omega equation. They propose that synoptic-scale vertical motions act to “1) produce a large

area of tropospheric-deep lift over the low-level cyclonic vorticity maximum, thereby creating a favorable environment for strong upward motion and thunderstorm initiation when mesoscale lift is also present; and 2) destabilize the air and/or remove any capping trade wind inversions through that ascent if the air is neutrally buoyant or stable over large areas.” Certainly the results of this study confirm 2). Agreement with the first assumption is not entirely complete, however, with regards to the depth of the large-scale vertical velocities. In the Subtropics and Gulf of Mexico composites the depth of the rising motion did extend throughout the troposphere. The tropical composite showed some weak rising motion at mid to upper levels on the eastern edge of the wave, but on the western edge, where Bracken and Bosart (2000) showed forcing for ascent, the rising motion in this study was limited to the low levels. Their simplified omega equation measured the forcing for omega at only one layer, assuming that to be representative of the vertical motion through the depth of the troposphere. It is perhaps this coarseness relative to the present study which resulted in the discrepancy.

The Student’s t-test was applied to the omega fields constituting the composites to see if there were any areas where the difference in the means of the developing and dissipating systems was statistically significant. Despite what appeared to be distinct differences in the omega field of the two composites in all three basins, only the omega field of the tropical Atlantic showed a consistent signal of statistical significance. The rising motion at low levels ahead of the developing composite was significantly greater than in the dissipating composite. Using this result, the 850-hPa omega was chosen to be used as an additional discriminant in the Tropical Cyclone Formation Guidance Product, or simply genesis product. Although it did improve the genesis product’s performance as measured by the Brier skill score, the behavior of the normalized coefficient assigned to the 850-hPa omega remains unclear. The analysis suggested that the greater the sinking motion, the greater the probability of formation, which is in direct conflict with the physical reasoning supported by the composite analysis. Thus, the 850-hPa omega is not a viable candidate for an additional discriminant in the genesis product. Perhaps omega could better serve the genesis product in the screening step, by eliminating from consideration those data points dominated by subsidence.

As a new tool, the global balance equations, along with the associated omega equation can be applied to a myriad of atmospheric problems. They will be found most useful perhaps, in the study of those

phenomena occurring at low latitudes, such as the study of tropical cyclones, or systems which cover a large portion of the globe, such as tropical cyclones undergoing extratropical transition, and Rossby wave trains.

REFERENCES

- Adams, J. C., and P. N. Swarztrauber, 1999: SPHEREPACK 3.0: A model development facility. *Mon. Wea. Rev.*, **127**, 1872–1878.
- Aiyyer, A. R., and J. Molinari, 2008: MJO and tropical cyclogenesis in The Gulf of Mexico and eastern Pacific: Case study and idealized numerical modeling. *J. Atmos. Sci.*, **65**, 2691–2704.
- Andrews, D. G., J. R. Holton, and C. B. Leovy, 1987: *Middle Atmosphere Dynamics*. Academic Press, 489 pp.
- Arakawa, A., 2000: A personal perspective on the early years of general circulation modeling at UCLA. *General circulation model development: Past, present, and future*, D. A. Randall Ed., Academic Press, 1–66.
- Baumhefner, D. P., 1968: Application of a diagnostic numerical model to the tropical atmosphere. *Mon. Wea. Rev.*, **96**, 218–228.
- Belousov, S. L., 1962: *Tables of Normalized Associated Legendre Polynomials*. Pergamon Press, 379 pp.
- Bister, M. and K. A., Emanuel, 1997: The genesis of Hurricane Guillermo: TEXMEX analyses and a modeling study. *Mon. Wea. Rev.*, **125**, 2662–2682.
- Blackburn, M., 1985: Interpretation of ageostrophic winds and implications for jet stream maintenance. *J. Atmos. Sci.*, **42**, 2604–2620.
- Bluestein, H. B., 1992: *Synoptic-Dynamic Meteorology in Midlatitudes. Vol.1*. Oxford University Press, 431 pp.
- Bluestein, H. B., 1993: *Synoptic-Dynamic Meteorology in Midlatitudes. Vol.2*. Oxford University Press, 594 pp.
- Bracken, W. E., and L. F. Bosart, 2000: The role of synoptic-scale flow during tropical cyclogenesis over the North Atlantic Ocean. *Mon. Wea. Rev.*, **128**, 353–376.
- Burpee, R. W., 1972: The origin and structure of easterly waves in the lower troposphere of North Africa. *J. Atmos. Sci.*, **29**, 77–90.
- Carlson, T. N., 1998: *Mid-Latitude Weather Systems*. American Meteorological Society, 507 pp.
- Charney, J. G., 1948: On the scale of atmospheric motions. *Geofys. Publ.*, **17**, 1–17.

- Charney, J. G., 1949: On a physical basis for numerical prediction of large-scale motions in the atmosphere. *J. Meteor.*, **6**, 371–385.
- Charney, J. G., 1955: The use of the primitive equations of motion in numerical prediction. *Tellus*, **7**, 22–26.
- Charney, J. G., 1960: Integration of the primitive and balance equations. *International Symposium on Numerical Weather Prediction*, Tokyo, Meteorological Society of Japan.
- Charney, J. G., 1963: A note on large-scale motions in the Tropics. *J. Atmos. Sci.*, **20**, 607–609.
- Charney, J. G., 1971: Geostrophic turbulence. *J. Atmos. Sci.*, **28**, 1087–1095.
- Charney, J. G., and P. G. Drazin, 1961: Propagation of planetary-scale disturbances from the lower into the upper atmosphere. *J. Geophys. Res.*, **66**, 83–109.
- Charney, J. G., R. Fjortoft, and J. von Neumann, 1950: Numerical integration of the barotropic vorticity equation. *Tellus*, **2**, 237–254.
- Charney, J. G., and M. E. Stern, 1962: On the stability of internal baroclinic jets in a rotating atmosphere. *J. Atmos. Sci.*, **19**, 159–172.
- Cossuth, J. H., R. D. Knabb, and D. P. Brown, 2010: Climatology of dvorak classifications to support operational probabilistic tropical cyclogenesis forecasts. *29th Conf. on Hurricane and Tropical Meteorology*, Tuscon, AZ, Amer. Meteor. Soc.
- Daley, R. W., 1983: Linear non-divergent mass-wind laws on the sphere. *Tellus*, **35**.
- DeMaria, M., 2009: A simplified dynamical system for tropical cyclone intensity prediction. *Mon. Wea. Rev.*, **137**, 68–82.
- DeMaria, M., and J. Kaplan, 2001: An updated statistical hurricane intensity prediction scheme (SHIPS) for the Atlantic and Eastern North Pacific Basins. *Wea. Forecasting*, **14**, 326–337.
- DeMaria, M., J. A. Knaff, and B. H. Connell, 2001: A tropical cyclone genesis parameter for the tropical Atlantic. *Wea. Forecasting*, **16**, 219–233.
- DiMego, G. J., and L. F. Bosart, 1982: The transformation of Tropical Storm Agnes into an extratropical cyclone. Part I: The observed fields and vertical motion computations. *Mon. Wea. Rev.*, **110**, 385–411.
- Doswell, C. A. I., 1987: The distinction between large-scale and mesoscale contribution to severe convection: A case study example. *Wea. Forecasting*, **2**, 3–16.
- Dunion, J. P., 2011: Rewriting the climatology of the tropical north Atlantic and Caribbean sea atmosphere. *J. Climate*, **24**, 893–908.
- Dunion, J. P., and C. S. Velden, 2004: The impact of the Saharan air layer on Atlantic tropical cyclone activity. *Bull. Amer. Meteor. Soc.*, **85**, 353–365.
- Dunkerton, T. J., M. T. Montgomery, and Z. Wang, 2009: Tropical cyclogenesis in a tropical wave critical layer: Easterly waves. *Atmos. Chem. Phys.*, **9**, 5587–5646.
- Dvorak, V. F., 1975: Tropical cyclone intensity analysis and forecasting from satellite imagery. *Mon. Wea. Rev.*, **103**, 420–430.

- Dvorak, V. F., 1984: Tropical cyclone intensity analysis using satellite data. Tech. rep., NOAA Tech. Rep. NESDIS 11, 47 pp., Washington, D. C.
- Frank, N. L., 1969: The “inverted V” cloud pattern — an easterly wave? *Mon. Wea. Rev.*, **97**, 130–140.
- Frank, W. M., 1977: The structure and energetics of the tropical cyclone I. storm structure. *Mon. Wea. Rev.*, **105**, 1119–1135.
- Frank, W. M., 1987: Tropical cyclone formation. *A Global View of Tropical Cyclones*.
- Fulton, S. R., and W. H. Schubert, 1985: Vertical normal mode transforms: Theory and application. *Mon. Wea. Rev.*, **113**, 647–658.
- Gill, A. E., 1982: *Atmosphere-Ocean Dynamics*. Academic Press, 662 pp.
- Gray, W. M., 1968: Global view of the origin of tropical disturbances and storms. *Mon. Wea. Rev.*, **96**, 669–700.
- Gray, W. M., 2000: General characteristics of tropical cyclones. *Storms*, R.A. Pielke, Sr. and R.A. Pielke, Jr., Ed., Routledge Press, 145–163.
- Haltiner, G. J., 1971: *Numerical Weather Prediction*. John Wiley and Sons, 317 pp.
- Holton, J. R., 1992: *An Introduction to Dynamic Meteorology 3rd ed.* Academic Press, 511 pp.
- Hopsch, S. B., C. D. Thorncroft, and K. R. Tyle, 2010: Analysis of easterly wave structures and their role in influencing tropical cyclogenesis. *Mon. Wea. Rev.*, **138**, 1399–1419.
- Hoskins, B. J., I. Draghici, and H. C. Davies, 1978: A new look at the ω -equation. *Quart. J. Roy. Meteor. Soc.*, **104**, 31–38.
- Hoskins, B. J., M. E. McIntyre, and A. W. Robertson, 1985: On the use and significance of isentropic potential vorticity maps. *Quart. J. Roy. Meteor. Soc.*, **111**, 877–946.
- Jordan, C. L., 1958: Mean soundings for the West Indies area. *J. Meteor.*, **15**, 91–97.
- Kiladis, G. N., M. C. Wheeler, P. T. Haertel, K. H. Straub, and P. E. Roundy, 2009: Convectively coupled equatorial waves. *Rev. Geophys.*, **47**, RG2003,doi:10.1029/2008RG000 266.
- Krishnamurti, T. N., 1968a: A diagnostic balance model for studies of weather systems of low and high latitudes, Rossby number less than 1. *Mon. Wea. Rev.*, **96**, 197–207.
- Krishnamurti, T. N., 1968b: A study of a developing wave cyclone. *Mon. Wea. Rev.*, **96**, 208–217.
- Kuo, H. L., 1959: Finite-amplitude three-dimensional harmonic waves on the spherical earth. *J. Meteor.*, **16**, 524–534.
- Landsea, C. W., 1993: A climatology of intense (or major) Atlantic hurricanes. *Mon. Wea. Rev.*, **121**, 1703–1713.
- Landsea, C. W., G. D. Bell, W. M. Gray, and S. B. Goldenberg, 1998: The extremely active 1995 Atlantic hurricane season: Environmental conditions and verification of seasonal forecasts. *Mon. Wea. Rev.*, **126**, 1174–1193.

- Lorenz, E. N., 2006: Reflections on the conception, birth, and childhood of numerical weather prediction. *Annu. Rev. Earth Planet. Sci.*, **34**, 37–45.
- Martin, J. E., 2006: The role of shearwise and transverse quasigeostrophic vertical motions in the midlatitude cyclone life cycle. *Mon. Wea. Rev.*, **134**, 1174–1193.
- McBride, J. L., 1981: Observational analysis of tropical cyclone formation. Part I: Basic description of data sets. *J. Atmos. Sci.*, **38**, 1117–1131.
- McBride, J. L., and R. M. Zehr, 1981: Observational analysis of tropical cyclone formation. Part II: Comparison of non-developing versus developing systems. *J. Atmos. Sci.*, **38**, 1132–1151.
- Mekonnen, A., C. D. Thorncroft, and A. R. Aiyyer, 2006: Analysis of convection and its association with African easterly waves. *J. Climate*, **19**, 5405–5421.
- Miller, A., and H. A. Panofsky, 1958: Large-scale vertical motions and weather in January, 1953. *Bull. Amer. Meteor. Soc.*, **39**, 8–13.
- Miller, R. J., A. J. Schrader, C. R. Sampson, and T. L. Tsui, 1990: The Automated Tropical Cyclone Forecasting System (ATCF). *Wea. Forecasting*, **5**, 653–660.
- Munk, W. H., 1950: On the wind-driven ocean circulation. *J. Meteor.*, **7**, 79–93.
- Musgrave, K. D., C. A. Davis, and M. T. Montgomery, 2008: Numerical simulations of the formation of hurricane Gabrielle (2001). *Mon. Wea. Rev.*, **136**, 3151–3167.
- O'Brien, J., 1970: Alternative solutions to the classical vertical velocity problem. *J. Appl. Meteor.*, **9**, 197–203.
- Palmén, E. H., 1948: On the formation and structure of tropical cyclones. *Geophysica*, **3**, 26–38.
- Pauley, P. M., and S. J. Nieman, 1992: A comparison of quasigeostrophic and nongeostrophic vertical motions for a model-simulated rapidly intensifying marine extratropical cyclone. *Mon. Wea. Rev.*, **120**, 1108–1134.
- Pedlosky, J., 1987: *Geophysical Fluid Dynamics*. Springer, 710 pp.
- Phillips, N. A., 1958: Geostrophic errors in predicting the Appalachian storm of November 1950. *Geophysica*, **6**, 389–405.
- Phillips, N. A., 1963: Geostrophic motion. *Rev. Geophys.*, **1**, 123–205.
- Raisanen, J., 1995: Factors affecting synoptic-scale vertical motions: A statistical study using a generalized omega equation. *Mon. Wea. Rev.*, **123**, 2447–2460.
- Reed, R. J., D. C. Norquist, and E. E. Recker, 1977: The structure and properties of African wave disturbances as observed during phase III of GATE. *Mon. Wea. Rev.*, **105**, 317–333.
- Reynolds, R. W., and T. M. Smith, 1993: An improved real-time global sea surface temperature analysis. *J. Climate*, **6**, 114–119.
- Riehl, H., 1948: On the formation of typhoons. *J. Meteor.*, **5**, 247–264.

- Sampson, C. R., and A. J. Schrader, 2000: The Automated Tropical Cyclone Forecasting System (Version 3.2). *Bull. Amer. Meteor. Soc.*, **81**, 1231–1240.
- Sardeshmukh, P. D., and B. J. Hoskins, 1984: Spatial smoothing on the sphere. *Mon. Wea. Rev.*, **112**, 2524–2529.
- Schubert, W. H., R. K. Taft, and L. G. Silvers, 2009: Shallow water quasi-geostrophic theory on the sphere. *J. Adv. Model. Earth Syst.*, **1**, 1–11.
- Schumacher, A. B., M. DeMaria, and J. A. Knaff, 2009: Objective estimation of the 24-h probability of tropical cyclone formation. *Wea. Forecasting*, **1**, 456–471.
- Shea, D. J., and W. M. Gray, 1973: The hurricane's inner core region. I. symmetric and asymmetric structure. *J. Atmos. Sci.*, **30**, 1544–1564.
- Sinclair, M. R., and M. J. Revell, 2000: Classification and composite diagnosis of extratropical cyclogenesis events in the southwest Pacific. *Mon. Wea. Rev.*, **128**, 1089–1105.
- Sutcliffe, R. C., 1947: A contribution to the problem of development. *Quart. J. Roy. Meteor. Soc.*, **73**, 370–383.
- Trenberth, K. E., 1978: On the interpretation of the diagnostic quasigeostrophic omega equation. *Mon. Wea. Rev.*, **106**, 131–137.
- Vallis, G. K., 2006: *Atmospheric and Oceanic Fluid Dynamics: Fundamentals and Large-scale Circulation*. Cambridge University Press, 745 pp.
- Verkley, W. T. M., 2009: A balanced approximation of the one-layer shallow-water equations on the sphere. *J. Atmos. Sci.*, **66**, 1735–1748.
- Williams, G. J., R. K. Taft, B. D. McNoldy, and W. H. Schubert, 2012: Shock-like structures in the tropical cyclone boundary layer. *J. Adv. Model. Earth Syst.*, Submitted.
- Willoughby, H. E., 1998: Tropical cyclone eye thermodynamics. *Mon. Wea. Rev.*, **126**, 3053–3067.

Appendix A

DERIVATION OF THE VERTICAL TRANSFORM PAIR FOR ω

In chapter 3, the equations governing the forward (3.13a) and inverse (3.13b) transform pair for ω were presented without derivation. In this appendix, each equation will be derived, starting with (3.13b).

A.1 Derivation of the inverse transform for ω

Assume the inverse transform of ω takes the form

$$\omega(\lambda, \mu, p) = \sum_{\ell=0}^{\infty} \omega_{\ell}(\lambda, \mu) \alpha_{\ell} A_{\ell}(p), \quad (\text{A.1})$$

where α_{ℓ} is a value which makes the quantity $\alpha_{\ell} A_{\ell}(p)$ unitless, such that $\omega(\lambda, \mu, p)$ and $\omega_{\ell}(\lambda, \mu)$ have the same units. The continuity equation can then be written as

$$\nabla \cdot \sum_{\ell=0}^{\infty} \mathbf{v}_{\ell}(\lambda, \mu) V_{\ell}(p) + \frac{\partial}{\partial p} \sum_{\ell=0}^{\infty} \omega_{\ell}(\lambda, \mu) \alpha_{\ell} A_{\ell}(p) = 0$$

or

$$\sum_{\ell=0}^{\infty} [\nabla \cdot \mathbf{v}_{\ell}(\lambda, \mu)] V_{\ell}(p) + \sum_{\ell=0}^{\infty} \omega_{\ell} \alpha_{\ell} \frac{dA_{\ell}(p)}{dp} = 0$$

Now choose $\alpha_{\ell} = \frac{c_{\ell}^2}{p_B - p_T}$, multiply by $\frac{V_{\ell'}(p)}{p_B - p_T}$, and integrate from p_T to p_B :

$$\sum_{\ell=0}^{\infty} \nabla \cdot \mathbf{v}_{\ell}(\lambda, \mu) \left(\frac{1}{p_B - p_T} \right) \int_{p_T}^{p_B} V_{\ell}(p) V_{\ell'}(p) dp + \sum_{\ell=0}^{\infty} \frac{\omega_{\ell}}{p_B - p_T} \left(\frac{c_{\ell}^2}{p_B - p_T} \right) \int_{p_T}^{p_B} \frac{dA_{\ell}(p)}{dp} V_{\ell'}(p) dp = 0$$

where the summation and integration have been switched. If $\frac{dA_{\ell}(p)}{dp} = -\frac{V_{\ell}(p)}{c_{\ell}^2}$ then

$$\sum_{\ell=0}^{\infty} \left[\nabla \cdot \mathbf{v}_{\ell}(\lambda, \mu) - \frac{\omega_{\ell}}{p_B - p_T} \right] \left(\frac{1}{p_B - p_T} \right) \int_{p_T}^{p_B} V_{\ell}(p) V_{\ell'}(p) dp = 0$$

Using the orthonormality condition of the vertical structure function:

$$\frac{1}{p_B - p_T} \int_{p_T}^{p_B} V_\ell V_{\ell'} dp = \begin{cases} 1 & \ell' = \ell \\ 0 & \ell' \neq \ell. \end{cases}$$

gives

$$\omega_\ell = p_B - p_T (\nabla \cdot \mathbf{v}_\ell)$$

for each ℓ .

$$\text{Now, for } \frac{dA_\ell(p)}{dp} = -\frac{V_\ell(p)}{c_\ell^2}$$

$$\frac{dA_\ell(p)}{dp} = \frac{d}{dp} \left(\frac{p^2}{R\bar{\Gamma}} \frac{dV_\ell}{dp} \right)$$

or

$$\frac{d}{dp} \left[A_\ell(p) - \frac{p^2}{R\bar{\Gamma}} \frac{dV_\ell}{dp} \right] = 0$$

by (3.14). Integrating gives

$$A_\ell(p) = \frac{p^2}{R\bar{\Gamma}} \frac{dV_\ell}{dp} + C$$

Looking at (A.1), it can be seen that C must be zero in order for $\omega(\lambda, \mu, p)$ to remain bounded. Therefore,

$\alpha_\ell A_\ell(p) = \frac{c_\ell^2}{p_B - p_T} \frac{p^2}{R\bar{\Gamma}} \frac{dV_\ell}{dp}$. This gives the inverse transform of

$$\omega(\lambda, \mu, p) = \sum_{\ell=0}^{\infty} \omega_\ell(\lambda, \mu) \frac{c_\ell^2 p^2}{R\bar{\Gamma} (p_B - p_T)} \frac{dV_\ell}{dp}.$$

Which is the same as (3.13b).

A.2 Derivation of the forward transform for ω

In order to compute $\omega_\ell(\lambda, \mu)$ from $\omega(\lambda, \mu, p)$ start with the Sturm-Liouville equation (3.14) which is repeated here

$$\frac{d}{dp} \left(\frac{p^2}{R\bar{\Gamma}} \frac{dV_\ell}{dp} \right) + \frac{V_\ell}{c_\ell^2} = 0 \quad (\text{A.2})$$

with boundary conditions

$$\frac{dV_\ell}{dp} = 0 \quad \text{at } p = p_T \quad (\text{A.3a})$$

$$p \frac{dV_\ell}{dp} + \frac{\bar{\Gamma}}{T} V_\ell = 0 \quad \text{at } p = p_B, \quad (\text{A.3b})$$

and c_ℓ^{-2} the eigenvalue. In order to derive the orthonormality condition on V_ℓ , apply (A.3b) to $V_{\ell'}$ and multiply by V_ℓ and add to (A.3b) applied to V_ℓ and multiplied by $V_{\ell'}$

$$\begin{aligned} -V_{\ell'} \frac{d}{dp} \left(\frac{p^2}{R\bar{\Gamma}} \frac{dV_\ell}{dp} \right) &= \frac{V_\ell}{c_\ell^2} V_{\ell'} \\ V_\ell \frac{d}{dp} \left(\frac{p^2}{R\bar{\Gamma}} \frac{dV_{\ell'}}{dp} \right) &= -\frac{V_{\ell'}}{c_{\ell'}^2} V_\ell \\ \frac{d}{dp} \left(V_\ell \frac{p^2}{R\bar{\Gamma}} \frac{dV_{\ell'}}{dp} - V_{\ell'} \frac{p^2}{R\bar{\Gamma}} \frac{dV_\ell}{dp} \right) &= \left(\frac{1}{c_\ell^2} - \frac{1}{c_{\ell'}^2} \right) V_\ell V_{\ell'} \end{aligned}$$

Multiply both sides by $\frac{1}{p_B - p_T}$ and integrate from p_T to p_B :

$$\frac{1}{p_B - p_T} \int_{p_T}^{p_B} \frac{d}{dp} \left(V_\ell \frac{p^2}{R\bar{\Gamma}} \frac{dV_{\ell'}}{dp} - V_{\ell'} \frac{p^2}{R\bar{\Gamma}} \frac{dV_\ell}{dp} \right) dp = \frac{\left(\frac{1}{c_\ell^2} - \frac{1}{c_{\ell'}^2} \right)}{p_B - p_T} \int_{p_T}^{p_B} V_\ell V_{\ell'} dp$$

which results in

$$\left[\frac{p^2}{R\bar{\Gamma}} \left(V_\ell \frac{dV_{\ell'}}{dp} - V_{\ell'} \frac{dV_\ell}{dp} \right) \right]_{p_T}^{p_B} = \frac{\left(\frac{1}{c_\ell^2} - \frac{1}{c_{\ell'}^2} \right)}{p_B - p_T} \int_{p_T}^{p_B} V_\ell V_{\ell'} dp$$

With the lower boundary condition (A.3b) the equation may be written

$$-\left[\frac{p^2}{R\bar{\Gamma}} \left(\frac{\bar{\Gamma}}{p\bar{T}} V_\ell V_{\ell'} - \frac{\bar{\Gamma}}{p\bar{T}} V_{\ell'} V_\ell \right) \right]_{p_B} - \left[\frac{p^2}{R\bar{\Gamma}} \left(V_\ell \frac{dV_{\ell'}}{dp} - V_{\ell'} \frac{dV_\ell}{dp} \right) \right]_{p_T} = \frac{\left(\frac{1}{c_\ell^2} - \frac{1}{c_{\ell'}^2} \right)}{p_B - p_T} \int_{p_T}^{p_B} V_\ell V_{\ell'} dp.$$

The quantity in the first set of brackets is 0, and because of the boundary condition (A.3a) the quantity in the second brackets also vanishes, leaving the result:

$$\frac{\left(\frac{1}{c_\ell^2} - \frac{1}{c_{\ell'}^2} \right)}{p_B - p_T} \int_{p_T}^{p_B} V_\ell V_{\ell'} dp = 0$$

or

$$\frac{1}{p_B - p_T} \int_{p_T}^{p_B} V_\ell V_{\ell'} dp = \begin{cases} 1 & \ell' = \ell \\ 0 & \ell' \neq \ell. \end{cases}$$

Orthonormality condition obeyed by $\frac{dV_\ell}{dp}$

$$\begin{aligned} \frac{1}{p_B - p_T} \int_{p_T}^{p_B} V_\ell V_{\ell'} dp &= -\frac{c_\ell^2}{p_B - p_T} \int_{p_T}^{p_B} V_{\ell'} \frac{d}{dp} \left(\frac{p^2}{R\bar{\Gamma}} \frac{dV_\ell}{dp} \right) dp \\ &= -\frac{c_\ell^2}{p_B - p_T} \left[\int_{p_T}^{p_B} \frac{d}{dp} \left(V_{\ell'} \frac{p^2}{R\bar{\Gamma}} \frac{d}{dp} \right) dp - \int_{p_T}^{p_B} \frac{p^2}{R\bar{\Gamma}} \frac{dV_{\ell'}}{dp} \frac{dV_\ell}{dp} dp \right] \\ &= \begin{cases} 1 & \ell' = \ell \\ 0 & \ell' \neq \ell. \end{cases} \end{aligned}$$

Evaluating the first integral and factoring out a minus sign gives:

$$\frac{c_\ell^2}{p_B - p_T} \left[- \left(V_{\ell'} \frac{p^2}{R\bar{\Gamma}} \frac{dV_\ell}{dp} \right)_{p_T} + \int_{p_T}^{p_B} \frac{p^2}{R\bar{\Gamma}} \frac{dV_{\ell'}}{dp} \frac{dV_\ell}{dp} dp \right] = \begin{cases} 1 & \ell' = \ell \\ 0 & \ell' \neq \ell. \end{cases}$$

Because $\frac{dV_\ell}{dp} = 0$ at $p = p_T$ the above equation can be written

$$\frac{c_\ell^2}{p_B - p_T} \left[- \left(V_{\ell'} \frac{p^2}{R\bar{\Gamma}} \frac{dV_\ell}{dp} \right)_{p_B} + \int_{p_T}^{p_B} \frac{p^2}{R\bar{\Gamma}} \frac{dV_{\ell'}}{dp} \frac{dV_\ell}{dp} dp \right] = \begin{cases} 1 & \ell' = \ell \\ 0 & \ell' \neq \ell. \end{cases}$$

Using $V_\ell = -\frac{p\bar{T}}{\Gamma} \frac{dV_\ell}{dp}$ at $p = p_B$ the form of the orthonormality condition on $\frac{dV_\ell}{dp}$ can be written:

$$\frac{c_\ell^2}{p_B - p_T} \left[\int_{p_T}^{p_B} \frac{p^2}{R\bar{\Gamma}} \frac{dV_{\ell'}}{dp} \frac{dV_\ell}{dp} dp + \left(\frac{p^3 \bar{T}}{R\bar{\Gamma}^2} \frac{dV_\ell}{dp} \frac{dV_{\ell'}}{dp} \right)_{p_B} \right] = \begin{cases} 1 & \ell' = \ell \\ 0 & \ell' \neq \ell. \end{cases}$$

From Appendix

$$\omega(\lambda, \mu, p) = \sum_{\ell=0}^{\infty} \omega_\ell(\lambda, \mu) \frac{c_\ell^2 p^2}{R\bar{\Gamma} (p_B - p_T)} \frac{dV_\ell}{dp}. \quad (\text{A.4})$$

This equation holds at the boundaries, and in this case, at the lower boundary:

$$\omega(\lambda, \mu, p) = \sum_{\ell=0}^{\infty} \omega_\ell(\lambda, \mu) \left[\frac{c_\ell^2 p^2}{R\bar{\Gamma} (p_B - p_T)} \frac{dV_\ell}{dp} \right]_{p_B}. \quad (\text{A.5})$$

Now multiply (A.4) by $\frac{dV_{\ell'}}{dp}$ and integrate from p_T to p_B , and multiply (A.5) by $\frac{p\bar{T}}{\Gamma} \frac{dV_{\ell'}}{dp}$. Adding the two equations gives:

$$\int_{p_T}^{p_B} \omega(\lambda, \mu, p) \frac{dV_{\ell'}}{dp} dp + \left[\omega(\lambda, \mu, p) \frac{p\bar{T}}{\Gamma} \frac{dV_{\ell'}}{dp} \right]_{p_B} = \sum_{\ell=0}^{\infty} \omega_\ell(\lambda, \mu) \left\{ \int_{p_T}^{p_B} \frac{p^2}{R\bar{\Gamma}} \frac{dV_\ell}{dp} \frac{dV_{\ell'}}{dp} dp + \left[\frac{p^3 \bar{T}}{R\bar{\Gamma}^2} \frac{dV_\ell}{dp} \frac{dV_{\ell'}}{dp} \right]_{p_B} \right\}$$

From the orthonormality condition on $\frac{dV_\ell}{dp}$ the expression in the braces assumes one of two values:

$$\int_{p_T}^{p_B} \frac{p^2}{R\bar{\Gamma}} \frac{dV_\ell}{dp} \frac{dV_{\ell'}}{dp} dp + \left[\frac{p^3 \bar{T}}{R\bar{\Gamma}^2} \frac{dV_\ell}{dp} \frac{dV_{\ell'}}{dp} \right]_{p_B} = \begin{cases} \frac{p_B - p_T}{c_\ell^2} & \ell' = \ell \\ 0 & \ell' \neq \ell. \end{cases}$$

Using that result, the forward transform is given by

$$\omega_\ell(\lambda, \mu) = \frac{c_\ell^2}{p_B - p_T} \left\{ \int_{p_T}^{p_B} \omega(\lambda, \mu, p) \frac{dV_\ell}{dp} dp + \left[\omega(\lambda, \mu, p) \frac{p\bar{T}}{\bar{\Gamma}} \frac{dV_\ell}{dp} \right]_{p_B} \right\}.$$